8. SITE 985[1]

Shipboard Scientific Party[2]

HOLE 985A

Position: 66°56.490′N, 6°27.012′W

Start hole: 1400 hr, 3 August 1995

End hole: 0415 hr, 7 August 1995

Time on hole: 86.25 hr (3.59 days)

Seafloor (drill pipe measurement from rig floor, mbrf): 2797.8

Total depth (drill pipe measurement from rig floor, mbrf): 3385.7

Distance between rig floor and sea level (m): 11.2

Water depth (drill pipe measurement from sea level, m): 2787.6

Penetration (mbsf): 587.9

Coring totals:

Type: APC
Number: 17
Cored: 155.2 m
Recovered: 159.33 m, 102.7%

Type: XCB
Number: 45
Cored: 432.7 m
Recovered: 394.09 m, 91.1%

Total:
Number: 62
Cored: 587.9 m
Recovered: 553.42 m, 94.1%

Formation:

Unit I: 0–17.2 mbsf; Holocene to late Pleistocene; clayey nannofossil ooze, nannofossil clay with silt, silty clay
Unit II: 17.2–99.2 mbsf; late Pleistocene to early Pliocene; silty clay, clay with silt, clay, clayey nannofossil ooze
Unit III: 99.2–155.2 mbsf; early Pliocene to late Miocene; clay with silt
Unit IV: 155.2–465.0 mbsf; late Miocene to ?late Oligocene; indurated clay, clay with silt, clay with glauconite
Unit V: 465.0–587.9 mbsf; ?early Miocene to ?late Oligocene; indurated clay and silty clay

HOLE 985B

Position: 66°56.498′N, 6°27.001′W

Start hole: 0415 hr, 7 August 1995

End hole: 2115 hr, 7 August 1995

Time on hole: 17.00 hr (0.71 days)

Seafloor (drill pipe measurement from rig floor, mbrf): 2799.1

Total depth (drill pipe measurement from rig floor, mbrf): 2926.0

Distance between rig floor and sea level (m): 11.3

Water depth (drill pipe measurement from sea level, m): 2787.8

Penetration (mbsf): 126.9

Coring totals:

Type: APC
Number: 14
Cored: 126.9 m
Recovered: 129.44 m, 102.0%

Formation:

Unit I: 0–17.2 mbsf; Holocene to late Pleistocene; clayey nannofossil ooze, nannofossil clay with silt, silty clay
Unit II: 17.2–99.2 mbsf; late Pleistocene to early Pliocene; silty clay, clay with silt, clay, clayey nannofossil ooze
Unit III: 99.2–155.2 mbsf; early Pliocene to late Miocene; clay with silt

Principal results: The sediments recovered at Site 985 (ICEP-3) are predominantly fine-grained siliciclastics. The dominant lithologies include silty clays, clays with silt, and clays. Biocarbonates are restricted to the upper parts of the sedimentary sequence. Clays and silty clays containing biosilica are encountered only between 240 and 290 mbsf. Disseminated volcanic ash, ash pods, and ash layers occur throughout the sedimentary sequence. Dropstones are confined to the upper sedimentary sequence (0–70 mbsf). The sequence was dated by means of magnetic polarity records to the latest Miocene, below which it became difficult to correlate to the geomagnetic polarity time scale. The underlying sequence thus has poor age constraints. Siliceous microfossils and arenaceous benthic foraminifers provide some age information in the lower section, indicating that the drilled sequence ends in the upper Oligocene.

Multisensor track (MST) investigations document that a complete section has been recovered over the upper 131 mbsf (Holocene to latest Miocene) with good overlap across core breaks. Within the last 7 Ma, sedimentation rates are highest in the last 3 Ma (13–36 m/m.y.) and drop to 10–20 m/m.y. in the middle and early Pliocene. Somewhat higher sedimentation rates (about 25 m/m.y.) are documented for the latest Miocene. The thick early to middle Miocene clay-rich unit precluded significant recovery of Paleogene sediments, and the lack of carbonate-bearing Oligocene sediments at the site was disappointing. Thus, our hopes of retrieving quantitative Paleogene paleoclimatic information from this site were not fulfilled.

Five lithostratigraphic units were recovered: Unit I (0–17.2 mbsf; Holocene to late Pleistocene) is defined largely on the basis of relatively abundant biocarbonates (up to 30%) and higher color spectral reflectance than underlying units. The sediments are composed of interbedded layers of gray clayey nannofossil ooze with foraminifers; dark gray nannofossil clay with silt; dark gray silty clay with nannofossils; brown and dark grayish brown clay with silt; and very dark gray to dark grayish brown silty clays. The cyclic, interbedded nature of the sediments testifies to their glacial/interglacial origin.

Unit II (17.2–99.2 mbsf; late Pleistocene to early Pliocene), is defined, in part, by the diminished presence of biocarbonate which occurs as a variable sedimentary component, averaging 7%. The unit is composed largely of silty clay, clay with silt, and clay. X-ray diffraction (XRD) and smear slide analysis both demonstrate an increase in quartz, plagioclase, and pyroxene within Unit II relative to the underlying sediments. Both reflectance values and natural gamma-ray counts decrease noticeably at the

[1]Jansen, E., Raymo, M.E., Blum, P., et al., 1996. *Proc. ODP, Init. Repts.*, 162: College Station, TX (Ocean Drilling Program).

[2]Shipboard Scientific Party is given in the list preceding the Table of Contents.

boundary with the underlying unit. Both Unit I and II contain dropstones, in contrast to the underlying units.

Unit III (99.2–155.2 mbsf; late Miocene to early Pliocene) is characterized by the occurrence of clay with silt and by the absence of biogenic sediments. Isolated spikes of inorganic carbonate are superimposed on a carbonate-free background. XRD analysis of the bulk sediments reveals that plagioclase, quartz, and pyroxene are present to a lesser extent than in Units I and II. Unit IV (155.2–465 mbsf; late Oligocene to late Miocene) comprises the bulk of the sedimentary sequence at Site 985. These sediments are distinguished from those of Units III and V by the transition from silty clay and clay with silt to lithologies in which indurated clays are dominant. Other characteristics of this lithofacies include very low magnetic susceptibility values and the absence of biocarbonates. Yellowish brown carbonate concretions are observed in Unit IV, some of which are composed of fluorapatite, and may be similar in composition to the yellowish orange layers found at shallower depths.

Unit IV can be subdivided into three distinct subunits. Subunit IVA (155.2–241.5 mbsf) is distinguished from the underlying sediments by higher magnetic susceptibility and natural gamma-ray values and by the absence of biosilica. Two carbonate-rich layers in Subunit IVA that may act as barriers to the diffusion of interstitial waters are noteworthy. XRD analysis of the upper layer indicates that it is composed of poorly crystallized carbonate. These layers yield high velocity measurements and bound sediments with interstitial waters that have anomalously low chloride, sodium, and salinity content, and a hydrocarbon gas content with unusually high proportions of C_{2+} gases relative to methane. Reduced diversity of arenaceous benthic foraminifers also characterizes this interval. The causes for these anomalies are not known. Subunit IVB (241.5–289.6 mbsf) is defined by the presence of biosilica. Subunit IVC (289.6–465 mbsf) is distinguished from Subunit IVB by the absence of biosilica and by a gradual increase in natural gamma-ray counts.

Unit V (465–578.9 mbsf; late Oligocene[?] to early Miocene[?]) is comprised of indurated dark greenish gray to very dark greenish gray clay; olive gray to dark greenish gray silty clay; and very dark greenish gray clay with glauconite and glauconitic clay. These sediments are distinguished from the overlying sediments by a sharp increase in magnetic susceptibility.

Changes in sediment physical properties appear to be correlated with the few prominent seismic reflectors of the site, some of which appear to reflect erosional surfaces or condensed sections.

BACKGROUND AND OBJECTIVES

Site 985 (ICEP-3) is located on a gentle slope of the Iceland Plateau into the deeper Norway Basin, at 2788 m water depth, about 1000 m deeper than Site 907 (Fig. 1). It was targeted on a University of Bergen seismic line showing an approximately 800-m-thick sediment sequence with little internal seismic structure, the seismic character being quite similar to that of Site 907. The site was a second-priority site for Leg 162, and was drilled due to operational constraints and considerations. Drilling at Site 985 served two main purposes: first, it is part of a paleoenvironmental transect together with Site 907. Second, our objective was to recover a pelagic Paleogene sequence on crust with an assumed normal subsidence history.

Site 985 is a part of a paleoenvironmental transect from Norway to Greenland, designed to study the history of advection of temperate, saline Atlantic waters into the Norwegian-Greenland Sea ("the Nordic heat pump"), the position of the mixing front between these warm waters and the cold, partly ice-covered Arctic waters (the Arctic Front) and the position of the front delineating the less saline, ice-covered Polar Waters of the East Greenland Current. This transect, therefore, covers the climatically sensitive and variable thermal gradient between polar areas near east Greenland and temperate areas off Norway. Sites drilled on the Vøring Plateau during ODP Leg 104 (Eldholm, Thiede, Taylor, et al., 1987; Eldholm et al., 1989) anchor the eastern end of the transect, and Site 987 (EGM-4) on the Greenland continental margin forms its western end (Fig. 1). Site 985 is located between these end-members, at the present wintertime location of the Arctic Front on the warm-water side of Site 907. The records from Site 985 are intended to (1) monitor the history of oceanic and climatic fronts moving east and west across the Norwegian-Greenland Sea, (2) derive an open-ocean record of ice-rafted debris (IRD) and carbonate accumulation, and (3) document the history of formation of northern-source deep waters. Piston and ODP cores from the southern Nordic Seas document that warm phases were short, variable, and seldom occurred in the late Quaternary. Each interglacial was unique in terms of ocean circulation and the heat advected to the region (Henrich and Baumann, 1994; Eide et al., in press; Fronval and Jansen, in press). Extending the late Quaternary record back in time will enable a clearer picture of the long-term evolution of these short interglacial warm spells and the relationships between them,

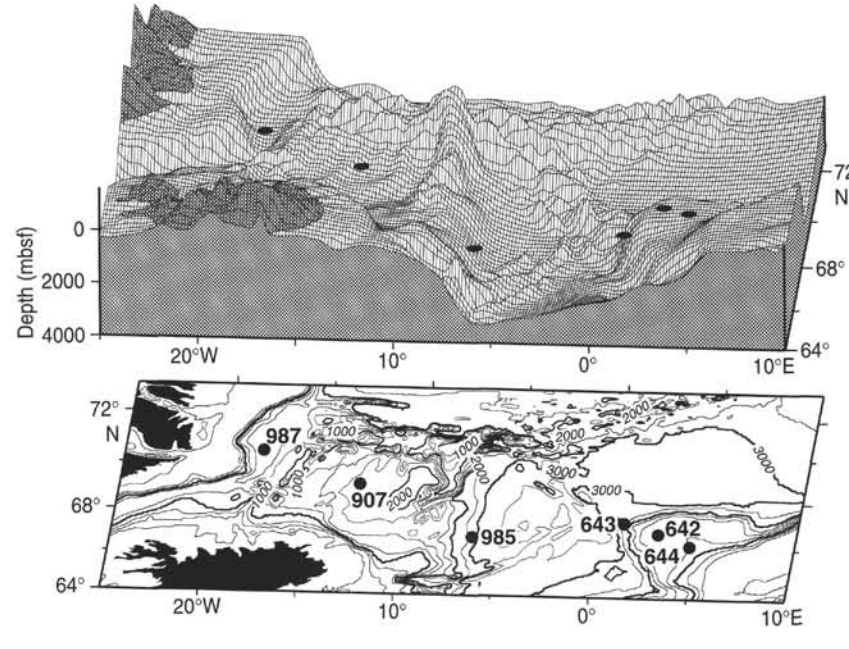

Figure 1. Bathymetry of the Nordic Seas paleoenvironmental transect, showing location of Leg 104, 151, and 162 drill sites. Bathymetric data (in meters) from ETOPO5.

ocean circulation patterns, and the glaciation history on Milankovitch time scales. This will provide insight into the climatic sensitivity of the Nordic Seas and their possible role as an early responder to orbital climate forcing (Imbrie et al., 1992, 1993; Koç and Jansen, 1994).

The second objective of this site was to recover Paleogene sections. The site is located on Eocene Anomaly 22 crust (about 50 Ma) (Talwani and Eldholm, 1977) (Fig. 2). The approximately 800-m sediment cover should contain both Neogene and Paleogene sections from which information on the paleoceanographic evolution of this high-latitude area can be obtained. DSDP and ODP drilling has so far recovered only sporadic Paleogene sections from the Nordic Seas (Leg 38: Talwani, Udintsev, et al., 1976; Leg 104: Eldholm, Thiede,

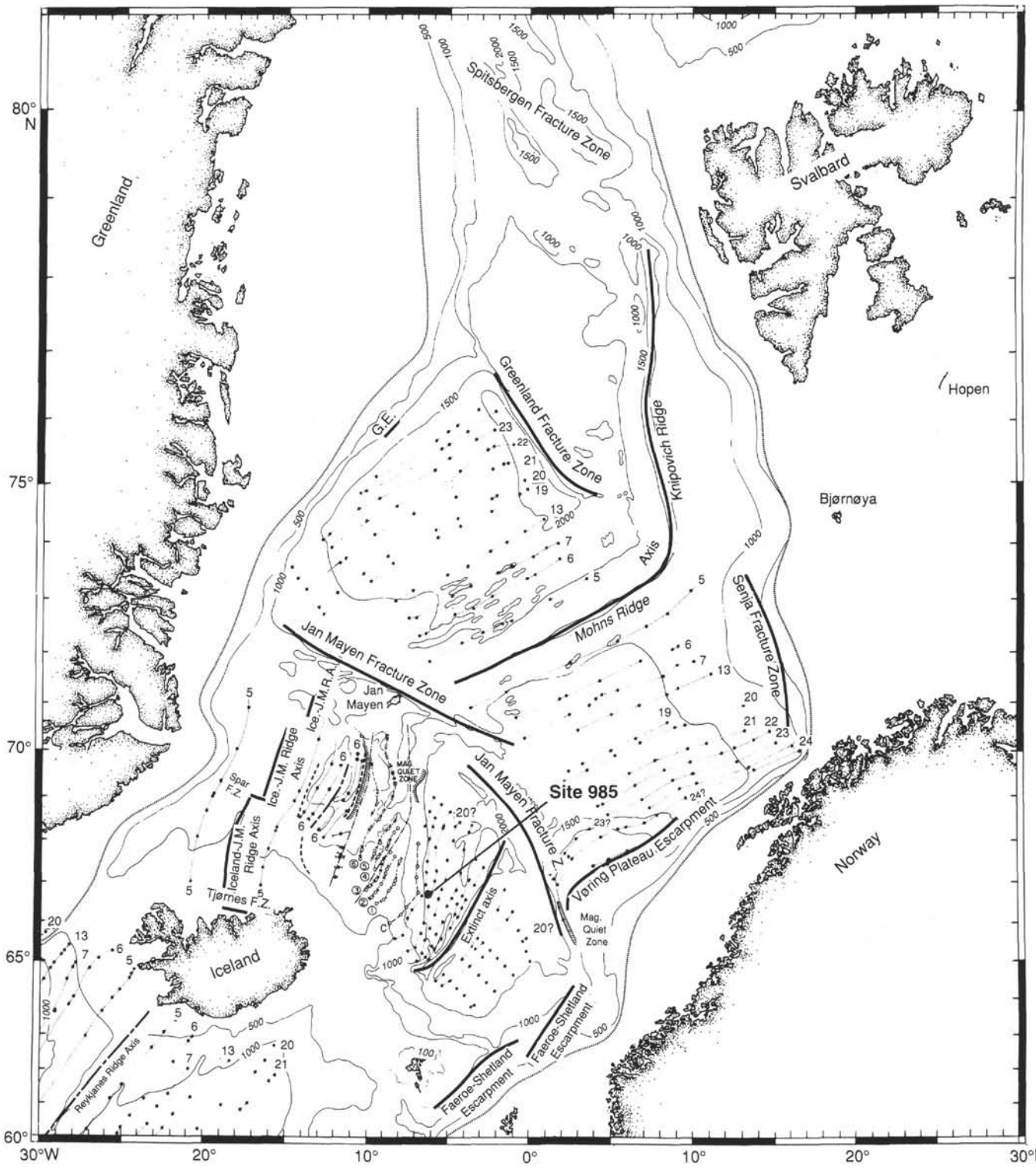

Figure 2. Position of Site 985 on magnetic anomaly map of Talwani and Eldholm (1977). G.E. = Greenland Escarpment (after Talwani and Eldholm, 1977).

Taylor, et al., 1987; Leg 151: Myhre, Thiede, Firth, et al., 1995), and an important objective of drilling Site 985 was to obtain Paleogene sections. Prior drilling has documented that carbonate-bearing Oligocene sediments exist in the region, but poor recovery and diagenetic overprinting have precluded stable isotope studies of these sections. Such investigations would cast light on Paleogene equator-to-pole temperature gradients and how meridional heat flux differed in the past, as well as provide insight into paleotemperatures and ocean circulation in the Nordic Seas during the Paleogene, and possible linkages with the Atlantic Ocean. Because the site is located on the Greenland side of the (now extinct) Aegir spreading axis, on oceanic crust with assumed normal subsidence history and in an area where excessive heat flux with associated strong diagenesis is not likely to have occurred, it was thought that drilling at Site 985 would be well-suited for such studies. Drilling at Site 985 would also help constrain the tectonic history of the Jan Mayen microcontinent, a continental fragment that rifted off east Greenland when spreading moved away from the Aegir Ridge during Anomaly 7 time (Talwani and Eldholm, 1977).

OPERATIONS

According to the plan in the Leg 162 Prospectus, Site 985 should have been EGM-4 on the East Greenland Margin. The ice data available to the shipboard party during the drilling of Hole 907C showed the EGM-4 drill site positioned on the edge of the 20% ice concentration line. Just hours before getting underway, an updated SSMI report was obtained that placed the EGM-4 drill site 20 nmi "outside" the 20% ice concentration line. Based on this promising outlook, and with a plan to survey alternate sites up to 10 nmi east of the proposed site EGM-4, the vessel departed for EGM-4 at 1445 hr on 2 August 1995. Less than 1 hr after getting underway, a faxed "interpreted" SAR image with data from 2 August was received indicating that the EGM-4 drill site was 15 nmi "inside" what was referred to as "closed ice." In addition to being more recent, the SAR data is considered more accurate then the more general SSMI information. This new information made the EGM-4, as well as its alternate sites EGM-4a-d, essentially undrillable at that time.

In the normal course of events, we would have then proceeded to our next first-priority site, SVAL-1. However, we had to remain near Iceland to wait for resupplies of some critical items. The ship had only enough core liners on board to complete a limited amount of drilling (about 700 m) and was running very low on acetone. A resupply was scheduled to take place via rendezvous with the supply boat *Strakur* prior to departure for the northern drill sites. Hence the decision was made to steam towards ICEP-3, a second-priority alternate site. While underway, the computer file containing the SAR photo was picked up from the ODP directory and the interpreted information regarding EGM-4 ice conditions received earlier was confirmed.

The drilling plan for ICEP-3 was to core a single APC/XCB hole as deep as possible in the time before the resupply ship arrived. The PPSP had approved drilling to a depth of 500 mbsf but the co-chief scientists felt that any major scientific rewards would most likely be attained at deeper depths. As a result they asked for and received permission to extend the depth of Hole 985A to 650 mbsf, time permitting. There was to be no core orientation or temperature measurements taken at this site.

After completing the pre-site survey (see "Seismic Stratigraphy" section, this chapter), the vessel returned to the drilling location based on GPS coordinates. The positioning beacon was deployed at 1358 hr on 3 August, initiating Hole 985A.

A standard APC/XCB bottom-hole assembly was used for all holes at Site 985, including a nonmagnetic drill collar. The mudline was established for each hole. The APC firing depth was offset by a few meters for Hole 985B relative to Hole 985A to establish a continuous sediment section over the double-cored interval. Position, depths, and coring totals for each hole are summarized at the top of this chapter. All cores are listed in Table 1.

Routine piston coring at Hole 985A proceeded until Cores 985A-14H to 17H failed to bleed off pressure, indicating incomplete stroke. XCB coring was initiated with Core 18X and continued with excellent recovery. Coring was temporarily halted when the methane/ethane ratio dropped from 100,000+ in Core 985A-36X to 6 on Core 37X; gas concentrations were very small (see "Organic Geochemistry" section, this chapter). In addition to the abrupt reduction in gas ratio, trace amounts of higher hydrocarbons up through IC6 were detected. At that time cutting of Core 985A-40X had just been completed and coring operations were halted until additional analyses could be evaluated. The hydrocarbon trends returned to normal in Cores 985A-38X and 39X, and the results from Core 40X were completely back to normal. Throughout the coring cycle there was no change in formation properties or drilling parameters. Coring resumed and continued without incident through Core 985A-62X, where the scientific target had been reached.

Upon completion of coring operations, a wiper trip was made in preparation for wireline logging. Overpull of 30 to 50 kilopounds was experienced. There was 9 m of fill identified on bottom. The hole was again circulated with 2 times annular volume of seawater while the go-devil was pumped downhole. The pipe was then pulled to a logging depth of 90.1 mbsf, with 10 to 20 kilopounds drag. Wireline logging was not successful in this hole. The first run with the Quad combination tool was deployed to only 23 m below the bit and all efforts to exceed that point failed. After a consultation with the co-chief scientist and the loggers, it was decided that any further logging attempts on Hole 985A be abandoned.

The vessel was offset 15 m north for spudding Hole 985B. APC coring proceeded without incident until the last remaining core liner had been used with Core 985B-14H. Fortunately, the supply boat was expected within a few hours.

The drilling line was cut and slipped prior to tripping the drill string back to the vessel. During the trip, the supply boat *Strakur* arrived (1715 hr). After several unsuccessful attempts to come alongside due to "thruster wash," the captain decided to release the beacon, retract the hydrophones, and turn the vessel to give the supply boat more of a lee to come alongside. During the process the drillship was allowed to drift with the current. The beacon was recovered at 1820 hr, and at 1845 hours the *Strakur* was alongside, discharging her cargo.

The core liners, acetone, mail, and other requested supplies were taken aboard. Shipboard mail and a small airfreight package were discharged to the supply boat, along with a Borehole Research Group logging trainee who had elected to leave his field of study and requested to return to shore. At 1915 hr on 7 August 1995, the *Strakur* departed for a small harbor just north of Reykjavik.

The pipe trip continued throughout the loading/unloading process and at 2115 hr that same day the vessel was secured and underway for Site 986 (SVAL-1).

COMPOSITE DEPTHS

Continuity of the sedimentary sequence at Site 985 was documented for the upper 131 mbsf (meters below seafloor), extending from the upper Miocene through the Holocene. Sufficient overlap between the 14 cores drilled in Hole 985B and the upper part of Hole 985A allowed a composite section to be developed for this site, as described in the "Composite Depth" section, "Explanatory Notes" chapter (this volume). Due to severe disturbance of Core 985B-3H, correlations between it and Cores 985A-2H and 3H were uncertain, and thus no adjustments of the relative depths of these cores were made. Core 985A-3H may also be somewhat disturbed. The depth

Table 1. Coring summary for Site 985.

Core	Date (Aug. 1995)	Time (UTC)	Depth (mbsf)	Length cored (m)	Length recovered (m)	Recovery (%)
162-985A-						
1H	3	1945	0.0–7.7	7.7	7.70	100.0
2H	3	2025	7.7–17.2	9.5	9.83	103.0
3H	3	2055	17.2–26.7	9.5	9.77	103.0
4H	3	2130	26.7–36.2	9.5	9.94	104.0
5H	3	2210	36.2–45.7	9.5	9.96	105.0
6H	3	2250	45.7–55.2	9.5	9.82	103.0
7H	3	2325	55.2–64.7	9.5	9.85	103.0
8H	3	2355	64.7–74.2	9.5	9.58	101.0
9H	4	0035	74.2–83.7	9.5	9.73	102.0
10H	4	0125	83.7–93.2	9.5	9.77	103.0
11H	4	0205	93.2–102.7	9.5	9.84	103.0
12H	4	0245	102.7–112.2	9.5	9.79	103.0
13H	4	0325	112.2–121.7	9.5	9.79	103.0
14H	4	0405	121.7–131.2	9.5	9.34	98.3
15H	4	0450	131.2–140.7	9.5	10.08	106.1
16H	4	0530	140.7–148.9	8.2	8.24	100.0
17H	4	0610	148.9–155.2	6.3	6.30	100.0
18X	4	0745	155.2–164.7	9.5	9.86	104.0
19X	4	0850	164.7–174.2	9.5	9.74	102.0
20X	4	0955	174.2–183.8	9.6	5.32	55.4
21X	4	1105	183.8–193.4	9.6	9.84	102.0
22X	4	1200	193.4–203.0	9.6	9.84	102.0
23X	4	1250	203.0–212.6	9.6	9.95	103.0
24X	4	1340	212.6–222.2	9.6	6.47	67.4
25X	4	1435	222.2–231.8	9.6	9.74	101.0
26X	4	1545	231.8–241.5	9.7	9.53	98.2
27X	4	1625	241.5–251.1	9.6	8.45	88.0
28X	4	1705	251.1–260.7	9.6	7.35	76.5
29X	4	1755	260.7–270.3	9.6	9.01	93.8
30X	4	1840	270.3–280.0	9.7	8.84	91.1
31X	4	1930	280.0–289.6	9.6	9.70	101.0
32X	4	2020	289.6–299.2	9.6	9.81	102.0
33X	4	2110	299.2–308.8	9.6	9.32	97.1
34X	4	2205	308.8–318.5	9.7	8.23	84.8
35X	4	2255	318.5–328.1	9.6	9.77	102.0
36X	4	2350	328.1–337.7	9.6	9.86	103.0
37X	5	0115	337.7–347.3	9.6	9.81	102.0
38X	5	0215	347.3–356.9	9.6	9.81	102.0
39X	5	0320	356.9–366.5	9.6	9.38	97.7
40X	5	0420	366.5–375.7	9.2	9.90	107.0
41X	5	0625	375.7–385.5	9.8	9.90	101.0
42X	5	0725	385.5–395.3	9.8	9.91	101.0
43X	5	0830	395.3–405.0	9.7	9.93	102.0
44X	5	0950	405.0–414.7	9.7	10.03	103.4
45X	5	1055	414.7–424.4	9.7	9.53	98.2
46X	5	1200	424.4–434.0	9.6	9.91	103.0
47X	5	1250	434.0–443.6	9.6	9.88	103.0
48X	5	1330	443.6–453.2	9.6	9.83	102.0
49X	5	1420	453.2–462.7	9.5	9.28	97.7
50X	5	1515	462.7–472.3	9.6	9.92	103.0
51X	5	1625	472.3–481.9	9.6	9.57	99.7
52X	5	1750	481.9–491.5	9.6	9.84	102.0
53X	5	1910	491.5–501.1	9.6	9.81	102.0
54X	5	2040	501.1–510.7	9.6	9.87	103.0
55X	5	2215	510.7–520.4	9.7	9.81	101.0
56X	6	0005	520.4–530.0	9.6	9.16	95.4
57X	6	0210	530.0–539.6	9.6	4.99	52.0
58X	6	0440	539.6–549.2	9.6	3.13	32.6
59X	6	0705	549.2–558.9	9.7	4.64	47.8
60X	6	0935	558.9–568.6	9.7	8.40	86.6
61X	6	1210	568.6–578.2	9.6	5.52	57.5
62X	6	1530	578.2–587.9	9.7	1.70	17.5
			Coring totals:	587.9	553.40	94.1
162-985B-						
1H	7	0550	0.0–3.4	3.4	3.42	100.0
2H	7	0630	3.4–12.9	9.5	9.76	103.0
3H	7	0710	12.9–22.4	9.5	9.79	103.0
4H	7	0750	22.4–31.9	9.5	9.36	98.5
5H	7	0830	31.9–41.4	9.5	9.79	103.0
6H	7	0910	41.4–50.9	9.5	9.60	101.0
7H	7	0950	50.9–60.4	9.5	9.85	103.0
8H	7	1035	60.4–69.9	9.5	9.42	99.1
9H	7	1115	69.9–79.4	9.5	9.82	103.0
10H	7	1155	79.4–88.9	9.5	9.67	102.0
11H	7	1230	88.9–98.4	9.5	9.82	103.0
12H	7	1310	98.4–107.9	9.5	9.66	101.0
13H	7	1345	107.9–117.4	9.5	9.87	104.0
14H	7	1420	117.4–126.9	9.5	9.61	101.0
			Coring totals:	126.9	129.40	102.0

offsets that comprise the composite depth section at Site 985 are given in Table 2.

MST data used in the correlations are displayed on the composite depth scale in Figure 3 (see also back pocket). Magnetic susceptibility was the primary parameter used to develop the composite section. Gamma-ray attenuation porosity (GRAPE) density, natural gamma radiation, and percentage spectral reflectance in the 650–700-nm band (see "Lithostratigraphy" section, this chapter) were used to confirm the hole-to-hole correlations. Natural gamma radiation and GRAPE density exhibited a moderate positive correlation; each showed a weak negative correlation with susceptibility through the depth range of the composite section. The relative independence of the three parameters made the splice more precise by allowing features that were not apparent in one data set to be correlated in another.

Although overlap between adjacent holes was excellent through most of the section, stretching and compression within the cored sequence occurred over most intervals. Because much of this distortion was on a scale of less than 9 m, it was not possible to align every sedimentary feature using only the composite depth scale adjustments. Within-core, decimeter to centimeter-scale depth adjustments would be required to align all sedimentary features simultaneously.

The mcd scale grows relative to the mbsf scale in both holes by about 8% over the range of the composite section (Fig. 4). The expansion of the sequence, less than the 10% commonly found at the sites south of Iceland, is caused by physical expansion of the cores after recovery and by stretching of the sequence during the coring process.

After construction of the composite depth section for Site 985, a single spliced record was developed, as described in the "Explanatory Notes" chapter (this volume). The tie points between the cores used to construct the splice are given in Table 3. Due to the disturbance in Core 985B-3H, Core 985A-3H was appended to the base of Core 985A-2H, and so the splice includes the core break at the bottom of Core 985A-2H. In the upper four sections of Core 985A-3H, the bedding is at an angle of up to 45° from horizontal, probably due to coring disturbance. The composite section continues down to 138 mcd, below which the remainder of the Hole 985A cores have been appended to the composite section with no adjustment of their relative depths. The spliced GRAPE density, natural gamma radiation, and magnetic susceptibility data are shown in Figure 5.

LITHOSTRATIGRAPHY

The sediments recovered at Site 985 are predominantly fine-grained siliciclastics. The dominant lithologies include silty clays, clays with silt, and clays. Yellowish orange color bands containing inorganic carbonate and clay are found in the upper sediments, while yellowish brown concretions, at least some of which contain fluorapatite, are more common toward the base of the sequence. In contrast, biocarbonates in amounts >10% are restricted to the upper part of the sedimentary sequence and occur in clayey nannofossil ooze with foraminifers and silty clay with nannofossils. Clays and silty clays containing biosilica are encountered only between 240 and 290 mbsf. Sulfides, although less common than at other sites drilled during Leg 162, are found throughout the section, predominantly as disseminated pyrite, pyrite layers, and concretions.

Disseminated volcanic ash, ash pods, and ash layers occur throughout the sedimentary sequence. Discrete ash layers (>1.0 cm thick) are most common in the upper 150 mbsf. While individual ash shards generally appear colorless under smear slide examination, the ash layers range in color from light gray to black, with darker ash layers more common. The darker coloration in these layers appears due to the presence of sulfides in association with the colorless volcanic ash. Much of the ash, particularly in the deeper sediments, is altered and occurs with pyrite, zeolites, and other ash-derived clays. Dropstones (>1.0 cm in size) are confined to the upper sedimentary se-

Table 2. Site 985 composite depths.

Core, section	Length (cm)	Depth (mbsf)	Depth (mcd)	Offset (mcd – mbsf)
162-985A-				
1H-1	150	0.00	0.22	0.22
1H-2	150	1.50	1.72	0.22
1H-3	150	3.00	3.22	0.22
1H-4	150	4.50	4.72	0.22
1H-5	150	6.00	6.22	0.22
1H-CC	20	7.50	7.72	0.22
2H-1	150	7.70	8.87	1.17
2H-2	150	9.20	10.37	1.17
2H-3	150	10.70	11.87	1.17
2H-4	150	12.20	13.37	1.17
2H-5	150	13.70	14.87	1.17
2H-6	150	15.20	16.37	1.17
2H-7	61	16.70	17.87	1.17
2H-CC	22	17.31	18.48	1.17
3H-1	150	17.20	18.37	1.17
3H-2	150	18.70	19.87	1.17
3H-3	150	20.20	21.37	1.17
3H-4	150	21.70	22.87	1.17
3H-5	150	23.20	24.37	1.17
3H-6	150	24.70	25.87	1.17
3H-7	54	26.20	27.37	1.17
3H-CC	23	26.74	27.91	1.17
4H-1	150	26.70	28.07	1.37
4H-2	150	28.20	29.57	1.37
4H-3	150	29.70	31.07	1.37
4H-4	150	31.20	32.57	1.37
4H-5	150	32.70	34.07	1.37
4H-6	150	34.20	35.57	1.37
4H-7	65	35.70	37.07	1.37
4H-CC	29	36.35	37.72	1.37
5H-1	150	36.20	37.88	1.68
5H-2	150	37.70	39.38	1.68
5H-3	150	39.20	40.88	1.68
5H-4	150	40.70	42.38	1.68
5H-5	150	42.20	43.88	1.68
5H-6	150	43.70	45.38	1.68
5H-7	69	45.20	46.88	1.68
5H-CC	27	45.89	47.57	1.68
6H-1	150	45.70	48.17	2.47
6H-2	150	47.20	49.67	2.47
6H-3	150	48.70	51.17	2.47
6H-4	150	50.20	52.67	2.47
6H-5	150	51.70	54.17	2.47
6H-6	150	53.20	55.67	2.47
6H-7	58	54.70	57.17	2.47
6H-CC	24	55.28	57.75	2.47
7H-1	150	55.20	59.11	3.91
7H-2	150	56.70	60.61	3.91
7H-3	150	58.20	62.11	3.91
7H-4	150	59.70	63.61	3.91
7H-5	150	61.20	65.11	3.91
7H-6	150	62.70	66.61	3.91
7H-7	62	64.20	68.11	3.91
7H-CC	23	64.82	68.73	3.91
8H-1	150	64.70	69.41	4.71
8H-2	150	66.20	70.91	4.71
8H-3	150	67.70	72.41	4.71
8H-4	150	69.20	73.91	4.71
8H-5	150	70.70	75.41	4.71
8H-6	150	72.20	76.91	4.71
8H-7	26	73.70	78.41	4.71
8H-CC	32	73.96	78.67	4.71
9H-1	150	74.20	79.12	4.92
9H-2	150	75.70	80.62	4.92
9H-3	150	77.20	82.12	4.92
9H-4	150	78.70	83.62	4.92
9H-5	150	80.20	85.12	4.92
9H-6	150	81.70	86.62	4.92
9H-7	47	83.20	88.12	4.92
9H-CC	26	83.67	88.59	4.92
10H-1	150	83.70	89.24	5.54
10H-2	150	85.20	90.74	5.54
10H-3	150	86.70	92.24	5.54
10H-4	150	88.20	93.74	5.54
10H-5	150	89.70	95.24	5.54
10H-6	150	91.20	96.74	5.54
10H-7	51	92.70	98.24	5.54
10H-CC	26	93.21	98.75	5.54
11H-1	150	93.20	99.54	6.34
11H-2	150	94.70	101.04	6.34
11H-3	150	96.20	102.54	6.34
11H-4	150	97.70	104.04	6.34
11H-5	150	99.20	105.54	6.34
11H-6	150	100.70	107.04	6.34
11H-7	58	102.20	108.54	6.34
11H-CC	26	102.78	109.12	6.34
12H-1	150	102.70	109.68	6.98
12H-2	150	104.20	111.18	6.98
12H-3	150	105.70	112.68	6.98
12H-4	150	107.20	114.18	6.98
12H-5	150	108.70	115.68	6.98
12H-6	150	110.20	117.18	6.98
12H-7	60	111.70	118.68	6.98
12H-CC	19	112.30	119.28	6.98
13H-1	150	112.20	119.69	7.49
13H-2	150	113.70	121.19	7.49
13H-3	150	115.20	122.69	7.49
13H-4	150	116.70	124.19	7.49
13H-5	150	118.20	125.69	7.49
13H-6	150	119.70	127.19	7.49
13H-7	51	121.20	128.69	7.49
13H-CC	28	121.71	129.20	7.49
14H-1	110	121.70	129.54	7.84
14H-2	150	122.80	130.64	7.84
14H-3	150	124.30	132.14	7.84
14H-4	150	125.80	133.64	7.84
14H-5	150	127.30	135.14	7.84
14H-6	150	128.80	136.64	7.84
14H-7	43	130.30	138.14	7.84
14H-CC	31	130.73	138.57	7.84
15H-1	150	131.20	139.04	7.84
15H-2	150	132.70	140.54	7.84
15H-3	150	134.20	142.04	7.84
15H-4	150	135.70	143.54	7.84
15H-5	150	137.20	145.04	7.84
15H-6	150	138.70	146.54	7.84
15H-7	58	140.20	148.04	7.84
15H-CC	50	140.78	148.62	7.84
16H-1	150	140.70	148.54	7.84
16H-2	150	142.20	150.04	7.84
16H-3	150	143.70	151.54	7.84
16H-4	150	145.20	153.04	7.84
16H-5	150	146.70	154.54	7.84
16H-6	49	148.20	156.04	7.84
16H-CC	25	148.69	156.53	7.84
17H-1	150	148.90	156.74	7.84
17H-2	150	150.40	158.24	7.84
17H-3	150	151.90	159.74	7.84
17H-4	150	153.40	161.24	7.84
17H-CC	30	154.90	162.74	7.84
18X-1	150	155.20	163.04	7.84
18X-2	150	156.70	164.54	7.84
18X-3	150	158.20	166.04	7.84
18X-4	150	159.70	167.54	7.84
18X-5	150	161.20	169.04	7.84
18X-6	150	162.70	170.54	7.84
18X-7	45	164.20	172.04	7.84
18X-CC	41	164.65	172.49	7.84
19X-1	150	164.70	172.54	7.84
19X-2	150	166.20	174.04	7.84
19X-3	150	167.70	175.54	7.84
19X-4	150	169.20	177.04	7.84
19X-5	150	170.70	178.54	7.84
19X-6	150	172.20	180.04	7.84
19X-7	49	173.70	181.54	7.84
19X-CC	25	174.19	182.03	7.84
20X-1	150	174.20	182.04	7.84
20X-2	150	175.70	183.54	7.84
20X-3	150	177.20	185.04	7.84
20X-4	69	178.70	186.54	7.84
20X-CC	13	179.39	187.23	7.84
21X-1	150	183.80	191.64	7.84
21X-2	150	185.30	193.14	7.84
21X-3	150	186.80	194.64	7.84
21X-4	150	188.30	196.14	7.84
21X-5	150	189.80	197.64	7.84
21X-6	150	191.30	199.14	7.84
21X-7	45	192.80	200.64	7.84
21X-CC	39	193.25	201.09	7.84
22X-1	150	193.40	201.24	7.84
22X-2	150	194.90	202.74	7.84
22X-3	150	196.40	204.24	7.84
22X-4	150	197.90	205.74	7.84
22X-5	150	199.40	207.24	7.84
22X-6	150	200.90	208.74	7.84
22X-7	46	202.40	210.24	7.84
22X-CC	38	202.86	210.70	7.84
23X-1	150	203.00	210.84	7.84
23X-2	150	204.50	212.34	7.84
23X-3	150	206.00	213.84	7.84
23X-4	150	207.50	215.34	7.84
23X-5	150	209.00	216.84	7.84
23X-6	150	210.50	218.34	7.84
23X-7	50	212.00	219.84	7.84
23X-CC	45	212.50	220.34	7.84
24X-1	150	212.60	220.44	7.84
24X-2	150	214.10	221.94	7.84

Table 2 (continued).

Core, section	Length (cm)	Depth (mbsf)	Depth (mcd)	Offset (mcd – mbsf)
24X-3	150	215.60	223.44	7.84
24X-4	150	217.10	224.94	7.84
24X-5	33	218.60	226.44	7.84
24X-CC	14	218.93	226.77	7.84
25X-1	150	222.20	230.04	7.84
25X-2	150	223.70	231.54	7.84
25X-3	150	225.20	233.04	7.84
25X-4	150	226.70	234.54	7.84
25X-5	150	228.20	236.04	7.84
25X-6	150	229.70	237.54	7.84
25X-7	48	231.20	239.04	7.84
25X-CC	26	231.68	239.52	7.84
26X-1	150	231.80	239.64	7.84
26X-2	150	233.30	241.14	7.84
26X-3	150	234.80	242.64	7.84
26X-4	150	236.30	244.14	7.84
26X-5	150	237.80	245.64	7.84
26X-6	150	239.30	247.14	7.84
26X-7	21	240.80	248.64	7.84
26X-CC	32	241.01	248.85	7.84
27X-1	150	241.50	249.34	7.84
27X-2	150	243.00	250.84	7.84
27X-3	150	244.50	252.34	7.84
27X-4	150	246.00	253.84	7.84
27X-5	150	247.50	255.34	7.84
27X-6	69	249.00	256.84	7.84
27X-CC	26	249.69	257.53	7.84
28X-1	150	251.10	258.94	7.84
28X-2	150	252.60	260.44	7.84
28X-3	150	254.10	261.94	7.84
28X-4	150	255.60	263.44	7.84
28X-5	98	257.10	264.94	7.84
28X-CC	37	258.08	265.92	7.84
29X-1	150	260.70	268.54	7.84
29X-2	150	262.20	270.04	7.84
29X-3	150	263.70	271.54	7.84
29X-4	150	265.20	273.04	7.84
29X-5	150	266.70	274.54	7.84
29X-6	113	268.20	276.04	7.84
29X-CC	38	269.33	277.17	7.84
30X-1	150	270.30	278.14	7.84
30X-2	150	271.80	279.64	7.84
30X-3	150	273.30	281.14	7.84
30X-4	150	274.80	282.64	7.84
30X-5	150	276.30	284.14	7.84
30X-6	99	277.80	285.64	7.84
30X-CC	35	278.79	286.63	7.84
31X-1	150	280.00	287.84	7.84
31X-2	150	281.50	289.34	7.84
31X-3	150	283.00	290.84	7.84
31X-4	150	284.50	292.34	7.84
31X-5	150	286.00	293.84	7.84
31X-6	150	287.50	295.34	7.84
31X-7	32	289.00	296.84	7.84
31X-CC	38	289.32	297.16	7.84
32X-1	150	289.60	297.44	7.84
32X-2	150	291.10	298.94	7.84
32X-3	150	292.60	300.44	7.84
32X-4	150	294.10	301.94	7.84
32X-5	150	295.60	303.44	7.84
32X-6	150	297.10	304.94	7.84
32X-7	42	298.60	306.44	7.84
32X-CC	39	299.02	306.86	7.84
33X-1	150	299.20	307.04	7.84
33X-2	150	300.70	308.54	7.84
33X-3	150	302.20	310.04	7.84
33X-4	150	303.70	311.54	7.84
33X-5	150	305.20	313.04	7.84
33X-6	150	306.70	314.54	7.84
33X-CC	32	308.20	316.04	7.84
34X-1	150	308.80	316.64	7.84
34X-2	150	310.30	318.14	7.84
34X-3	150	311.80	319.64	7.84
34X-4	150	313.30	321.14	7.84
34X-5	150	314.80	322.64	7.84
34X-6	39	316.30	324.14	7.84
34X-CC	34	316.69	324.53	7.84
35X-1	150	318.50	326.34	7.84
35X-2	150	320.00	327.84	7.84
35X-3	150	321.50	329.34	7.84
35X-4	150	323.00	330.84	7.84
35X-5	150	324.50	332.34	7.84
35X-6	150	326.00	333.84	7.84
35X-7	44	327.50	335.34	7.84
35X-CC	33	327.94	335.78	7.84
36X-1	150	328.10	335.94	7.84
36X-2	150	329.60	337.44	7.84
36X-3	150	331.10	338.94	7.84
36X-4	150	332.60	340.44	7.84
36X-5	150	334.10	341.94	7.84
36X-6	150	335.60	343.44	7.84
36X-7	46	337.10	344.94	7.84
36X-CC	40	337.56	345.40	7.84
37X-1	150	337.70	345.54	7.84
37X-2	150	339.20	347.04	7.84
37X-3	150	340.70	348.54	7.84
37X-4	150	342.20	350.04	7.84
37X-5	150	343.70	351.54	7.84
37X-6	150	345.20	353.04	7.84
37X-7	43	346.70	354.54	7.84
37X-CC	38	347.13	354.97	7.84
38X-1	150	347.30	355.14	7.84
38X-2	150	348.80	356.64	7.84
38X-3	150	350.30	358.14	7.84
38X-4	150	351.80	359.64	7.84
38X-5	150	353.30	361.14	7.84
38X-6	150	354.80	362.64	7.84
38X-7	46	356.30	364.14	7.84
38X-CC	35	356.76	364.60	7.84
39X-1	150	356.90	364.74	7.84
39X-2	150	358.40	366.24	7.84
39X-3	150	359.90	367.74	7.84
39X-4	150	361.40	369.24	7.84
39X-5	150	362.90	370.74	7.84
39X-6	150	364.40	372.24	7.84
39X-CC	38	365.90	373.74	7.84
40X-1	150	366.50	374.34	7.84
40X-2	150	368.00	375.84	7.84
40X-3	150	369.50	377.34	7.84
40X-4	150	371.00	378.84	7.84
40X-5	150	372.50	380.34	7.84
40X-6	150	374.00	381.84	7.84
40X-7	54	375.50	383.34	7.84
40X-CC	36	376.04	383.88	7.84
41X-1	150	375.70	383.54	7.84
41X-2	150	377.20	385.04	7.84
41X-3	150	378.70	386.54	7.84
41X-4	150	380.20	388.04	7.84
41X-5	150	381.70	389.54	7.84
41X-6	150	383.20	391.04	7.84
41X-7	49	384.70	392.54	7.84
41X-CC	41	385.19	393.03	7.84
42X-1	150	385.50	393.34	7.84
42X-2	150	387.00	394.84	7.84
42X-3	150	388.50	396.34	7.84
42X-4	150	390.00	397.84	7.84
42X-5	150	391.50	399.34	7.84
42X-6	150	393.00	400.84	7.84
42X-7	51	394.50	402.34	7.84
42X-CC	40	395.01	402.85	7.84
43X-1	150	395.30	403.14	7.84
43X-2	150	396.80	404.64	7.84
43X-3	150	398.30	406.14	7.84
43X-4	150	399.80	407.64	7.84
43X-5	150	401.30	409.14	7.84
43X-6	150	402.80	410.64	7.84
43X-7	54	404.30	412.14	7.84
43X-CC	39	404.84	412.68	7.84
44X-1	150	405.00	412.84	7.84
44X-2	150	406.50	414.34	7.84
44X-3	150	408.00	415.84	7.84
44X-4	150	409.50	417.34	7.84
44X-5	150	411.00	418.84	7.84
44X-6	150	412.50	420.34	7.84
44X-7	55	414.00	421.84	7.84
44X-CC	48	414.55	422.39	7.84
45X-1	150	414.70	422.54	7.84
45X-2	150	416.20	424.04	7.84
45X-3	150	417.70	425.54	7.84
45X-4	150	419.20	427.04	7.84
45X-5	150	420.70	428.54	7.84
45X-6	150	422.20	430.04	7.84
45X-7	18	423.70	431.54	7.84
45X-CC	35	423.88	431.72	7.84
46X-1	150	424.40	432.24	7.84
46X-2	150	425.90	433.74	7.84
46X-3	150	427.40	435.24	7.84
46X-4	150	428.90	436.74	7.84
46X-5	150	430.40	438.24	7.84
46X-6	150	431.90	439.74	7.84
46X-7	53	433.40	441.24	7.84
46X-CC	38	433.93	441.77	7.84
47X-1	150	434.00	441.84	7.84
47X-2	150	435.50	443.34	7.84
47X-3	150	437.00	444.84	7.84
47X-4	150	438.50	446.34	7.84
47X-5	150	440.00	447.84	7.84
47X-6	150	441.50	449.34	7.84

Table 2 (continued).

Core, section	Length (cm)	Depth (mbsf)	Depth (mcd)	Offset (mcd – mbsf)
47X-7	39	443.004	50.84	7.84
47X-CC	49	443.39	451.23	7.84
48X-1	150	443.60	451.44	7.84
48X-2	150	445.10	452.94	7.84
48X-3	150	446.60	454.44	7.84
48X-4	150	448.10	455.94	7.84
48X-5	150	449.60	457.44	7.84
48X-6	150	451.10	458.94	7.84
48X-7	47	452.60	460.44	7.84
48X-CC	36	453.07	460.91	7.84
49X-1	150	453.20	461.04	7.84
49X-2	150	454.70	462.54	7.84
49X-3	150	456.20	464.04	7.84
49X-4	150	457.70	465.54	7.84
49X-5	150	459.20	467.04	7.84
49X-6	137	460.70	468.54	7.84
49X-CC	41	462.07	469.91	7.84
50X-1	150	462.70	470.54	7.84
50X-2	150	464.20	472.04	7.84
50X-3	150	465.70	473.54	7.84
50X-4	150	467.20	475.04	7.84
50X-5	150	468.70	476.54	7.84
50X-6	150	470.20	478.04	7.84
50X-7	57	471.70	479.54	7.84
50X-CC	35	472.27	480.11	7.84
51X-1	150	472.30	480.14	7.84
51X-2	150	473.80	481.64	7.84
51X-3	150	475.30	483.14	7.84
51X-4	150	476.80	484.64	7.84
51X-5	150	478.30	486.14	7.84
51X-6	150	479.80	487.64	7.84
51X-7	27	481.30	489.14	7.84
51X-CC	30	481.57	489.41	7.84
52X-1	150	481.90	489.74	7.84
52X-2	150	483.40	491.24	7.84
52X-3	150	484.90	492.74	7.84
52X-4	150	486.40	494.24	7.84
52X-5	150	487.90	495.74	7.84
52X-6	150	489.40	497.24	7.84
52X-7	45	490.90	498.74	7.84
52X-CC	39	491.35	499.19	7.84
53X-1	150	491.50	499.34	7.84
53X-2	150	493.00	500.84	7.84
53X-3	150	494.50	502.34	7.84
53X-4	150	496.00	503.84	7.84
53X-5	150	497.50	505.34	7.84
53X-6	150	499.00	506.84	7.84
53X-7	44	500.50	508.34	7.84
53X-CC	37	500.94	508.78	7.84
54X-1	150	501.10	508.94	7.84
54X-2	150	502.60	510.44	7.84
54X-3	150	504.10	511.94	7.84
54X-4	150	505.60	513.44	7.84
54X-5	150	507.10	514.94	7.84
54X-6	150	508.60	516.44	7.84
54X-7	44	510.10	517.94	7.84
54X-CC	43	510.54	518.38	7.8
55X-1	150	510.70	518.54	7.84
55X-2	150	512.20	520.04	7.84
55x-3	150	513.70	521.54	7.84
55X-4	150	515.20	523.04	7.84
55X-5	150	516.70	524.54	7.84
55X-6	150	518.20	526.04	7.84
55X-7	41	519.70	527.54	7.84
55X-CC	40	520.11	527.95	7.84
56X-1	150	520.40	528.24	7.84
56X-2	150	521.90	529.74	7.84
56X-3	150	523.40	531.24	7.84
56X-4	150	524.90	532.74	7.84
56X-5	150	526.40	534.24	7.84
56X-6	144	527.90	535.74	7.84
56X-CC	22	529.34	537.18	7.84
57X-1	150	530.00	537.84	7.84
57X-2	150	531.50	539.34	7.84
57X-3	144	533.00	540.84	7.84
57X-CC	55	534.44	542.28	7.84
58X-1	150	539.60	547.44	7.84
58X-2	132	541.10	548.94	7.84
58X-CC	31	542.42	550.26	7.84
59X-1	150	549.20	557.04	7.84
59X-2	150	550.70	558.54	7.84
59X-3	92	552.20	560.04	7.84
59X-4	37	553.12	560.96	7.84
59X-CC	35	553.49	561.33	7.84
60X-1	150	558.90	566.74	7.84
60X-2	150	560.40	568.24	7.84
60X-3	150	561.90	569.74	7.84
60X-4	150	563.40	571.24	7.84
60X-5	150	564.90	572.74	7.84
60X-6	66	566.40	574.24	7.84
60X-CC	24	567.06	574.90	7.84
61X-1	70	568.60	576.44	7.84
61X-2	138	569.30	577.14	7.84
61X-3	150	570.68	578.52	7.84
61X-4	150	572.18	580.02	7.84
61X-CC	44	573.68	581.52	7.84
62X-1	150	578.20	586.04	7.84
62X-CC	20	579.70	587.54	7.84
162-985B-				
1H-1	150	0.00	0.00	0.00
1H-2	150	1.50	1.50	0.00
1H-3	28	3.00	3.00	0.00
1H-CC	14	3.28	3.28	0.00
2H-1	150	3.40	5.24	1.84
2H-2	150	4.90	6.74	1.84
2H-3	150	6.40	8.24	1.84
2H-4	150	7.90	9.74	1.84
2H-5	150	9.40	11.24	1.84
2H-6	150	10.90	12.74	1.84
2H-7	53	12.40	14.24	1.84
2H-CC	23	12.93	14.77	1.84
3H-1	150	12.90	14.74	1.84
3H-2	150	14.40	16.24	1.84
3H-3	150	15.90	17.74	1.84
3H-4	150	17.40	19.24	1.84
3H-5	150	18.90	20.74	1.84
3H-6	150	20.40	22.24	1.84
3H-7	53	21.90	23.74	1.84
3H-CC	26	22.43	24.27	1.84
4H-1	150	22.40	24.56	2.16
4H-2	150	23.90	26.06	2.16
4H-3	150	25.40	27.56	2.16
4H-4	150	26.90	29.06	2.16
4H-5	150	28.40	30.56	2.16
4H-6	150	29.90	32.06	2.16
4H-CC	36	31.40	33.56	2.16
5H-1	150	31.90	34.58	2.68
5H-2	150	33.40	36.08	2.68
5H-3	150	34.90	37.58	2.68
5H-4	150	36.40	39.08	2.68
5H-5	150	37.90	40.58	2.68
5H-6	150	39.40	42.08	2.68
5H-7	61	40.90	43.58	2.68
5H-CC	18	41.51	44.19	2.68
6H-1	150	41.40	44.81	3.41
6H-2	150	42.90	46.31	3.41
6H-3	150	44.40	47.81	3.41
6H-4	150	45.90	49.31	3.41
6H-5	150	47.40	50.81	3.41
6H-6	150	48.90	52.31	3.41
6H-7	42	50.40	53.81	3.41
6H-CC	18	50.82	54.23	3.41
7H-1	150	50.90	54.85	3.95
7H-2	150	52.40	56.35	3.95
7H-3	150	53.90	57.85	3.95
7H-4	150	55.40	59.35	3.95
7H-5	150	56.90	60.85	3.95
7H-6	150	58.40	62.35	3.95
7H-7	60	59.90	63.85	3.95
7H-CC	25	60.50	64.45	3.95
8H-1	150	60.40	65.83	5.43
8H-2	150	61.90	67.33	5.43
8H-3	103	63.40	68.83	5.43
8H-4	59	64.43	69.86	5.43
8H-5	130	65.02	70.45	5.43
8H-6	150	66.32	71.75	5.43
8H-7	150	67.82	73.25	5.43
8H-CC	50	69.32	74.75	5.43
9H-1	150	69.90	75.16	5.26
9H-2	150	71.40	76.66	5.26
9H-3	150	72.90	78.16	5.26
9H-4	150	74.40	79.66	5.26
9H-5	150	75.90	81.16	5.26
9H-6	150	77.40	82.66	5.26
9H-7	62	78.90	84.16	5.26
9H-CC	20	79.52	84.78	5.26
10H-1	150	79.40	86.05	6.65
10H-2	150	80.90	87.55	6.65
10H-3	150	82.40	89.05	6.65
10H-4	150	83.90	90.55	6.65
10H-5	150	85.40	92.05	6.65
10H-6	150	86.90	93.55	6.65
10H-7	43	88.40	95.05	6.65
10H-CC	24	88.83	95.48	6.65
11H-1	150	88.90	96.01	7.11
11H-2	150	90.40	97.51	7.11
11H-3	150	91.90	99.01	7.11

Table 2 (continued).

Core, section	Length (cm)	Depth (mbsf)	Depth (mcd)	Offset (mcd – mbsf)
11H-4	150	93.40	100.51	7.11
11H-5	150	94.90	102.01	7.11
11H-6	150	96.40	103.51	7.11
11H-7	61	97.90	105.01	7.11
11H-CC	21	98.51	105.62	7.11
12H-1	150	98.40	105.41	7.01
12H-2	150	99.90	106.91	7.01
12H-3	150	101.40	108.41	7.01
12H-4	150	102.90	109.91	7.01
12H-5	150	104.40	111.41	7.01
12H-6	150	105.90	112.91	7.01
12H-7	57	107.40	114.41	7.01
12H-CC	9	107.97	114.98	7.01
13H-1	150	107.90	116.54	8.64
13H-2	150	109.40	118.04	8.64
13H-3	150	110.90	119.54	8.64
13H-4	150	112.40	121.04	8.64
13H-5	150	113.90	122.54	8.64
13H-6	150	115.40	124.04	8.64
13H-7	63	116.90	125.54	8.64
13H-CC	24	117.53	126.17	8.64
14H-1	150	117.40	126.73	9.33
14H-2	150	118.90	128.23	9.33
14H-3	150	120.40	129.73	9.33
14H-4	150	121.90	131.23	9.33
14H-5	150	123.40	132.73	9.33
14H-6	150	124.90	134.23	9.33
14H-7	33	126.40	135.73	9.33
14H-CC	28	126.73	136.06	9.33

Note: Depths are from the top of each section.

quence (0–70 mbsf) and consist primarily of angular to subrounded igneous or metamorphic rock fragments.

The lithostratigraphic units and subunits at Site 985 are defined on the basis of data obtained from seven sources: (1) visual core descriptions, (2) smear slide examination, (3) bulk calcium carbonate measurements, (4) spectral reflectance measurements, (5) magnetic susceptibility measurements, (6) natural gamma-ray measurements, and (7) X-ray diffraction analysis of bulk sediments. These data allow us to delineate five lithostratigraphic units, the fourth of which is subdivided into three subunits. Lithostratigraphic unit boundaries occur at 17.2, 99.2, 155.2, and 465.0 mbsf. Subunit boundaries within Unit IV occur at 241.5 and 289.6 mbsf. The lithologic descriptions of these units and subunits follow.

Description of Lithostratigraphic Units

Unit I

Interval:
Cores 162-985A-1H through 2H
Cores 162-985B-1H through 2H
Age: Holocene to late Pleistocene
Depth: 0 to 17.2 mbsf

Unit I is defined largely on the basis of relatively abundant biocarbonates and spectral reflectance values between 10% and 20% for the 650–700-nm range (Fig. 6). These sediments contain up to 30% carbonate, but average 12.1% ± 10.0% carbonate (see "Organic Geochemistry" section, this chapter). Carbonate content generally decreases with increasing depth. The sediments of Unit I are composed of interbedded layers of gray clayey nannofossil ooze with foraminifers, dark gray nannofossil clay with silt, dark gray silty clay with nannofossils, brown and dark grayish brown clay with silt, and very dark gray to dark grayish brown silty clays. The color changes are gradational and cyclic throughout the unit. Bioturbation is slight to moderate in intensity. Five dropstones greater than 1.0 cm were recovered from the darker sediment layers of this Unit (Table 4).

Pyrite is present in small quantities in concretions or pods, and is discernible by XRD analysis. XRD analysis also reveals that quartz, plagioclase, pyroxene, and clay minerals are important components of the bulk sediments in this interval. Smear slide analysis, which also detects the presence of opaque minerals, is consistent with bulk sediment XRD. Several thin (<1.0 cm) ash layers, ash pods, and a single ash layer 2.0 cm thick are present near the base of the unit. All ash layers >1.0 cm thick are listed in Table 5. Slight alteration of the colorless volcanic shards in these ashes is suggested by the presence of zeolites and ash-derived clays in smear slides. The 2.0-cm ash layer has a sharp basal contact and gradational upper contacts.

Unit II

Interval:
Sections 162-985A-3H-1 through 11H-4
Sections 162-985B-3H-1, 0 cm, through 12H-2, 105 cm
Age: late Pleistocene to early Pliocene
Depth: 17.2 to 99.2 mbsf

Unit II is defined, in part, by the diminished presence of biocarbonate which occurs as a variable sedimentary component, averaging 6.9%. These sediments are mainly grayish brown to dark greenish brown and dark gray to very dark greenish gray silty clay and clay with silt. Biocarbonate-bearing sediments consist of gray to dark greenish gray clayey nannofossil ooze, silty clay with nannofossils, and nannofossil clay. Bioturbation is slight to moderate, and color changes are gradational. Centimeter-scale color variations in the form of faint grayish green color banding occurs throughout. XRD and smear slide analyses both indicate higher abundance of quartz, plagioclase, and pyroxene within Unit II relative to the underlying sediments. Spectral reflectance values in Unit II are lower than in Unit I, averaging 10% ± 5% throughout the interval. Both reflectance values and natural gamma-ray counts decrease noticeably downsection and define the boundary with the underlying unit.

Several other lithologic components are found within this unit. The earliest appearance of dropstones (>1.0 cm) at Site 985 occurs within Unit II in Section 985A-7H-5 at 125 cm (62.45 mbsf), and in Section 985B-7H-6 at 9 cm (58.49 mbsf). The dropstones of Units I and II were recovered from darker sediment layers. Centimeter-scale, indurated yellowish orange color bands, composed of clay with inorganic calcite, are also present.

Within Unit II, 16 gray to black ash layers >1.0 cm thick with sharp basal contacts and gradational upper boundaries were identified in Hole 985A (e.g., Fig. 7). In addition, 17 ash layers >1.0 cm were observed in Hole 985B (Table 5). These ashes average 5.8 and 5.9 cm in thickness, respectively. Because the ash layers in Hole 985A and 985B do not correspond precisely in depth, there must be a minimum of 24 ash layers >1.0 cm thick in Unit II (Table 5; Fig. 8). More detailed analytical studies of the dark layers of Unit II will be necessary to distinguish dark pyritic layers from ash layers in these sediments. Disseminated pyrite, pyrite-filled burrows, and discrete pyrite layers are scattered throughout.

Unit III

Interval:
Sections 162-985A-11H-5 through 17H-CC
Sections 162-985B-12H-2, 105 cm, through 14H-CC (base of hole)
Age: early Pliocene to late Miocene
Depth: 99.2 to 155.2 mbsf

Unit III is characterized by the occurrence of clay with silt, and the absence of biogenic sediments. Low-amplitude variations in spectral reflectance, with mean values of 8% ± 2%, are characteristic, along with increases in natural gamma-ray counts and in the number and amplitude magnetic susceptibility spikes. In Unit III, isolated spikes of inorganic carbonate are superimposed on a carbonate-free background (see "Organic Geochemistry" section, this chapter).

The main sediment components of Unit III display much less variation in color than those of the preceding units. They are composed

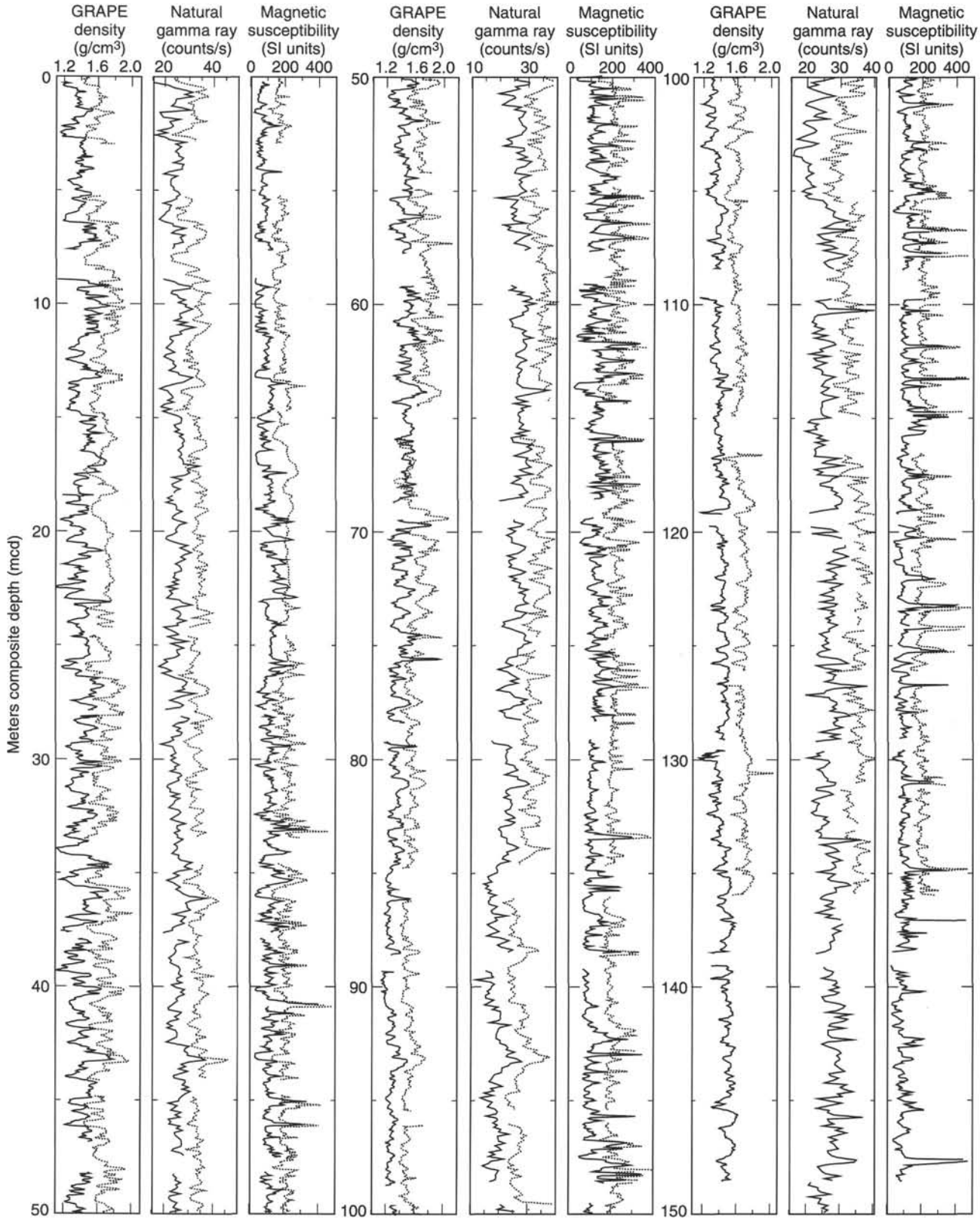

Figure 3. GRAPE density, natural gamma radiation, and magnetic susceptibility data from Site 985 on the mcd (meters composite depth) scale. Line for Hole 985B (dotted) has been horizontally offset from line for Hole 985A (solid) for better display; therefore, values on horizontal scale are the true values only for Hole 985A. (See also back pocket.)

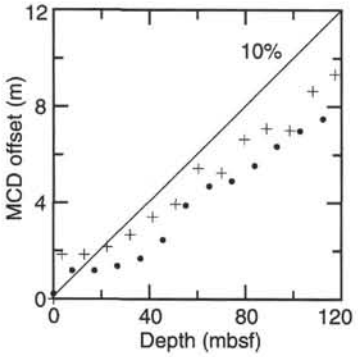

Figure 4. Depth offsets of the Site 985 mcd scale relative to mbsf depth, indicating the "growth" of the composite depth scale. Solid circles = Hole 985A; crosses = Hole 985B.

almost entirely of dark greenish gray and very dark greenish gray clay with silt. XRD analysis of the bulk sediments reveals that plagioclase, quartz, and pyroxene are less abundant than in Units I and II. The sediments are slightly to moderately bioturbated and color mottling is present. The interbedding of these two lithologies gives the sediments a more pronounced greenish color banding than was present in Unit II.

Several types of concretions and discrete lithologic layers occur in Unit III. Indurated yellowish orange color bands, less common than those of Unit II, are present at the top of Unit III (Core 162-985A-12H, 102.7–112.3 mbsf). Yellowish brown concretions are first observed in Unit IV in the interval 162-985A-12H-3, 101–104 cm, at 106.71–106.74 mbsf (Fig. 9). XRD analysis reveals at least some of these concretions are composed of fluorapatite, and may be similar in composition to the yellowish orange layers found at shallower depths. Seven ash layers, averaging 4.1 cm in thickness, were observed in Hole 985A, and 14 ash layers, averaging 2.8 cm in thickness, were observed in Hole 985B (Table 5). As in Unit II, pyrite concretions and black bands, which may contain pyrite and/or ash, are scattered throughout. The presence of zeolites and pyrites in association with ash layers suggests that some of the ash in Unit III is slightly altered.

Unit IV

Interval: Sections 162-985A-18X-1, 0 cm, through 50X-2, 30 cm
Age: late Miocene to late Oligocene(?)
Depth: 155.2 to 465 mbsf

The sediments of Unit IV comprise the bulk of the sedimentary sequence at Site 985. These sediments are distinguished from those of Units III and V by the switch from a lithology above and below Unit IV in which silty clay and clay with silt dominates, to one in which clay with silt is present but indurated clay is dominant. Shipboard bulk mineral XRD analyses reveal that these clays are composed of smectite, chlorite, kaolinite, micas, and mixed layer clays. XRD-estimated plagioclase and quartz content in Unit IV is similar to that of Unit III, but pyroxene is absent from Unit IV sediments. Sediment coloration in Unit IV ranges from gray to very dark greenish gray in the clay and from dark greenish gray to dark grayish brown in the clay with silt. Dark greenish color banding is present in Unit IV, but is not as pronounced as in Unit III. The sediments are moderately bioturbated and color mottling is present. Thirteen discrete ash layers, averaging 4.1 cm in thickness, were observed in Unit IV (Table 5). Disseminated ash is present as a lithologic component of the bulk sediments.

Other characteristics of this lithofacies include very low magnetic susceptibility values and the absence of biocarbonates, although isolated inorganic carbonate layers occur. Yellowish orange layers are found in fewer numbers within Unit IV than in Units III and II. Yellowish brown concretions, some of which contain fluorapatite, are also present in Unit IV sediments. The presence of Sr isotopes in fluorapatite may provide age constraints in the deeper sediments at Site 985 using the Sr^{87}/Sr^{86} dating method (e.g., Elderfield, 1986; Smalley et al., 1989). Two lithified layers in Unit IV that may act as barriers to the diffusion of interstitial waters are noteworthy (see "Inorganic Geochemistry" section, this chapter). These layers occur at intervals 162-985A-32X-3, 101–131 cm (293.61–293.91 mbsf) and 985A-44X-6, 13–23 cm (412.63–412.73 mbsf). XRD analysis of the upper layer indicates that it is composed of poorly crystallized carbonate. The lower layer was not sampled for XRD analysis. These layers yield high velocity measurements (see "Physical Properties" section, this chapter) and bound sediments with interstitial waters that have low chloride, sodium, and salinity content (see "Inorganic Geochemistry" section, this chapter).

Unit IV can be subdivided into three distinct subunits (Table 6; Fig. 6). Subunit IVA (155.2–241.5 mbsf) is distinguished from the underlying Unit IV sediments by higher magnetic susceptibility and natural gamma-ray values, and by the absence of biosilica. Smear slide analysis of several ash layers within Subunit IVA reveals an increased zeolite content, suggesting greater alteration than shallower ash layers at Site 985. With the exception of discrete inorganic carbonate layers and concretions, these sediments are essentially barren of carbonate (see "Organic Geochemistry" section, this chapter).

Subunit IVB (241.5–289.6 mbsf) contains interbedded layers of clay, clay with ash, and clay with biosilica. Zeolite is present in Subunit IVB in quantities lower than in overlying Subunit IVA. The presence of biosilica is a defining characteristic for this subunit, which like Subunit IVA, is essentially barren of carbonate. Smear slide analysis indicates up to 15% biosilica in some layers, consisting of diatoms, sponge spicules, radiolarians, and silicoflagellates. This lithostratigraphic subunit exhibits several other differences relative to the sediments above and below. Interstitial water analysis indicates an increase in dissolved silica within this layer (see "Inorganic Geochemistry" section, this chapter). Also, physical properties measurements indicate greater water content and void space ratios within Subunit IVB (see "Physical Properties" section, this chapter).

Table 3. Site 985 splice tie points.

Hole, core, section (cm)	Depth (mbsf)	Depth (mcd)		Hole, core, section (cm)	Depth (mbsf)	Depth (mcd)
162-985-				162-985-		
B-1H-2, 8	1.58	1.58	tie to	A-1H-1, 136	1.36	1.58
A-1H-5, 86	6.86	7.08	tie to	B-2H-2, 35	5.24	7.08
B-2H-5, 89	10.28	12.12	tie to	A-2H-3, 25	10.95	12.12
A-2H-7, 55	17.25	18.42	tie to	A-3H-1, 4	17.24	18.41
A-3H-6, 131	26.01	27.18	tie to	B-4H-2, 113	25.02	27.18
B-4H-3, 107	26.47	28.63	tie to	A-4H-1, 56	27.26	28.63
A-4H-6, 89	35.09	36.46	tie to	B-5H-2, 38	33.78	36.46
B-5H-3, 113	36.03	38.71	tie to	A-5H-1, 83	37.03	38.71
A-5H-6, 124	44.94	46.62	tie to	B-6H-2, 31	43.21	46.62
B-6H-4, 70	46.60	50.01	tie to	A-6H-2, 34	47.54	50.01
A-6H-6, 23	53.42	55.89	tie to	B-7H-1, 104	51.94	55.89
B-7H-5, 56	57.46	61.41	tie to	A-7H-2, 80	57.50	61.41
A-7H-7, 22	64.42	68.33	tie to	B-8H-2, 100	62.90	68.33
B-8H-7, 70	68.52	73.95	tie to	A-8H-4, 4	69.24	73.95
A-8H-6, 118	73.38	78.09	tie to	B-9H-2, 143	72.83	78.09
B-9H-5, 22	76.12	81.38	tie to	A-9H-2, 76	76.46	81.38
A-9H-6, 115	82.85	87.77	tie to	B-10H-2, 22	81.12	87.77
B-10H-6, 134	88.24	94.89	tie to	A-10H-4, 116	89.35	94.89
A-10H-6, 4	91.24	96.78	tie to	B-11H-1, 77	89.67	96.78
B-11H-5, 65	95.54	102.65	tie to	A-11H-3, 11	96.31	102.65
A-11H-6, 52	101.22	107.56	tie to	B-12H-2, 65	100.55	107.56
B-12H-7, 26	107.66	114.67	tie to	A-12H-4, 50	107.69	114.67
A-12H-6, 145	111.65	118.63	tie to	B-13H-2, 59	109.99	118.63
B-13H-7, 5	116.94	125.58	tie to	A-13H-4, 139	118.09	125.58
A-13H-6, 28	119.98	127.47	tie to	B-14H-4, 74	118.14	127.47
B-14H-6, 29	125.19	134.52	tie to	A-14H-4, 88	126.68	134.52
A-62X-1, 143	579.63	587.47				

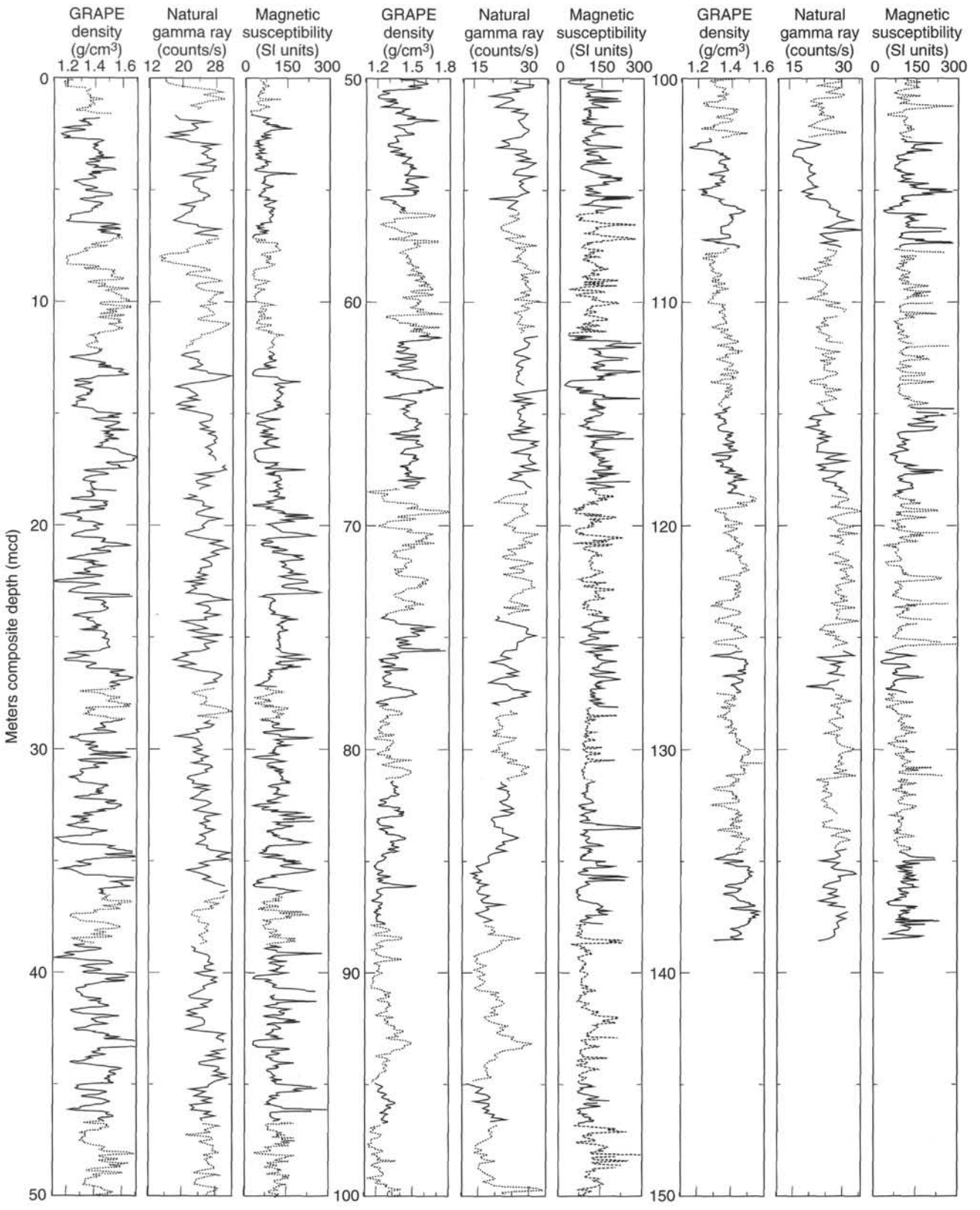

Figure 5. Spliced records of GRAPE density, natural gamma radiation, and magnetic susceptibility from Site 985. Tie points for forming the splice are given in Table 3. Holes are 985A (solid line) and 985B (dotted line).

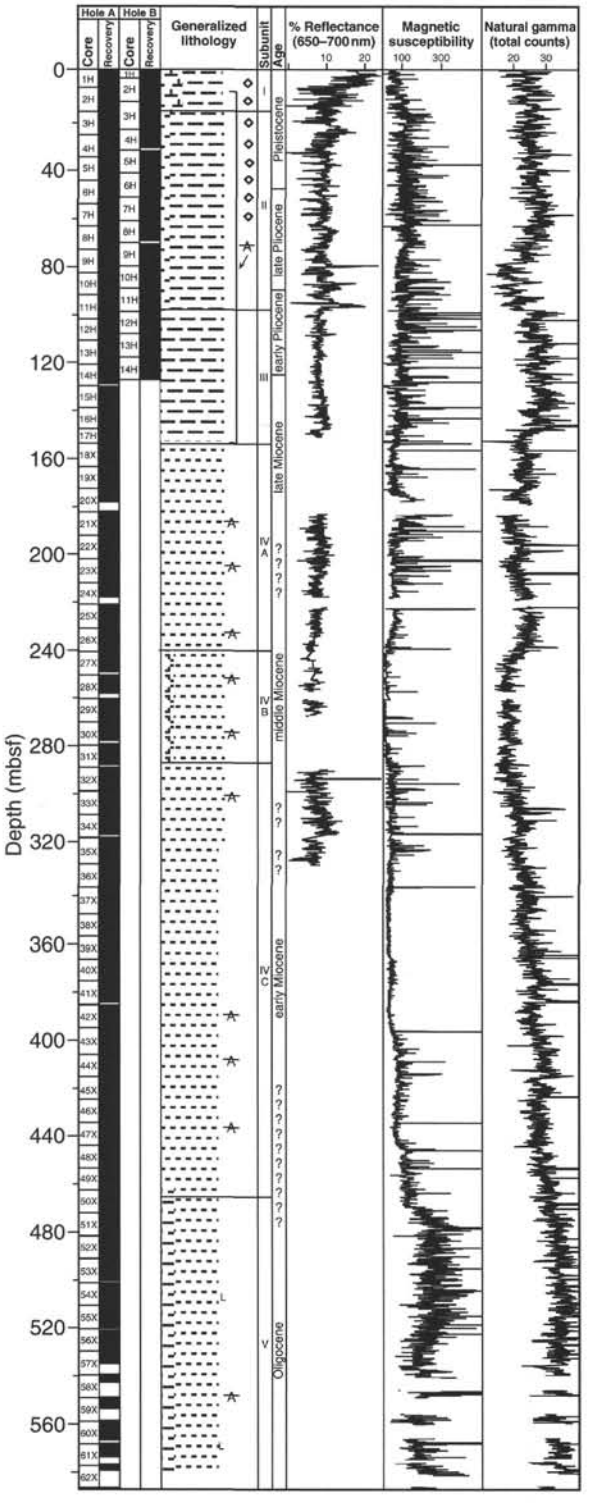

Figure 6. Core recovery, lithostratigraphy, age, spectral reflectance (red band), magnetic susceptibility, and natural gamma radiation of sediments recovered in Holes 985A and 985B. Cores containing ash layers (crossed A's, including bracketed area), dropstones (open diamonds), and limestone layers (letter "L") are shown in column adjacent to the lithostratigraphy. Spectral reflectance, magnetic susceptibility, and natural gamma radiation records are from Hole 985A. (Key to symbols used in the "Generalized Lithology" column can be found in fig. 4, "Explanatory Notes" chapter, this volume.)

Table 4. Summary table of dropstones greater than 1 cm in size found at Site 985.

Core, section, interval top (cm)	Depth (mbsf)	Size (cm)	Composition	Shape
162-985A-				
1H-5, 101	7.01	3.5	Sandstone	Subangular
3H-4, 30	22.00	3.0	Indurated ash	Angular
3H-4, 100	22.70	1.5	Indurated ash	Angular
5H-1, 16	36.36	1.4	Soft siltstone, brown	Subrounded
5H-2, 3	37.73	1.1	Brown siltstone	Subrounded
5H-3, 32	39.52	2.5	Gray-green gabbro	Subrounded
5H-4, 66	41.36	1.3	Buff sandstone	Subangular
7H-4, 32	60.02	1.1	Black crystalline	Subangular
7H-5, 125	62.45	1.3	Buff siltstone	Crumbles
162-985B-				
1H-1, 97	0.97	4.5	Dark granite	Angular
2H-3, 52	6.92	1.6	Black basalt	Angular
1H-CC, 0	3.28	3.0	Diorite	Angular
2H-4, 35	8.25	2.8	Granite	Angular
4H-1, 44	22.84	2.7	Plutonic igneous	Angular
4H-1, 49	22.89	1.1	Basalt	Angular
4H-1, 53	22.93	3.0	Gneiss	Subrounded
4H-2, 71	24.61	1.1	Plutonic igneous	Angular
4H-3, 29	25.69	1.0	Schist	Angular
4H-4, 77	27.67	1.6	Plutonic igneous	Angular
4H-5, 122	29.62	1.8	Plutoinic igneous	Angular
4H-6, 100	30.90	2.0	Siltstone	Subrounded
6H-3, 106	45.46	1.1	Green-gray siltstone	Subrounded
6H-5, 101	48.41	3.5	Gneiss	Subangular
6H-6, 57	49.47	1.5	Pyritic siltstone	Subrounded
7H-2, 122	53.62	1.5	Quartzitic igneous plutonic	Subrounded
7H-3, 54	54.44	2.2	Gray quartzite	Subrounded
7H-3, 100	54.90	1.1	Quartz	Subangular
7H-3, 130	55.20	1.4	Black siltstone	Subrounded
7H-3, 145	55.35	4.3	Orange-brown sandstone	Subrounded
7H-4, 113	56.53	4.7	Quartzitic igneous plutonic	Subrounded
7H-6, 9	58.49	1.0	Quartzitic igneous plutonic	Subangular

Subunit IVC (289.6–465 mbsf) is distinguished from Subunit IVB by the absence of biosilica and by a gradual downsection increase in natural gamma-ray counts. The base of Subunit IVC is defined by a sharp downsection increase in magnetic susceptibility (Fig. 6). Agglutinated foraminifers, which provide the primary shipboard age constraint in the lower section (see "Biostratigraphy" section, this chapter), were observed during visual core description of the sediments of Core 985A-37X (338.7 mbsf) and below in Subunit IVC.

Unit V

Interval: Sections 162-985A-50X-2, 30 cm, through 62X-CC
Age: early Miocene(?) to late Oligocene(?)
Depth: 465.0 to 587.9 mbsf

Unit V comprises the deepest sediments recovered at this site (Hole 985A) and are composed of indurated dark greenish gray to very dark greenish gray clay, olive gray to dark greenish gray silty clay, and very dark greenish gray clay with glauconite and glauconitic clay. These sediments are distinguished from the overlying sediments by a sharp increase in magnetic susceptibility. Smear slide analysis suggests an increase in silt-sized grains and reveals the presence of glauconite in some instances at greater than trace amounts. XRD analyses indicate increases in quartz, mica, and combined chlorite and kaolinite within Unit V. The plagioclase content of Unit V is similar to that of Unit IV.

As in Unit IV, yellowish brown concretions, some of which may be composed of fluorapatite, are present. In addition, two 8–9-cm thick, grayish brown to light gray limestone layers are found at intervals 162-985A-54X-4, 40–49 cm (506.0 mbsf), and 162-985A-61X-4, 122–130 cm (573.4 mbsf). The inorganic carbonates, which occur sporadically and were preferentially sampled, account for the increase in the average carbonate content of these sediments to 14.6% ± 23.8%. Background carbonate composition is similar to that of Unit IV. Once again, pyrite is present as disseminated particles, and as dis-

Table 5. List of the location, and thickness of ash layers >1.0 cm in thickness found in cores from Holes 985A and 985B.

Lithostratigraphic unit	Core, section, interval (cm)	Depth (mbsf)	Layer thickness (cm)
	162-985A-		
I	2H-3, 60–62	11.30	2.0
II	3H-4, 30–40	22.00	10.0
	3H-4, 100–107	22.70	7.0
	4H-3, 37–38	30.07	1.0
	4H-4, 48–49	31.68	1.0
	4H-5, 10–15	32.80	5.0
	4H-5, 97–102	33.67	5.0
	6H-2, 120–125	48.40	5.0
	6H-5, 22–23	51.92	1.0
	7H-4, 69–71	60.39	2.0
	7H-4, 134–138	61.04	4.0
	9H-3, 122–141	78.42	19.0
	9H-5, 54–56	80.74	2.0
	9H-6, 116–117	82.86	1.0
	9H-7, 13–16	83.33	3.0
	9H-CC, 4–7	83.71	3.0
	11H-3, 33–57	96.53	24.0
III	13H-3, 50–52	115.70	2.0
	13H-5, 85–86	119.05	1.0
	14H-2, 39–40	123.19	1.0
	14H-6, 46–49	129.26	3.0
	16H-2, 82–92	143.02	10.0
	17H-2, 88–96	151.28	8.0
	17H-2, 142–147	151.82	5.0
	17H-3, 132–135	153.22	3.0
IVA	21X-4, 67–70	188.97	3.0
	23X-1, 8–13	203.08	5.0
	23X-2, 98–99	205.48	1.0
	23X-7, 22–31	212.22	9.0
IVB	28X-3, 75–85	254.85	10.0
	30X-3, 114–122	274.44	8.0
IVC	42X-2, 53–54	387.53	1.0
	42X-2, 70–72	387.70	2.0
	44X-2, 118–120	407.68	2.0
	47X-5, 33–36	440.33	3.0
	47X-6, 124–126	442.74	2.0
	47X-6, 149–150, to 47X-7, 0–2	442.99	3.0
	47X-7, 12–16	443.12	4.0
V	59X-2, 83–84	551.53	1.0
	162-985B-		
I	2H-5, 123–125	10.63	2.0
II	5H-3, 0–10	34.90	10.0
	5H-7, 47–50	41.37	3.0
	7H-2, 15–17	52.55	2.0
	7H-6, 95–97	59.35	2.0
	7H-CC, 5–10	60.55	5.0
	9H-6, 65–85	78.05	20.0
	10H-2, 72–74	81.62	2.0
	10H-2, 109–110	81.99	1.0
	10H-2, 114–116	82.04	2.0
	10H-4, 141–146	85.31	5.0
	10H-5, 85–87	86.25	2.0
	11H-1, 21–25	89.11	4.0
	11H-1, 87–95	89.77	8.0
	11H-2, 62–67	91.02	5.0
	11H-2, 85–90	91.25	5.0
	11H-3, 15–17	92.05	2.0
	11H-5, 88–111	95.78	23.0
III	12H-1, 134–136	99.74	2.0
	12H-2, 92–94	100.82	2.0
	12H-4, 3–8	102.93	5.0
	12H-4, 57–59	103.47	2.0
	12H-5, 46–48	104.86	2.0
	12H-6, 30–31	106.20	1.0
	12H-6, 63–68	106.53	5.0
	12H-7, 59–63	107.99	4.0
	12H-7, 78–79	108.18	1.0
	13H-2, 127–131	110.67	4.0
	13H-3, 51–53	111.41	2.0
	14H-4, 22–28	122.12	6.0
	14H-3, 144–146	121.84	2.0
	14H-5, 85–86	124.25	1.0

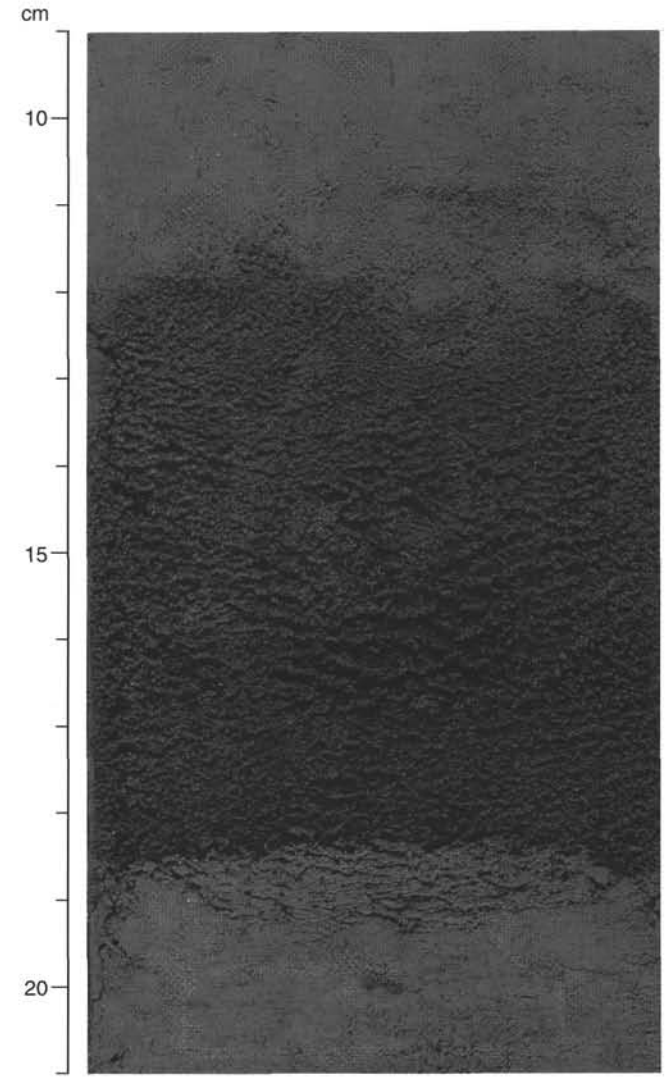

Figure 7. Ash layer with sharp basal and gradual upper contact. Located in Section 162-985A-10H-6, 12–19 cm, within lithostratigraphic Unit II.

crete nodules and concretions. Unit V sediments also contain disseminated, altered ash. A single ash layer 1.0 cm thick was observed in Unit V at interval 162-985A-59X-2, 83–84 cm.

Interpretation

These five lithostratigraphic units record the sedimentary response to climatic and tectonic changes at this site from late Oligocene or early Miocene time to Holocene. Tectonic events that may have influenced sedimentation at Site 985 include (1) seafloor spreading and ridge orientation in the Norwegian-Greenland Sea, (2) changes in the Greenland-Scotland Ridge sill depth (Wright and Miller, 1993), and (3) initiation of the final closure of the Isthmus of Panama (Wolf and Thiede, 1991). Potential climatic events that may have influenced the deposition of these sediments include the transition from relatively ice-free conditions in the Miocene, to weak Northern Hemisphere glaciation, and eventually to strong Northern Hemisphere glaciation from the late Pliocene to Holocene.

Seafloor spreading in the Norwegian-Greenland Sea was underway by Anomaly 24 time (early Eocene), but may have begun as early as Anomaly 29 time (Talwani and Eldholm, 1977; Myhre and

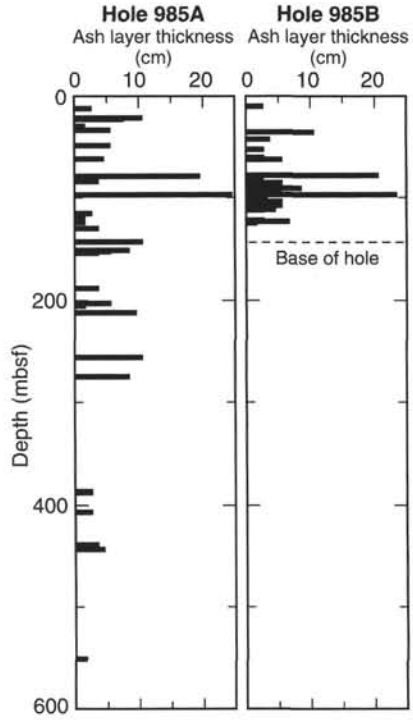

Figure 8. Thickness of ash layers greater than 1 cm plotted against depth at Site 985.

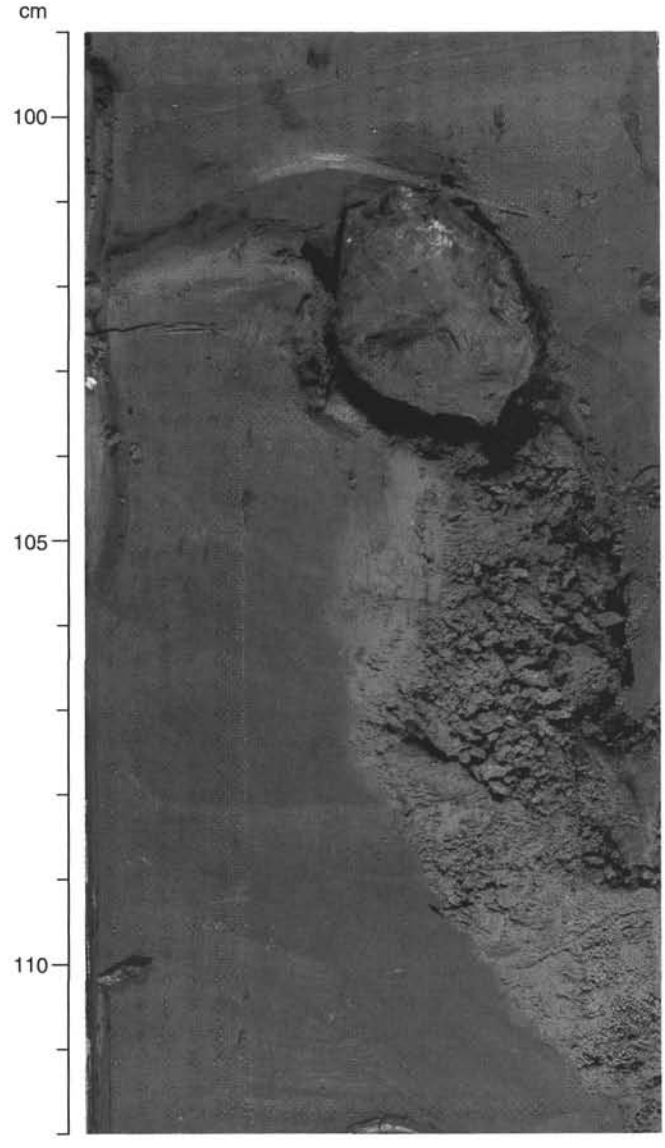

Figure 9. A concretion containing fluorapatite in Section 162-985A-12H-3, 101–104 cm, at 106.71–106.74 mbsf, within lithostratigraphic Unit III.

Thiede, 1995). Unit V sediments are believed to have been deposited during the late Oligocene/early Miocene when the basin was roughly half its modern dimensions and Site 985 was shallower and closer to land. During the deposition of Unit V, the site of active seafloor spreading, the Aegir spreading axis was located to the east of Site 985. The lack of an intervening bathymetric high between Greenland and Site 985 may have allowed for more effective transport of silt-sized continental material to Site 985.

Following Anomaly 7 time in the Oligocene/early Miocene, active spreading shifted from the Aegir spreading axis to the Kolbeinsey spreading axis, which is located to the west of Site 985 (Myhre and Thiede, 1995). This shift in the spreading axis, which occurred during the transition from Unit V to Unit IV, could have decreased the delivery of continentally derived silts to Site 985 by separating the site from Greenland with an intervening ridge. Unit IV sediments, which contain fewer silt-sized particles than Unit V, are thus interpreted to reflect Miocene deposition as the position of Site 985 moved farther from continental sediment source areas and subsided to greater depths.

Although age constraints are relatively weak in Units V and IV, bulk sedimentation rates at Site 985 appear to have remained between 20 and 30 m/m.y. from the Miocene to Holocene (see "Sedimentation Rates" section, this chapter). These sedimentation rates are somewhat higher than at nearby Site 907. It is thus likely that the higher clay content of these Miocene sediments reflect greater clay-fraction sedimentation rates during the Miocene than in the younger sediments at Site 985. The ultimate cause for the greater clay sedimentation rates during the Miocene is unclear.

The low biocarbonate content of the sediments of Units V and IV implies low production and/or enhanced dissolution during the early Miocene and late Oligocene at Site 985. Henrich (1989) reports the presence of a variety of inorganic concretions in sediments of similar age recovered from Site 643 in the Norwegian Sea. These included opal-CT, calcite, rhodochrosite, manganese-siderite, and fluorapatite concretions. We observe fluorapatite concretions and pyrite in the sediments at Site 985. Both of these minerals can form during the degradation of organic matter in carbon-rich sediments, suggesting that there was the potential to dissolve biocarbonates from the sediments of Units IV and V. The biosilica content of Subunit IVB and relatively high sediment organic carbon content (see "Organic Geochemistry" section, this chapter) both suggest enhanced productivity during this time interval.

The increased silt content of Unit III sediments, which were deposited in the late Miocene and early Pliocene, may mark the transition into the period of weak Northern Hemisphere glaciation and overall climatic cooling. The observed change in sediment lithology could have resulted from increased continental erosion, and thus greater delivery of silt-sized sediments to Site 985 through intermittent or weak ice-rafted-debris events (Fronval and Jansen, in press). A possible alternative to the above scenario involves greater bottom-

Table 6. Description of the lithostratigraphic units at Site 985.

Unit	Subunit	Depth (mbsf)	Thickness (m)	Age	Lithology and characteristic features
I		0–17.2	17.2	Holocene–Pleistocene	Interbedded clayey nannofossil ooze with foraminifers, clay with silt, silty clay, and silty clay with nannofossils. Few ashes, dropstones present, reflectance decrease at base.
II		17.2–99.2	82.0	Pleist.–early Plio.	Silty clay, clay with silt, clay, minor occurrence of biocarbonate. Ashes are common and dropstones are present, reflectance and natural gamma radiation decrease at base.
III		99.2–155.2	56.0	early Plio.–late Mio.	Indurated sediments composed of clay with silt, clay, absence of biogenic components. Ashes common to abundant, dropstones absent. Low-amplitude reflectance variations.
IV		155.2–465.0	306.8	late Mio.–late Oligo.(?)	
	IVA	155.2–241.5	86.3	late Mio.–mid. Mio.(?)	Clay, with very minor occurrence of clay with silt. Ashes rare, dropstones absent. Decrease in natural gamma radiation and magnetic susceptibility at base of unit.
	IVB	241.5–289.6	48.1	middle Miocene(?)	Clay with minor occurrence of biosilicious clays. Ashes rare and dropstones absent. Low magnetic susceptibility and natural gamma radiation.
	IVC	289.6–465.0	175.4	m. Mio.(?)–e. Mio.(?)	Clay, with minor occurrence of clay with silt. Ashes rare and dropstones absent. Low and gradually increasing magnetic susceptibility and natural gamma radiation.
V		465.0–587.9	122.9	e. Mio.(?)–l. Oligo.(?)	Clay, silty clay, clay with silt, and glauconitic clay. Ashes rare and dropstones absent. Sharp increase in magnetic susceptibility.

water delivery of silt-sized material to the site due to the enhancement of bottom-water production and bottom-current strength. This could be linked to either (1) climatic cooling, (2) deepening of the Greenland-Scotland Ridge sill depth (Wright and Miller, 1993), or (3) the initiation of the final closure of the Isthmus of Panama (Wolf and Thiede, 1991).

Units II and I record cyclic late Pliocene to Holocene variations between biocarbonate-bearing interglacial sediments and siliciclastic-rich glacial sediments. Late Pliocene to Holocene sedimentation rates at Site 985 were higher than at Sites 907 and 982, but much lower than at the southern drift sites (980/981, 983, and 984). The late Pliocene to Holocene lithologic cycles at Site 985 are also recorded in visual color variations and changes in spectral reflectance. These cycles are presumably related to orbital variations in the Milankovitch frequency bands. In accordance with this interpretation, paleomagnetic data from Site 985 suggest that the first occurrence of dropstones at the site takes place shortly after the onset of significant Northern Hemisphere glaciation some 2.5 m.y. ago (see "Paleomagnetism" section, this chapter).

BIOSTRATIGRAPHY

Site 985, centrally located in the Greenland-Norwegian Sea, yielded a sedimentary sequence of Oligocene to Holocene age. Calcareous microfossils (i.e., calcareous nannofossils and planktonic and benthic foraminifers) are present down to a depth of about 55 mbsf in Hole 985A. Calcareous nannofossils are also present through a short interval of about 15 m, centered at 90 mbsf in Hole 985A. Siliceous microfossils are rare at this site and only occur between about 240 and 280 mbsf. Agglutinated benthic foraminifers are recorded from about 300 mbsf to the bottom of the section. Limited biostratigraphic zonations have been achieved for this site and are summarized in Figure 10.

Calcareous Nannofossils

The abundance of Pleistocene calcareous nannofossils fluctuates considerably from Cores 162-985A-1H through 6H, as does that of reworked Cretaceous nannofossils in these cores. A few samples from this interval are barren of nannofossils. The nannofossils zonal boundaries indicated in Figure 10 have not been precisely located due to scarcity and sporadic occurrences of the marker species in the samples examined.

Sample 162-985A-5H-2, 122 cm, contains abundant *Coccolithus pelagicus* and rare *Gephyrocapsa* spp. A/B. The presence of the latter indicates an age younger than about 1.6 Ma (Pleistocene). The lowest interval with nannofossils was found in Cores 162-985A-9H and 10H. The presence of abundant *Reticulofenestra producta* and few *C. pelagicus* in the absence of *R. pseudoumbilicus* suggests a late Pliocene age. The sequence below Core 162-985A-10H is barren of nannofossils, apparently due to dissolution of carbonate.

Planktonic Foraminifers

Planktonic foraminifers are found only in the upper part of the Site 985 sequence; they are common in Samples 162-985-1H-CC and 2H-CC and rare in Samples 162-985-3H-CC and 4H-CC. Assemblages are dominated by *Neogloboquadrina pachyderma* (sinistrally coiling), indicating polar to subpolar paleoenvironmental conditions. The start of the acme zone of *N. pachyderma* (sinistrally coiling) is not found at this site because samples are barren of planktonic foraminifers (Fig. 10).

Benthic Foraminifers

Calcareous benthic foraminifers are recorded only in the upper part of Site 985. The mudline Sample 162-985A-1H-1, 0–1 cm, contains a relatively low-diversity fauna (16 species, 101 specimens) dominated by *Epistominella exigua, Cibicidoides wuellerstorfi, Oridorsalis umbonatus,* and *Triloculina frigida.* Rose Bengal-stained specimens account for nearly 15% of the total fauna; *O. umbonatus* is the dominant "live" taxon present at this site. Low-diversity calcareous benthic foraminiferal faunas, many exhibiting some degree of dissolution etching, are recorded down to Sample 162-985A-5H-2, 122–124 cm; the latter is highly unusual in that it contains nearly 63% *C. wuellerstorfi* (sample count = 123 specimens).

Agglutinated benthic foraminifers, devoid of calcareous cements, are generally present from Sample 162-985A-32X-CC to the base of the sequence. Barren samples are recorded at the following levels: 162-985A-33X-CC, 34X-CC, 35X-CC, and 37X-CC. Two assemblage zones are recognized from this lower sequence: the *Psamminopelta* sp. zone from about 300 to 370 mbsf and the *Psamminopelta* sp.–*Cyclammina amplectens* zone from about 370 mbsf to the base of the sequence. Kaminski et al. (1990) define this zonal boundary from ODP Site 643 on the basis of the last occurrence of *C. amplectens,* and they assign the *Psamminopelta* sp.–*C. amplectens* Zone to the Oligocene and the *Psamminopelta* sp. Zone to the upper Oligocene to lower Miocene. As at Site 643, the diversity and abundance of agglu-

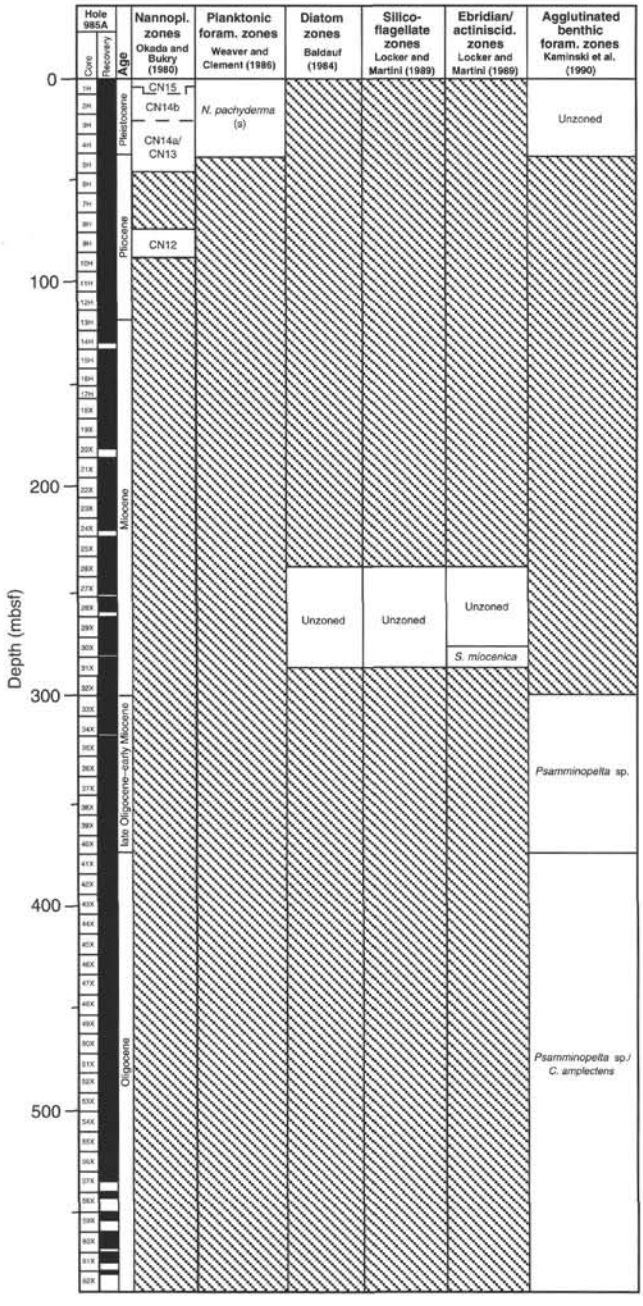

Figure 10. Biostratigraphic summary, Site 985. Hatched intervals indicate absence of fossils. Age boundaries for the Miocene/Pliocene and Pliocene/Pleistocene are based on paleomagnetic data. Other age information is based on agglutinated foraminifers and siliceous microfossil data.

Table 7. Summary of pass-through cryogenic magnetometer measurements at Site 985.

Measurement	Core sections
	162-985A-
25 mT 30 mT	1H-1 through 19X-6, 26X-6, 29X-4, 29X-5 2H-6, 4H-5 through 4H-7, 5H-1, 5H-6, 5H-7, 6H-6, 7H-1, 8H-1, 9H-5, 10H-2, 10H-3, 11H-1, 11H-2, 11H-4, 11H-5, 11H-6, 12H-3, 12H-4, 13H-6, 14H-2 through 14H-5, 15H-1, 16H-3 through 16H-6
	162-985B-
25 mT 30 mT	1H-1 through 14H-6 4H-2, 4H-6, 5H-4, 8H-1, 8H-4, 8H-5, 8H-7, 10H-1, 10H-6, 11H-2, 11H-4, 11H-5, 12H-2, 12H-6, 14H-3, 14H-6

tinated foraminifers decline markedly above this zonal boundary. It is interesting to note that these faunal changes parallel a similar reduction in pore-water salinity and chloride ion concentration (see "Inorganic Geochemistry" section, this chapter). However, it remains unclear whether these changes record reduced bottom-water salinity and associated faunal response during the upper Oligocene to lower Miocene, a diagenetic alteration of pore-water chemistry and associated reduction in agglutinated foraminiferal preservation, or have no common causal relationship.

Diatoms

At Site 985, only Samples 162-985A-27X-CC to 30X-CC contained siliceous microfossils. Diatom abundances varied from common to rare during this interval. The dominance of the heavily silicified species *Stephanogonia horridus* in all samples indicates poor preservation. The absence of several marker species prevented the assignation of sediments to a specific zone. However, assemblages in these samples consisted of several species restricted to the middle Miocene, including *Actinocyclus ingens* and *Denticulopsis lauta.*

Siliceous Flagellates

Siliceous flagellates (including silicoflagellates, ebridians, and actiniscidians) were recorded only in Samples 162-985A-26X-CC through 30X-CC. The abundance of these microfossils is generally low and preservation is poor.

Silicoflagellates

Beside fragments, skeletons of *Dictyocha* sp., *Distephanus crux,* and *Cannopilus hemisphaericus* were identified. *C. hemisphaericus* was found in Sample 162-985A-29-CC. The time range of this species is from the late Oligocene to early late Miocene.

Ebridians and Actiniscidians

The skeletons of ebridians and actiniscidians are more resistant against dissolution and therefore occur more frequently than silicoflagellates. Beside fragments, skeletons of three ebridian species (*Ammodochium serotinum, Spongebria miocenica,* and *Thranium* cf. *crassipes*) and of three actiniscidian species (*Actiniscus pentasterias, A. planatus,* and *Carduifolia gracilis*) were found. The co-occurrence of *S. miocenica* and of *A. planatus* in Sample 162-985A-30X-CC indicates the uppermost *Spongebria miocenica* Zone, which has its upper boundary at 14.4 Ma and belongs in the middle Miocene. This is consistent with co-occurrence of *C. hemisphaericus,* which ranges up to the early late Miocene.

PALEOMAGNETISM

At Site 985, archive halves of all 14 cores recovered from Hole 985B and the first 19 cores recovered from Hole 985A were measured using the pass-through cryogenic magnetometer with a 5-cm measurement interval. Below 180 mbsf in Hole 985A (below Core 985A-19H), erratic results indicated that drilling disturbance and "biscuiting" of the core compromised the measurements. Demagnetization was carried out at peak alternating fields of 25 mT for all core sections. Additional demagnetization steps at 30 mT were carried out on some core sections, as time allowed (Table 7). The ubiquitous drilling-induced remanence is steeply inclined downward, and therefore mimics a normal-polarity geomagnetic field which may mask reversed polarity intervals. This magnetic overprint can have relatively high coercivity and is not always fully removed at peak demagnetization fields of 30 mT, the largest demagnetization field available in conjunction with the pass-through cryogenic magnetometer.

Due to incomplete removal of the drill-string magnetization, reversed-polarity intervals are often represented by low inclination data and are more poorly defined than normal polarity intervals (Fig. 11). Dropstones contributed to core deformation and resulting remagnetization. Ash layers were often observed to have been remagnetized either as a result of iron sulfide authigenesis or mechanical rotation of magnetite grains in a lower viscosity (less cemented) ashy medium. In addition, the upper 25%–50% of the top section of most cores appears particularly susceptible to the high coercivity (drill-string) remagnetization, which is not always removed at peak alternating fields of 25 or 30 mT.

At the 25-mT demagnetization level, magnetization intensities lie in the 1–40 mA/m range for almost all measured cores. Below 180 mbsf in Hole 985A, magnetization intensities decrease by about an order of magnitude, possibly as a result of magnetite dissolution in sulfide-rich pore waters and/or drilling disturbance.

The polarity zone records for Holes 985A and 985B can be correlated, although the correlation is hampered by poor definition of reversed-polarity zones (Fig. 11). The apparent top of the Gauss Chron (Chron 2An) does not correlate in the two holes. The Gilbert Chron (Chron 3n) is better defined in Hole 985B than in Hole 985A. These differences are probably due to differences in the degree of drilling disturbance, partly induced by dropstone occurrence and/or possibly by variable degrees of (magnetic) iron sulfide authigenesis.

The correlation of the polarity record to the geomagnetic polarity time scale (GPTS) is based entirely on pattern fit of the polarity zones to the GPTS. At this site, the biostratigraphy does not provide useful constraints. The correlation of polarity zones to the GPTS implies variations in sedimentation rate, particularly in the upper Gilbert and Gauss Chrons (Fig. 12; Table 8). The magnetostratigraphic interpretation below the Gauss/Matuyama boundary remains tentative, although the correlation is strengthened by the correlation of natural gamma radiation between Sites 907 and 985 (Fig. 13), which indicates that the polarity chron assignments are consistent for the two sites.

SEDIMENTATION RATES

A sedimentary section 580 m thick was recovered at Site 985. Sedimentation rate reconstructions were based primarily on magnetic polarity events from Holes 985A and 985B (see "Paleomagnetism" section, this chapter). Because the sediments at Site 985 were largely barren of microfossils, biostratigraphic events were not used for sedimentation rate estimates in the upper 155 m (see "Biostratigraphy" section, this chapter). However, because the paleomagnetic data were unreliable in the XCB-cored interval of Hole 985A (below 155 mbsf or 163 mcd in Hole 985A; see "Paleomagnetism" section, this chapter), biostratigraphic information from the rare nonbarren intervals provided the only shipboard age control for the lowermost portion of the sequence. The Site 985 composite depth section (see "Composite Depths" section, this chapter) was used to relate events recorded in Holes 985A and 985B to a common depth scale.

Sedimentation rates were calculated for both the meters below seafloor (mbsf) depth scale and the meters composite depth (mcd) depth scale. Figure 14 and Table 9 present sedimentation rates as a function of age and composite depth for Site 985. Several intervals of relatively high sedimentation rate occur from 1.77 to 1.95 Ma (38 mcd/m.y.), from 3.13 to 3.23 Ma (39 mcd/m.y.), and from 4.78 to 4.88 Ma (43 mcd/m.y.). Because the interpretation of the paleomagnetic sequence is not constrained by biostratigraphy, it cannot be ruled out that these "spikes" of less than 200-k.y. duration are artifacts. This is true particularly in the Gilbert Chron, where interpretation of the paleomagnetic data is uncertain (see "Paleomagnetism" section, this chapter). Likewise, below the C3Ar/C3Bn boundary at 6.79 Ma (154 mbsf or 162 mcd in Hole 985A), constraints on average

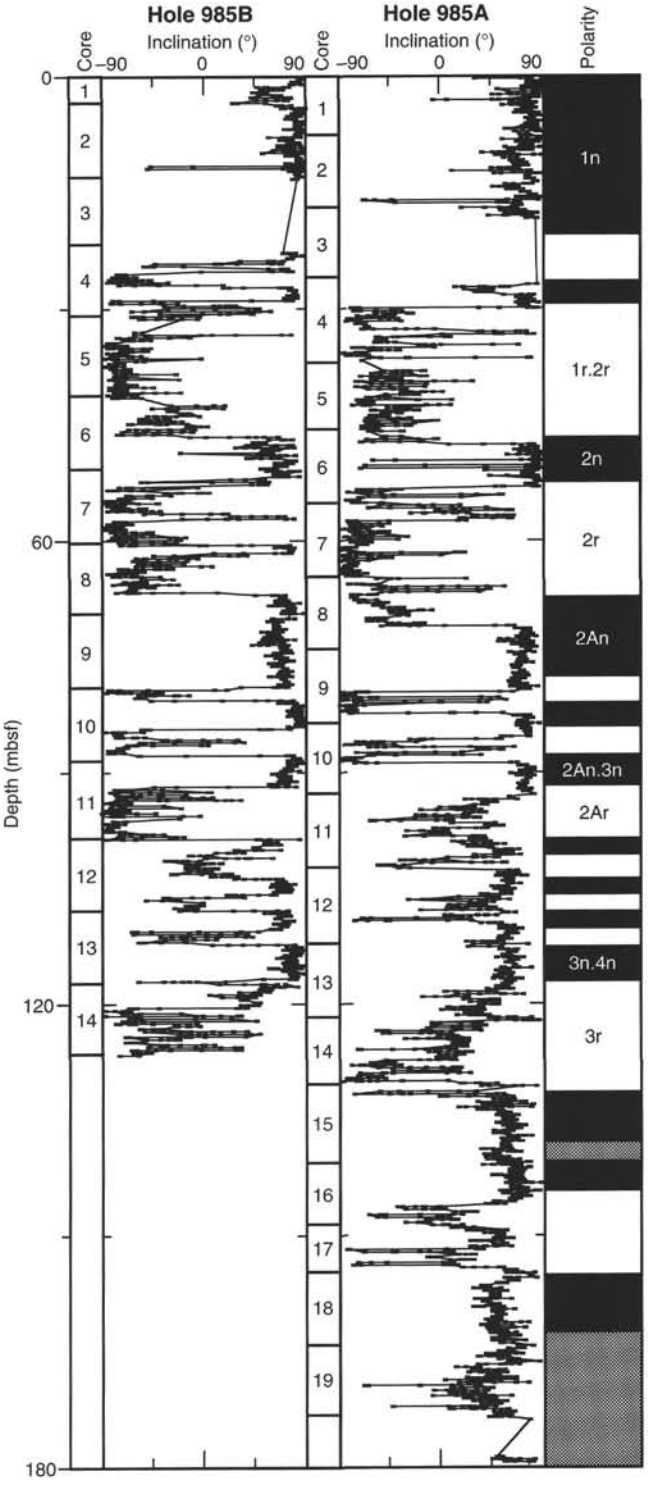

Figure 11. Inclination of the magnetization vector vs. depth (mbsf) for Holes 985A and 985B after AF demagnetization at peak fields of 25 mT. Polarity chron nomenclature after Cande and Kent (1992).

sedimentation rates are speculative. However, siliceous microfossils and agglutinated benthic foraminifers provide age control over the lower portion of the sequence. In particular, the uppermost *Spongebria miocenica* Zone (14.4 Ma) is at approximately 279 mbsf (287 mcd) in Hole 985A. Use of this event yields a sedimentation rate of

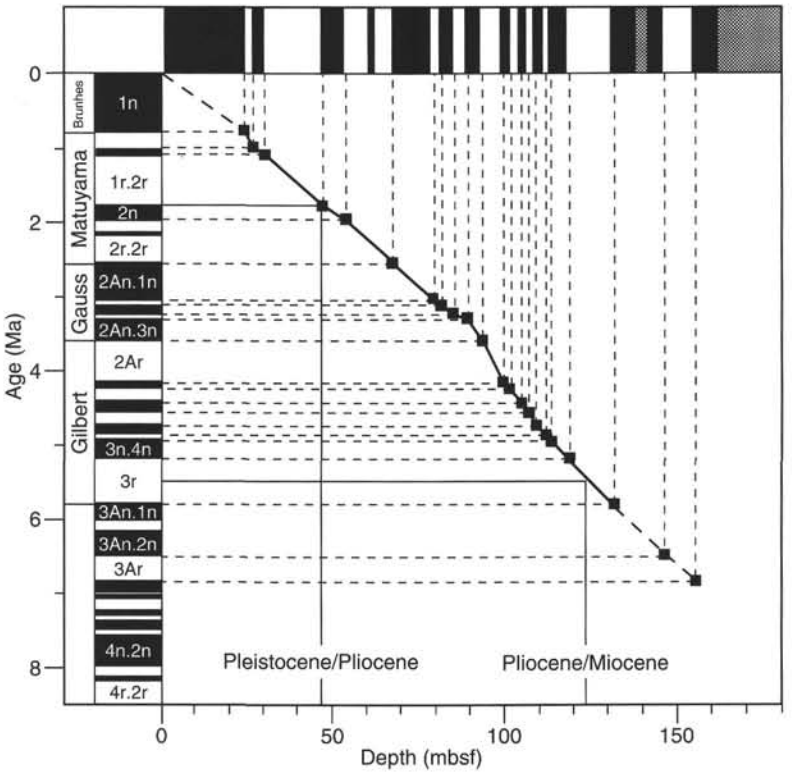

Figure 12. Tentative correlation of polarity zones in Holes 985A and 985B to the geomagnetic polarity time scale. Ages of polarity chrons from Cande and Kent (1995).

Table 8. Preliminary positions of polarity chron boundaries at Site 985.

Core, section, interval (cm)	Depth (mbsf)	Interpreted boundary	Age (Ma)	Comments
162-985A-				
4H-3, 0	29.70	Jaramillo (bottom)	1.07	Section break
6H-2, 5	47.25	Olduvai (top)	1.77	
6H-6, 65	53.85	Olduvai (bottom)	1.95	
8H-5, 20	70.90	Matuyama/Gauss	2.58	
9H-4, 70	79.40	Kaena (top)	3.04	
9H-6, 45	82.15	Kaena (bottom)	3.11	
10H-2, 35	85.55	Mammoth (top)	3.22	
10H-4, 50	88.70	Mammoth (bottom)	3.33	
11H-1, 15	93.35	Gauss/Gilbert	3.58	Poorly defined
15H-2, 30	133.00	Gilbert/C3An	5.89	Poorly defined
16H-4, 90	146.10	C3An/C3Ar	6.57	Poorly defined
17H-4, 45	153.85	C3Ar/C3Bn	6.93	Poorly defined
162-985B-				
4H-2, 10	24.00	Brunhes/Matuyama	0.78	Poorly defined
4H-3, 65	26.65	Jaramillo (top)	0.99	
4H-5, 30	28.70	Jaramillo (bottom)	1.07	
6H-4, 35	46.25	Olduvai (top)	1.77	
7H-2, 30	52.70	Olduvai (bottom)	1.95	
8H-6, 30	66.62	Matuyama/Gauss	2.58	
9H-7, 10	79.00	Kaena (top)	3.04	
10H-1, 100	80.40	Kaena (bottom)	3.11	
10H-4, 35	84.25	Mammoth (top)	3.22	
10H-6, 65	87.50	Mammoth (bottom)	3.33	
11H-2, 140	91.80	Gauss/Gilbert	3.58	
12H-1, 0	98.40	Cochiti (top)	4.18	Core break
12H-2, 55	100.45	Cochiti (bottom)	4.29	
12H-4, 70	103.60	Nunivak (top)	4.48	
12H-6, 0	105.90	Nunivak (bottom)	4.62	Section break
12H-7, 35	107.75	Sidufjall (top)	4.80	
13H-2, 105	110.45	Sidufjall (bottom)	4.89	
13H-4, 35	112.15	Thvera (top)	4.98	
13H-6, 145	116.85	Thvera (bottom)	5.23	

16 m/m.y. from 6.79 to 14.40 Ma, slightly lower than the sedimentation rates from the late Miocene (Table 9). The presence of certain agglutinated benthic foraminifer taxa from Section 162-985A-32X-CC to the base of the sequence places the base of Hole 985A in the Oligocene (see "Biostratigraphy" section, this chapter). Given an Oligocene age for the base of Hole 985A (580 mbsf), sedimentation rates over the lowermost portion (bottom 300 m) of Site 985 must be ≤30 m/m.y.

ORGANIC GEOCHEMISTRY

The shipboard organic geochemistry program at Site 985 consisted of analyses of volatile hydrocarbons, determinations of inorganic carbon, total nitrogen, total carbon, and total sulfur, and pyrolysis measurements (for methods, see "Explanatory Notes" chapter, this volume).

Volatile Hydrocarbons

As part of the shipboard safety and pollution monitoring program, concentrations of hydrocarbon gases were measured in every core using the standard ODP headspace-sampling technique. Headspace samples from Cores 2H through 5H were taken from Hole 985B. The methane content remained very low throughout the sediment sequence at Site 985 (2–12 ppm; Fig. 15; Table 10). However, a sudden increase of methane with higher hydrocarbons (to C_6, hexane) was detected between 344 and 363 mbsf with methane, reaching a maximum concentration of 80 ppm (Samples 162-985A-37X-5, 0–5 cm, through 39X-5, 0–5 cm; Fig. 15; Table 10). In this interval, the concentrations of iso-hexane (IC_6) and *n*-hexane (NC_6) rose to 116 and 148 ppm in Core 162-985A-37X (344 mbsf), respectively. C_1/C_{2+} ra-

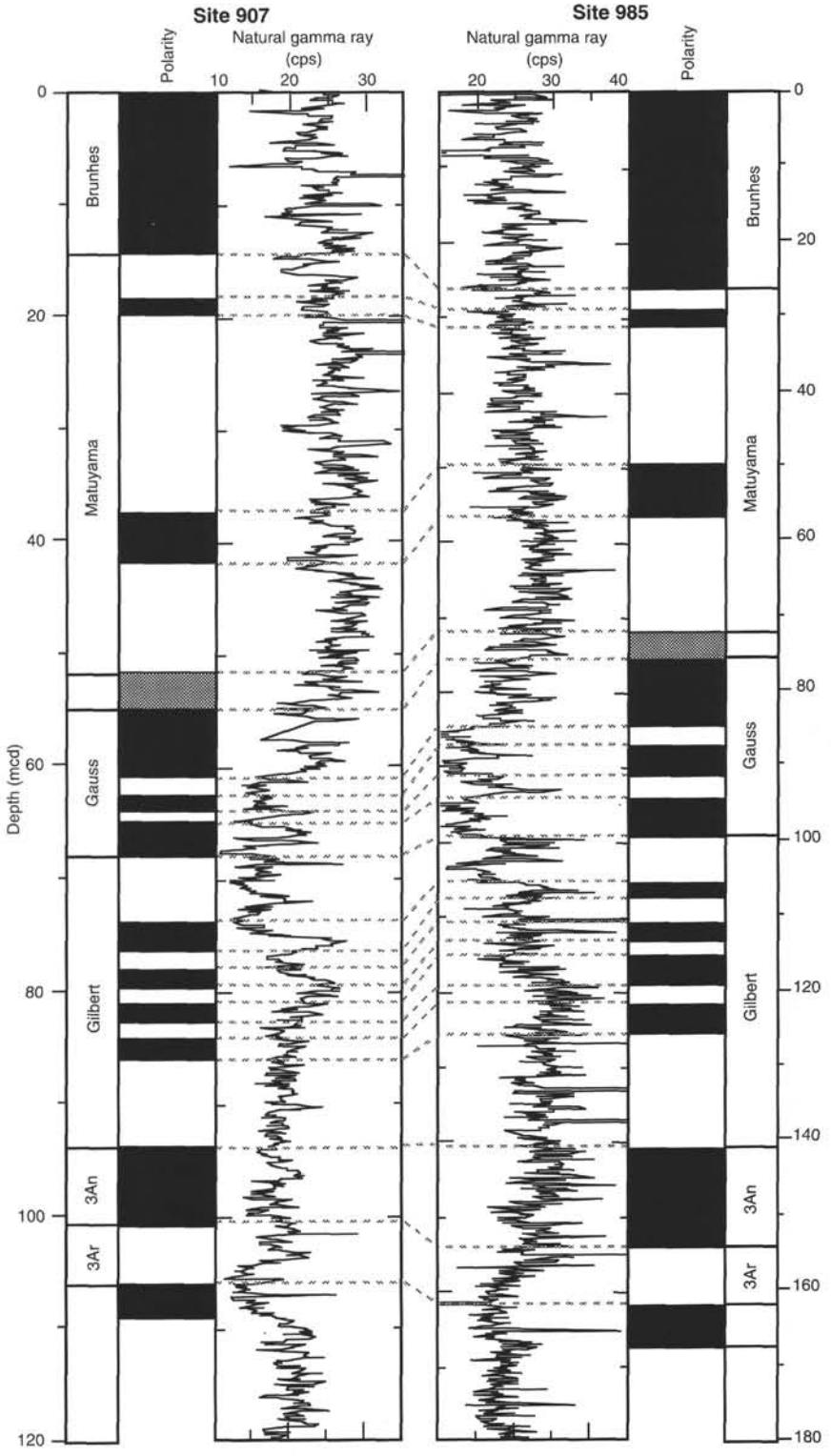

Figure 13. Correlation of natural gamma radiation records (from the shipboard multisensor track) for Sites 907 and 985. The natural gamma-ray correlation supports the Pliocene-Pleistocene polarity chron correlation at the two sites.

tios were 0.15, 0.12, and 0.09 within this interval, suggesting that the concentrations of the longer-chain hydrocarbon gases were anomalous in comparison to methane (Fig. 16). Sulfate values from pore waters never reached zero (see "Inorganic Geochemistry" section, this chapter), indicating that this anomaly cannot be explained by the normal process of microbial methanogenesis. This interval is also marked by a distinct decrease in the concentration of chloride, salinity, and sodium in interstitial water between 300 and 420 mbsf (see "Inorganic Geochemistry" section, this chapter). Furthermore, higher concentrations of total organic carbon were measured from several dark layers within this interval (Core 162-985A-37X; see "Lithostratigraphy" section, this chapter).

Possible causes of the abrupt increase of hydrocarbon gases include (1) contamination from core liner and/or drill oil, (2) decompo-

sition of gas hydrates during the coring process, (3) lateral migration of gas with large amounts of higher hydrocarbons from another source region, and (4) methanogenesis within dark organic-rich strata. It is possible that the hydrocarbon gas anomaly is related to contamination from the core liner and/or drill oil; however, this would not explain the chloride, salinity, and sodium anomaly. The decomposition of gas hydrates is one explanation for the decrease of salinity, sodium, and chloride in the pore waters (see "Inorganic Geochemistry" section, this chapter). However, if decomposition of gas hydrates occurred, large amounts of methane would be discharged, yet methane concentrations are lower than longer-chain hydrocarbons within the gas anomaly zone (Fig. 16). This result suggests that the source of the hydrocarbon gases is not from the direct decomposition of a clathrate. It is also possible that the hydrocarbon and pore-water anomalies are coincidental and have different origins; the interstitial anomaly occurs over a 120-m-thick section, whereas the gas anomaly is confined to a thickness of only 20 m.

Geochemical Composition of Dark Layers

As stated above, dark layers were observed in the zone of the hydrocarbon gases anomaly. Four sediment samples were taken from six dark layers that occurred in Core 162-985A-37X. Carbonate contents of these dark layers are very low, with values ranging from 0.7% and 0.9% (Table 11). Total organic carbon concentrations are very high, between 1.98% and 5.12%, with an average value of 3.67%

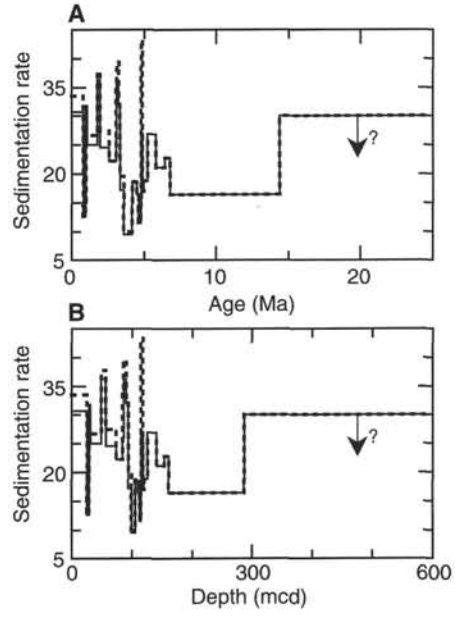

Figure 14. Site 985 sedimentation rates vs. age (**A**) and vs. composite depth (**B**). Solid lines indicate rates in mbsf/m.y.; dashed lines indicate rates in mcd/m.y.

Table 9. Age control points, Site 985.

Event	Age (Ma)	985A (mbsf)	985A (mcd)	985B (mbsf)	985B (mcd)	Avg. depth (mbsf)	Avg. depth (mcd)	Rate (mbsf/m.y.)	Rate (mcd/m.y.)
Core top	0.00	0.00	0.00	0.00	0.00	0.00	0.00		
								30.77	33.54
Brunhes/Matuyama	0.78			24.00	26.16	24.00	26.16		
								12.62	12.62
Jaramillo top	0.99			26.65	28.81	26.65	28.81		
								31.88	26.94
Jaramillo bottom	1.07	29.70	31.07	28.70	30.86	29.20	30.97		
								25.07	26.75
Olduvai top	1.77	47.25	49.72	46.25	49.66	46.75	49.69		
								36.25	37.75
Olduvai bottom	1.95	53.85	56.32	52.70	56.65	53.28	56.49		
								24.58	27.53
Matuyama/Gauss	2.58	70.90	75.61	66.62	72.05	68.76	73.83		
								22.21	22.26
Kaena top	3.05	79.40	84.32	79.00	84.26	79.20	84.29		
								25.94	34.62
Kaena bottom	3.13	82.15	87.07	80.40	87.05	81.28	87.06		
								36.25	39.35
Mammoth top	3.23	85.55	91.09	84.25	90.90	84.90	91.00		
								32.00	32.00
Mammoth bottom	3.33	88.70	94.24	87.50	94.15	88.10	94.20		
								17.21	19.63
Gauss/Gilbert	3.59	93.35	99.69	91.80	98.91	92.58	99.30		
								9.55	10.02
Cochiti top	4.20			98.40	105.41	98.40	105.41		
								18.64	18.64
Cochiti bottom	4.31			100.45	107.46	100.45	107.46		
								18.53	18.53
Nunivak top	4.48			103.60	110.61	103.60	110.61		
								16.43	16.43
Nunivak bottom	4.62			105.90	112.91	105.90	112.91		
								11.56	11.56
Sidufjall top	4.78			107.75	114.76	107.75	114.76		
								27.00	43.30
Sidufjall bottom	4.88			110.45	119.09	110.45	119.09		
								17.00	17.00
Thvera top	4.98			112.15	120.79	112.15	120.79		
								18.80	18.80
Thvera bottom	5.23			116.85	125.49	116.85	125.49		
								26.92	25.58
Gilbert/C3An	5.83	133.00	140.84			133.00	140.84		
								21.13	21.13
C3An/C3Ar	6.45	146.10	153.94			146.10	153.94		
								22.79	22.79
C3Ar/C3Bn	6.79	153.85	161.69			153.85	161.69		
								16.42	16.42
Spongebria miocenica, (S) top	14.40	278.79	286.63			278.79	286.63		
								<30.09	<30.09
Base of section	>24.40	579.70	587.54			579.70	587.54		

Notes: Ages are from Berggren et al. (1995). In parentheses: S = siliceous microfossil.

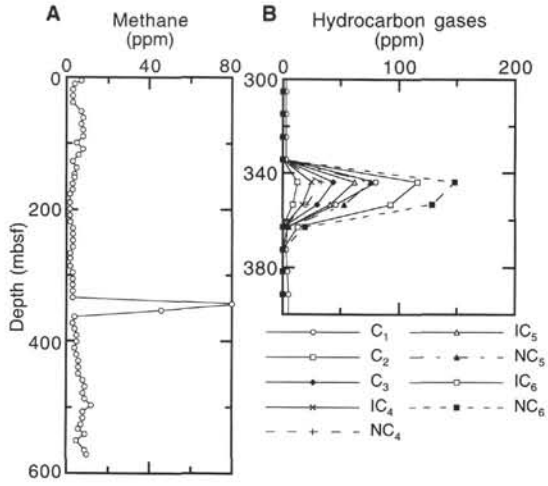

Figure 15. **A.** Methane concentration in Holes 985A and 985B. **B.** Concentrations of hydrocarbon gases between 300 and 400 mbsf in Hole 985A. C_1 = methane, C_2 = ethane, C_3 = propane, IC_4 = iso-butane, NC_4 = *n*-butane, IC_5 = iso-pentane, NC_5 = *n*-pentane, IC_6 = iso-hexane, and NC_6 = *n*-hexane.

(Table 11). Total nitrogen contents range from 0.13% to 0.33%, suggesting slightly higher values in comparison with those of the other sediments in Hole 985A (Table 11). Total sulfur values are very high, ranging between 7.32% and 16.36% (Table 11). According to the Rock-Eval pyrolysis data, these dark layers show a similar nature, except for one sample (162-985A-37X-5, 82–84 cm), which has relatively lower TOC content. Hydrogen index (HI) values range from 374 to 466 (Table 11), suggesting that organic matter of the dark layers may be of marine origin. As indicated by the HI and oxygen index (OI) data, samples of these dark layers contain immature Type II (oil-prone) organic matter. The productivity index (PI) is very low (0.02 to 0.04), and T_{max} varies between 409° and 418°C (Table 11), suggesting that immature organic material dominates the dark layers of Core 162-985A-37X. The existence of these dark layers with very high TOC content and immature marine organic material may be related to the abrupt generation of higher hydrocarbon gases. However, we have no definitive explanation for the relationship between hydrocarbon gas generation and these dark layers. Further qualitative and quantitative investigations of organic geochemical samples, such as detailed flux records of several biomarkers and isotopic composition of C_1 in the hydrocarbon gas mixtures, are required to address to this problem.

Carbon, Nitrogen, and Sulfur Concentration

Determinations of inorganic carbon, total carbon, total nitrogen, and total sulfur in Hole 985A are summarized in Table 12 and displayed in Figure 17. Data derived from dark layers are discussed above. Carbonate content fluctuated between 0.2% and 30.7% in the Pliocene and Pleistocene sections (0–110 mbsf; Fig. 17; Table 12). The high $CaCO_3$ content in the lower interval reflects nonbiogenic (inorganic) carbonate in the sediments. Total organic carbon (TOC) varies between 0% and 2.3%, with an average value of 0.35% (Fig. 17; Table 12). However, the average TOC content in the middle interval (17–276 mbsf; late to middle Miocene), at 0.71%, is considerably higher than that of the other intervals. This TOC enrichment is coincident with a high TOC interval of the same age found at Site 907. A similar TOC enrichment was observed in ODP Holes 642B and 643A, which were drilled on the Vøring Plateau (Holemann and Henrich, 1994). Total nitrogen contents are generally low in Hole 985A (0.03%–0.15%; Fig. 17; Table 12). Total sulfur values range from 0% to 5.1%, with an average of 0.32% (Fig. 17; Table 12). As with TOC, total sulfur also shows higher values in the middle to late Miocene section in Hole 985A (177–276 mbsf). The higher TOC and TS contents may suggest that the environment of deposition was more anoxic due to increased productivity and/or restricted deep-water ventilation in the Iceland Plateau region during the middle to late Miocene (see "Organic Geochemistry" section, "Site 907" chapter).

Composition of Organic Matter

C/N ratios vary between 0.5 and 15.8 in Hole 985A (Fig. 17; Table 12). These data suggest a mixture of marine and terrigenous organic carbon (Fig. 18) with a predominance of marine organic material. Most of the Rock-Eval pyrograms show an indistinct S_2 peak in Hole 985A. Pyrolysis pyrograms of immature sediments typically show poorly separated S_1 and S_2 peaks, which can give anomalous S_2, T_{max}, HI, and OI values (Peters, 1986). Thus, these results point to the occurrence of an immature type of organic matter (Table 13).

INORGANIC GEOCHEMISTRY

Interstitial water profiles at Site 985 are characteristic of sediments in which sulfate reduction and volcanic alteration are the primary reactions controlling the concentrations of dissolved constituents. The most striking feature of these profiles is the departure from diffusive trends between 280 and 480 mbsf. In this interval chloride, sodium, and salinity decrease abruptly. This interval also includes a sudden increase in headspace methane and longer-chain hydrocarbons above background levels from Cores 162-985A-37X to 39X (see "Organic Geochemistry" section, this chapter). The interval of anomalous pore-water concentrations is bounded, above and below, by high-velocity layers in Sections 162-985A-32X-3, 101 cm, and 44X-6, 13 cm (see "Physical Properties" section, this chapter). The first peak, at 293.61 mbsf, corresponds to a 30-cm carbonate layer and the second peak, at 412.63 mbsf, corresponds to a 10-cm limestone layer (see "Lithostratigraphy" section, this chapter). These layers may have acted as diffusion barriers and modified the pore-water chemistry at Site 985, resulting in nondiffusive profiles.

Sulfate concentrations decrease from 26.3 mM near the surface to 10.8 mM at the bottom of the hole (Fig. 19A; Table 14). Sulfate values never reach zero, indicating that sulfate reduction is incomplete and methanogenesis is not an important process in these sediments. As a result, Site 985 is marked by very low methane concentrations with the exception of Cores 162-985A-37X through 39X, where methane reaches values as high as 80 ppm (see "Organic Geochemistry" section, this chapter). Across the upper diffusion barrier at 293.61 mbsf, sulfate values decrease from 14.0 mM in Core 162-985A-30X to about 11.5 mM in Cores 36X to 42X. Ammonia increases from 10 μM near the surface to a maximum of 591 μM at 108 mbsf, reflecting production of ammonia within the zone of sulfate reduction (Fig. 19B; Table 14). Ammonia concentrations decrease markedly across the upper diffusion barrier at 293.6 mbsf, reaching a minimum of 228 μM in Section 162-985A-39X-4 (Fig. 19B; Table 14). Ammonia values increase from the minimum across the lower diffusion barrier at 412.6 mbsf, and then decrease again toward the bottom of the hole.

Alkalinity values are highest, and variable, in the upper 300 m of Hole 985A (Fig. 19C; Table 14). Alkalinity decreases sharply across the upper diffusion barrier to a minimum of 1.3 mM at about 450 mbsf. The low values of alkalinity throughout Site 985 suggest that sulfate reduction has not been extensive at this site. Phosphate values are very low and highly variable in Hole 985A, with values ranging between 2.2 μM and 9.6 μM (Fig. 19D; Table 14).

Calcium increases and magnesium decreases with depth as expected from in situ alteration of volcanic material and interaction

Table 10. Results of headspace gas analyses of Hole 985A and 985B samples.

Core, section, interval (cm)	Depth (mbsf)	C_1 (ppm)	$C_{2=}$ (ppm)	C_2 (ppm)	C_3 (ppm)	IC_4 (ppm)	NC_4 (ppm)	IC_5 (ppm)	NC_5 (ppm)	IC_6 (ppm)	NC_6 (ppm)	C_1/C_2	C_1/C_3	C_1/C_{2+}
162-985A-														
1H-4, 0–5	4.53	7												
162-985B-														
2H-5, 0–5	9.43	4												
3H-5, 0–5	18.93	3												
4H-5, 0–5	28.43	3												
5H-5, 0–5	37.93	3												
162-985A-														
6H-5, 0–5	51.73	7												
7H-5, 0–5	61.23	8												
8H-5, 0–5	70.73	7												
9H-5, 0–5	80.23	8												
10H-5, 0–5	89.73	8												
11H-5, 0–5	99.23	5												
12H-5, 0–5	108.73	8												
13H-5, 0–5	118.23	6												
14H-5, 0–5	127.33	3												
15H-5, 0–5	137.23	5												
16H-5, 0–5	146.73	4												
17H-3, 0–5	151.93	4												
18X-5, 0–5	161.23	3												
19X-5, 0–5	170.73	3												
20X-3, 0–5	177.23	2												
21X-5, 0–5	189.83	2												
22X-5, 0–5	199.43	2												
23X-5, 0–5	209.03	2												
24X-5, 0–5	218.63	2												
25X-5, 0–5	228.23	3												
26X-5, 0–5	237.83	3												
27X-5, 0–5	247.53	3												
28X-5, 0–5	257.13	3												
29X-5, 0–5	266.73	2												
30X-4, 0–5	274.83	2												
31X-5, 0–5	286.03	2												
32X-5, 0–5	295.63	3												
33X-5, 0–5	305.23	3												
34X-5, 0–5	314.83	3												
35X-5, 0–5	324.53	3												
36X-5, 0–5	334.13	3												
37X-5, 0–5	343.73	80	4.0	13.0	44.0	25.0	33.0	62.0	76.0	116.0	148.0	6.2	1.8	0.15
38X-5, 0–5	353.33	46	3.0	9.0	30.0	17.0	21.0	41.0	53.0	93.0	129.0	5.1	1.5	0.12
39X-5, 0–5	362.93	4			0.3	0.5	0.7	3.8	5.1	12.8	19.0		13.3	0.09
40X-5, 0–5	372.53	3												
41X-5, 0–5	381.73	4												
42X-5, 0–5	391.53	5												
43X-5, 0–5	401.33	5												
44X-5, 0–5	411.03	4												
45X-5, 0–5	420.73	5												
46X-5, 0–5	430.43	6												
47X-5, 0–5	440.03	6												
48X-5, 0–5	449.63	6												
49X-5, 0–5	459.23	8												
50X-5, 0–5	468.73	9												
51X-5, 0–5	478.33	8												
52X-5, 0–5	487.93	9												
53X-5, 0–5	497.53	12												
54X-5, 0–5	507.13	8												
55X-5, 0–5	516.73	8												
56X-5, 0–5	526.43	7												
57X-3, 0–5	533.03	6												
58X-2, 0–5	541.13	9												
59X-2, 0–5	550.73	5												
60X-5, 0–5	564.93	9												
61X-4, 0–5	572.21	10												

with oceanic basement below (Fig. 19E; Table 14). The plot of Ca vs. Mg shows two slopes separated by an inflection in the interval between the diffusion barriers (Fig. 19F). The $\Delta Ca/\Delta Mg$ slope in the upper 300 m is –0.6, which is followed by the inflection between about 320 and 420 mbsf, and a decrease in $\Delta Ca/\Delta Mg$ to –1.6 below the lower diffusion barrier. The upper slope of –0.6 may indicate the uptake of magnesium and release of calcium during in situ alteration of volcanic material to smectite and zeolite, whereas the slope of –1.6 below 420 mbsf is more typical of alteration of basaltic oceanic crust.

Potassium concentrations progressively decrease downhole from a maximum of 12.6 mM at the surface to a minimum of 1.2 mM at the bottom of Hole 985 (Fig. 19G; Table 14). An abrupt drop from 5.9 to 3.4 mM occurs across the upper diffusional barrier at 293.6 mbsf, and concentrations continue to decrease to the bottom of the hole. The decrease in potassium reflects uptake during the alteration of volcanic material to form K-bearing zeolites (e.g., clinoptilolite, phillipsite). Aside from a small decrease in the upper 50 m, lithium concentrations increase in the upper part of Hole 985A, reaching a maximum in Cores 162-985A-36X through 42X and then decrease toward the base of the hole (Fig. 19H; Table 14). The complex lithium profile is similar to that observed at Site 907, and the increase from about 250 to 400 mbsf probably reflects release of lithium during alteration of volcanic material.

The salinity, sodium, and chloride profiles are anomalous in that all three profiles exhibit a characteristic minimum in Cores 162-985A-36X, 39X, and 42X (Fig. 19I, -J, -K; Table 14). Relative to seawater values at the top of the core, the decrease in salinity, sodium, and chloride is 4, 40 mM, and 40 mM, respectively. These changes

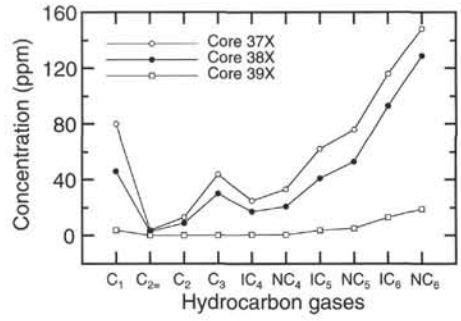

Figure 16. Concentrations of hydrocarbon gases in the gas anomaly interval (Cores 162-985A-37X through 39X). C_1 = methane, $C_{2=}$ = ethylene, C_2 = ethane, C_3 = propane, IC_4 = iso-butane, NC_4 = *n*-butane, IC_5 = iso-pentane, NC_5 = *n*-pentane, IC_6 = iso-hexane, and NC_6 = *n*-hexane.

represent a dilution of seawater by about 8% to 9%. The low-salinity horizon appears to be bounded above and below by dense, high-velocity layers mentioned earlier (see "Physical Properties" section, this chapter).

The cause of the low-salinity pore waters is enigmatic and we suggest several possibilities. No stored drill water was used during drilling Hole 985A; therefore, the low salinity zone cannot be explained by contamination by low-salinity drill water. Other explanations include (1) gas hydrate dissociation; (2) the migration of low-salinity water and gas to the site from elsewhere; (3) dehydration of clay minerals or hydrated calcium carbonate (e.g., ikaite, $CaCO_3 \cdot 6H_2O$); and (4) paleosalinity changes in the late Oligocene–early Miocene bottom waters of the Norwegian-Greenland Sea.

The existence of gas hydrates could explain the salinity, sodium, and chloride minima by freshwater dilution during hydrate decomposition; however, this explanation is difficult to reconcile with generally low methane values and with pore-water profiles of sulfate, ammonia, and alkalinity that suggest that sulfate reduction is incomplete. Furthermore, the concentration of longer-chain hydrocarbons is greater than methane in Cores 162-985A-37X to 39X (see "Organic Geochemistry" section, this chapter), suggesting that the source of the gas may not be from the direct decomposition of a clathrate. Alternatively, the low-salinity water and gas may have migrated laterally or vertically from a nearby source, but no evidence to support this interpretation is obvious from the seismic lines (see "Seismic Stratigraphy" section, this chapter).

We also considered the possibility that the low salinity resulted from the dehydration of clay minerals or, less likely, the dewatering of a hydrated carbonate, such as ikaite ($CaCO_3 \cdot 6H_2O$), as it was buried beyond its zone of stability. Transformation of clay minerals and zeolites can release fresh water to pore fluids, but shipboard XRD results do not indicate any major changes in clay mineralogy in this interval. The 30-cm limestone unit at 293.6 mbsf has an XRD pattern that is consistent with calcite that is poorly crystallized, as might be expected from decomposition of hydrated carbonate (see "Lithostratigraphy" section, this chapter). Dewatering of ikaite, which is more than 50% water by weight, could conceivably account for the low-salinity layer and might also explain the upper diffusive barrier, but does not address the occurrence of gas. Finally, it is possible that the pore waters record lowered salinity of bottom waters in the Norwegian-Greenland Sea during the late Oligocene–early Miocene. The zone of lowered salinity coincides with the occurrence of a low-diversity agglutinated benthic foraminiferal assemblage, potentially indicative of a change in paleoenvironment (see "Biostratigraphy" section, this chapter). A similar assemblage occurs in Site 643 on the Vøring Plateau, where pore-water chloride and salinity was low (539 mM and 32.5, respectively) in the one sample measured during this interval (Shipboard Scientific Party, 1987, p. 492). The problem inherent in a paleoceanographic explanation is that it would be difficult to get relatively low-salinity waters (30.5) to sink to deep or intermediate depths, especially if the Norwegian-Greenland Sea was open to the North Atlantic during the late Oligocene/early Miocene. Additional shore-based research will be necessary to choose among the proposed causes of the enigmatic salinity anomaly at Site 985.

The most pronounced feature of the silica profile in Hole 985A is the maximum of 982 µM that occurs between about 250 and 300 mbsf (Fig. 19L; Table 14). This interval corresponds to lithostratigraphic Subunit IVB, which contains high concentrations of biosiliceous material (see "Lithostratigraphy" and "Biostratigraphy" sections, this chapter). The profile of dissolved silica is controlled, therefore, by the availability of biogenic silica for dissolution. The profile of dissolved strontium increases with depth from 95 µM at the surface to 344 µM at the base of the hole (Fig. 19M; Table 14), probably indicating release of strontium to pore waters during alteration of volcanic material and calcite recrystallization.

PHYSICAL PROPERTIES

The primary objective of the physical properties program at Site 985 was to contribute to an understanding of syn- and postdepositional processes on the Iceland Plateau. Furthermore, the physical properties will help to establish the nature of lithologic/seismic boundaries within the sediments and clarify the geotechnical response of chert and ash layers. Lastly, we examine differences in physical properties due to the presence of hydrocarbons in the sediments. Physical properties measured were (1) index properties (water content and grain density), (2) bulk density (GRAPE), (3) undrained shear strength, (4) compressional wave velocity, (5) bulk magnetic susceptibility, and (6) natural gamma radiation. Bulk density and compressional wave velocity were measured both on whole-round core sections and split-core sections from Hole 985A. Laboratory procedures and techniques are discussed in the "Explanatory Notes" chapter (this volume). All physical properties data for Hole 985A are presented in Tables 15 through 17.

Results

Three geotechnical units (G1 to G3) have been defined on the basis of the character and trends of physical properties profiles. These criteria also have been used to define eight subunits.

Geotechnical Unit G1 (0–98 mbsf) is divided into two subunits (G1A and G1B). Subunit G1A (0–69 mbsf) corresponds to lithostratigraphic Unit I and upper part of lithostratigraphic Unit II, which are characterized as a nannofossil-rich and a silt-rich mud, respectively (see "Lithostratigraphy" section, this chapter). The lithostratigraphic units also contain several ash layers, dropstones, and dark, clay-rich layers. The physical properties profiles exhibit maximum variability of porosity, *P*-wave velocity, and natural gamma radiation within this subunit (Fig. 20). The average value of wet bulk density is 1.7 g/cm^3, with values ranging from 1.4 to 2.1 g/cm^3. Water content and porosity vary from 21% to 54% and 41% to 75%, respectively, with mean values of 36% and 60%, respectively. The *P*-wave velocity profiles show large variations as well as a decreasing trend with depth in this subunit (Fig. 20). The highest values correspond to dark, clay-rich layers, carbonate-rich layers, or ash layers that are thicker than 5 cm. Undrained shear strength profiles show a trend of gradual increase from approximately 4 kPa near the seafloor to 40 kPa at the lower boundary of geotechnical Subunit G1A. The magnetic susceptibility record shows increasing values in the upper 20 mbsf and fairly constant values between 20 and 100 mbsf, whereas the natural gamma radiation record exhibits little change in character and gradient.

Subunit G1B (69–98 mbsf) covers the lower part of lithostratigraphic Unit II, which is composed of silty mud containing nannofossils, ice-rafted debris, and ash layers. This subunit has relatively high

Table 11. Geochemical data from dark layers of Core 162-985A-37X.

Core, section, interval (cm)	Depth (mbsf)	IC (%)	$CaCO_3$ (%)	TC (%)	TOC (%)	TN (%)	TS (%)	C/N	C/S	T_{max} (°C)	S_1	S_2	S_3	PI	S_2/S_3	PC	HI	OI
162-985A-																		
37X-4, 24–27	342.44	0.11	0.9	3.49	3.38	0.24	7.32	14.1	0.5	418	0.22	12.52	1.59	0.02	7.88	1.06	371	47
37X-5, 82–84	344.52	0.08	0.7	2.07	1.98	0.13	7.73	15.2	0.3	520	0.19		1.27					64
37X-6, 16–18	345.36	0.09	0.7	5.21	5.12	0.33	16.36	15.5	0.3	412	0.28	18.28	1.88	0.01	9.73	1.54	357	37
37X-7, 31–34	347.01	0.09	0.7	4.28	4.19	0.31	11.23	13.5	0.4	409	0.49	14.25	1.64	0.03	8.71	1.22	340	39
	Average:	0.09	0.8	3.76	3.67	0.25	10.66	14.6	0.4	440	0.29	15.02	1.59	0.02	8.77	1.27	356	47

Note: IC = Inorganic carbon, $CaCO_3$ = calcium carbonate, TC = total carbon, TOC = total organic carbon, TN = total nitrogen, TS = total sulfur, C/N = total organic carbon/total nitrogen ratio, C/S = total organic carbon/total sulfur ratio, T_{max} = temperature (°C) of maximum hydrocarbon generation from kerogen, S_1 (mg HC/g rock) = volatile hydrocarbons; S_2 (mg HC/g rock) = kerogen-derived hydrocarbons, S_3 (mg CO_2/g rock) = organic CO_2 from kerogen, PI ($S_1 + S_2$) = productivity index, S_2/S_3 = kerogen-type index, PC ($0.083 \cdot [S_1 + S_2]$) = petroleum potential, HI ($100 \cdot S_2/TOC$) = hydrogen index; and OI ($100 \cdot S_3/TOC$) = oxygen index.

and very variable water content (25%–62%), porosity (49%–80%), and shear strength (38–144 kPa) values. Low natural gamma radiation values are another distinct characteristic of this subunit. The compressional wave velocity profiles show less variability than in Subunit G1A and a relatively low (1532 m/s) mean value.

Geotechnical Unit G2 (98–290 mbsf) is divided into four subunits (G2A to G2D). Subunit G2A (98–155 mbsf) corresponds with lithostratigraphic Unit III which is composed of silty mud. Subunit G2A shows a normal trend with depth to lower water content and porosity, and higher bulk density and *P*-wave velocity (from 1520 to 1545 m/s). It is also associated with higher natural gamma radiation values relative to those of Subunit G1B (Fig. 20). Undrained shear strength increases with less scatter than in Subunit G1B.

Geotechnical Subunit G2B (155–217 mbsf) comprises most of lithostratigraphic Subunit IVA, a clay-rich mudstone. The trend of the physical properties is similar to that observed in geotechnical Subunit G1B. Water content and porosity are high and variable (35% to 64% and 61% to 82%, respectively), and bulk density decreases accordingly to 1.31 g/cm^3. Compressional wave velocity continues its downhole increase and varies between 1523 and 1673 m/s, and there is a broad velocity peak between 182 and 200 mbsf. Values of undrained shear strength measured with the pocket penetrometer show a sharp increase at the upper boundary of Subunit G2B, indicating a more consolidated or indurated sediment in this subunit. Undrained shear strength values are at the upper boundary of the measurable range for the motorized vane, which, therefore, gives uncertain values. Geotechnical Subunit G2C (217–241.5 mbsf) includes the lowermost part of lithostratigraphic Subunit IVA, and shows a change back to low water content and porosity, and higher bulk density, similar to Subunit G2A. The lower boundary is associated with dark sediments and a prominent ash layer having high compressional velocities (up to 1909 m/s), and a clear downward drop in the susceptibility and natural gamma radiation values (Fig. 20).

Geotechnical Subunit G2D (241.5–290 mbsf) corresponds to lithostratigraphic Subunit IVB, which is a clay-rich mudstone containing 10%–15% biosilica. Porosity, grain density, and natural gamma radiation values are similar to those of Subunits G1B and G2B. Grain density shows maximum fluctuation (2.5–3.3) and magnetic susceptibility is at a minimum (mean value of 22 SI units) throughout Subunit G2D.

Geotechnical Unit G3 (290–480 mbsf) is divided into two subunits (G3A and G3B). Subunit G3A roughly corresponds to lithostratigraphic Subunit IVC, a clay-rich mudstone. The upper boundary of geotechnical Unit G3 is distinct and is associated with a high-velocity layer and an abrupt decrease in water content, porosity, and grain density (Fig. 20). The boundary also corresponds to the first occurrence of long-chained (>CH_4) hydrocarbons in the sediment (see "Inorganic Geochemistry" and "Organic Geochemistry" sections, this chapter). Free or adsorbed hydrocarbons were present down to 392 mbsf and may have been the reason why sediment volumes were difficult and sometimes impossible to measure in that interval. Subunit G3A shows a distinctly different trend from the cyclic changes in physical properties observed in the overlying units. Most of the properties display a gentle downcore change, except for the magnetic susceptibility which shows a stepwise increase with highest values in lowermost part of the subunit.

Geotechnical Subunit G3B (480 mbsf to total depth) includes most of lithostratigraphic Unit V, which is defined as a slightly silty, clayey mudstone. Most of the physical properties stay relatively constant throughout the subunit, with averages of 26% water content, 48% porosity, and 1.88 g/cm^3 bulk density. Compressional wave velocity shows a decrease just below the upper boundary, followed by an increase, and then fairly constant values below approximately 540 mbsf. Subunit G3B is also characterized by high magnetic susceptibility and natural gamma radiation values.

Discussion

The variability in physical properties of geotechnical Unit G1 is most likely caused by rapid changes in lithology, between carbonate-rich (nannofossil) sediments, ash layers, and dark clay-rich layers. In particular, the ash and clay-rich layers show up as distinct peaks in the velocity profiles.

A distinct boundary between geotechnical Subunits G1A and G1B is indicated in most of the physical properties profiles, but it is not identified as a change in the lithology, except that dropstones do not occur below this level. In general, zones of higher porosity and water content and lower bulk density are associated with more clay-rich sediment. The abrupt change in physical properties could therefore reflect a change from sediments containing coarser material (silt to gravel) associated with glaciations (in Subunit G1A) to more clay-rich sediments in Subunit G1B. This is supported by an early Pliocene age at the level of the Subunit G1A/G1B boundary.

The contact between geotechnical Units G1 and G2 is well defined both in the physical properties and lithology, and the combination of high bulk density and low water content, and porosity in Subunit G2A would suggest that the sediments contain more coarse material (silt) than the overlying unit.

The boundary between Subunits G2A and G2B is abrupt, and the undrained shear strength measurements (pocket penetrometer) mark the transition into more lithified sediments, characterized as claystones.

Geotechnical Subunit G2C is probably associated with seismic Reflector R1 (see "Seismic Stratigraphy" section, this chapter) and is characterized by high-velocity values. The lower boundary of this subunit is defined by a prominent ash layer, and by a well-defined change in most of the physical properties profiles. The transition is most likely attributed to a change in lithology into more silica-rich sediments in Subunit G2D (see "Lithostratigraphy" section, this chapter), reflected by the generally high grain density values.

Table 12. Summary of organic geochemical analyses of Hole 985A samples.

Core, section, interval (cm)	Depth (mbsf)	IC (%)	$CaCO_3$ (%)	TC (%)	TOC (%)	TN (%)	TS (%)	C/N	C/S
162-985A-									
1H-1, 101–102	1.01	1.36	11.3	1.33	0.00	0.04	0.00		
1H-3, 108–109	4.08	3.36	28.0	3.39	0.03	0.06	0.00	0.5	
1H-5, 131–132	7.31	1.58	13.2						
2H-1, 51–52	8.21	0.82	6.8	1.07	0.25	0.05	0.00	4.9	
2H-6, 52–53	15.72	0.17	1.4	1.23	1.06	0.09	0.07	11.8	15.2
3H-3, 126–127	21.46	1.16	9.7	1.21	0.05	0.04	0.00	1.3	
3H-6, 77–78	25.47	0.10	0.8						
4H-3, 50–51	30.20	0.22	1.8	0.50	0.28	0.05	0.00	5.5	
4H-6, 101–102	35.21	0.12	1.0						
5H-3, 60–61	39.80	0.15	1.2	0.23	0.08	0.04	0.00	1.9	
5H-4, 77–78	41.47	0.11	0.9						
5H-6, 103–104	44.73	0.17	1.4						
6H-1, 47–48	46.17	0.73	6.1	0.83	0.10	0.04	0.00	2.5	
6H-3, 132–133	50.02	0.78	6.5						
6H-4, 94–95	51.14	0.07	0.6	0.40	0.33	0.09	0.00	3.9	
6H-5, 48–49	52.18	1.64	13.7						
7H-1, 107–108	56.27	0.03	0.2	0.25	0.22	0.06	0.00	3.9	
7H-4, 79–80	60.49	0.02	0.2						
7H-6, 78–79	63.48	0.06	0.5	0.41	0.35	0.08	0.00	4.3	
8H-2, 106–107	67.26	0.07	0.6						
8H-5, 12–13	70.82	3.68	30.7	3.79	0.11	0.08	0.00	1.4	
8H-5, 140–141	72.10	0.07	0.6						
9H-3, 81–82	78.01	0.06	0.5	0.37	0.31	0.07	0.00	4.7	
9H-5, 47–48	80.67	1.93	16.1	2.16	0.23	0.08	0.00	2.9	
9H-5, 89–90	81.09	3.49	29.1						
10H-3, 128–129	87.98	0.35	2.9	0.63	0.28	0.05	0.00	5.8	
10H-4, 118–119	89.38	2.52	21.0	2.66	0.14	0.04	0.00	3.4	
10H-6, 118–119	92.38	0.08	0.7						
11H-1, 117–118	94.37	0.06	0.5	0.51	0.45	0.05	0.00	8.5	
11H-3, 107–108	97.27	3.69	30.7	3.85	0.16	0.09	0.00	1.8	
11H-6, 41–42	101.11	0.06	0.5						
12H-2, 73–74	104.93	0.06	0.5	0.25	0.19	0.05	0.00	3.9	
12H-4, 74–75	107.94	0.07	0.6						
12H-5, 74–75	109.44	2.00	16.7	2.29	0.29	0.04	0.00	7.9	
13H-2, 42–43	114.12	0.04	0.3	0.58	0.54	0.06	0.00	8.6	
13H-4, 42–43	117.12	0.06	0.5						
13H-6, 42–43	120.12	0.06	0.5						
14H-1, 86–87	122.56	0.09	0.7	0.35	0.26	0.09	0.03	2.9	7.6
14H-3, 86–87	125.16	0.07	0.6						
14H-5, 86–87	128.16	0.06	0.5						
15H-2, 57–58	133.27	0.06	0.5	0.35	0.29	0.05	0.66	6.4	0.4
15H-4, 57–58	136.27	0.06	0.5						
15H-6, 57–58	139.27	0.07	0.6						
16H-1, 135–136	142.05	0.06	0.5	0.41	0.35	0.05	0.00	6.6	
16H-4, 58–59	145.78	0.05	0.4						
17H-1, 85–86	149.75	0.05	0.4	0.26	0.21	0.09	0.00	2.5	
17H-3, 104–105	152.94	2.25	18.7	2.41	0.16	0.07	0.19	2.3	0.9
18X-2, 117–118	157.87	0.05	0.4	0.31	0.26	0.07	0.21	4.1	1.3
18X-6, 121–122	163.91	0.06	0.5						
19X-2, 26–27	166.46	0.06	0.5	0.25	0.19	0.06	0.20	3.5	1.0
19X-5, 53–54	171.23	0.05	0.4						
20X-2, 113–114	176.83	0.07	0.6	0.73	0.66	0.08	1.43	8.6	0.5
21X-2, 83–84	186.13	0.04	0.3	0.29	0.25	0.05	0.34	4.7	0.8
22X-4, 57–58	198.47	0.06	0.5	0.40	0.34	0.08	0.50	4.4	0.7
22X-6, 101–77	214.86	0.06	0.5	1.05	0.99	0.07	0.59	13.8	1.7
24X-4, 119–120	218.29	0.06	0.5						
25X-2, 143–144	225.13	0.06	0.5	0.57	0.51	0.08	0.70	6.6	0.7
25X-5, 97–98	229.17	0.06	0.5						
25X-6, 7–8	229.77	0.05	0.4						
26X-1, 126–127	233.06	0.05	0.4	0.48	0.43	0.07	1.15	6.6	0.4
26X-3, 78–79	235.58	0.05	0.4						
26X-5, 100–101	238.80	0.05	0.4	1.05	1.00	0.08	0.98	12.3	1.0
27X-2, 3–4	243.03	0.04	0.3						
27X-2, 58–59	243.58	0.04	0.3	2.34	2.30	0.15	5.10	15.8	0.5
27X-6, 49–50	249.49	0.05	0.4						
29X-2, 22–23	262.42	0.04	0.3	0.48	0.44	0.07	1.12	6.1	0.4
29X-3, 113–114	264.83	0.03	0.2						
29X-5, 119–120	267.89	0.04	0.3	0.37	0.33	0.06	0.36	5.2	0.9
30X-2, 82–83	272.62	0.04	0.3						
30X-4, 73–74	275.53	0.04	0.3	1.11	1.07	0.10	1.53	11.1	0.7
30X-5, 43–44	276.73	0.04	0.3						
31X-1, 62–63	280.62	0.05	0.4	0.33	0.28	0.05	0.13	6.0	2.1
31X-2, 45–46	281.95	0.05	0.4						
31X-6, 81–82	288.31	0.05	0.4	0.40	0.35	0.05	0.12	6.5	3.1
32X-2, 46–47	291.56	0.04	0.3						
32X-3, 101–102	293.61	7.07	58.9	7.04	0.00	0.05	0.04		
32X-5, 106–107	296.66	0.06	0.5						
33X-2, 58–59	301.28	0.05	0.4	0.22	0.17	0.05	0.11	3.6	1.5
33X-4, 58–59	304.28	0.05	0.4						
33X-6, 58–59	307.28	0.05	0.4	0.29	0.24	0.05	0.08	4.7	2.9
34X-1, 34–35	309.14	0.05	0.4						
34X-4, 34–35	313.64	0.05	0.4	0.28	0.23	0.05	0.08	4.3	2.9
34X-6, 36–29	323.28	0.05	0.4						
35X-6, 28–29	326.28	0.05	0.4	0.32	0.27	0.05	0.29	5.1	0.9
36X-1, 100–101	329.10	0.04	0.3						
36X-4, 100–101	333.60	0.03	0.2	0.37	0.34	0.06	0.10	6.1	3.4
37X-3, 58–59	341.28	0.04	0.3						
37X-5, 104–105	344.74	0.07	0.6	0.35	0.28	0.05	0.18	5.2	1.5

Table 12 (continued).

Core, section, interval (cm)	Depth (mbsf)	IC (%)	$CaCO_3$ (%)	TC (%)	TOC (%)	TN (%)	TS (%)	C/N	C/S
38X-3, 61–62	350.91	0.06	0.5						
38X-4, 63–64	352.43	0.06	0.5	0.30	0.24	0.05	0.16	4.8	1.5
38X-6, 20–21	355.00	0.06	0.5						
39X-2, 37–38	358.77	0.06	0.5	0.43	0.37	0.06	0.26	6.5	1.4
39X-5, 37–38	363.27	0.06	0.5						
40X-2, 100–101	369.00	0.54	4.5	1.00	0.46	0.06	0.12	8.4	3.9
40X-5, 100–101	373.50	0.13	1.1						
41X-2, 63–64	377.83	0.07	0.6	0.73	0.66	0.07	0.25	10.0	2.7
42X-1, 35–36	385.85	0.08	0.7	0.59	0.51	0.06	1.15	8.4	0.4
43X-2, 84–85	397.64	0.06	0.5	0.60	0.54	0.07	0.24	8.0	2.2
43X-5, 82–83	402.12	0.06	0.5						
43X-7, 11–12	404.41	0.06	0.5	0.57	0.51	0.07	0.22	7.6	2.3
44X-5, 62–63	411.62	0.06	0.5	0.59	0.53	0.04	0.05	12.7	10.7
45X-1, 63–64	415.33	0.08	0.7						
46X-7, 22–23	433.62	0.04	0.3	0.42	0.38	0.07	0.27	5.8	1.4
47X-1, 92–93	434.92	0.05	0.4						
47X-3, 104–105	438.04	0.19	1.6	0.45	0.26	0.06	0.17	4.3	1.5
47X-5, 39–40	440.39	0.04	0.3						
48X-1, 15–16	443.75	4.42	36.8	4.69	0.27	0.06	0.00	4.4	
48X-1, 56–57	444.16	0.05	0.4	0.39	0.34	0.06	0.15	5.5	2.3
48X-3, 88–89	447.48	0.04	0.3						
49X-2, 43–44	455.13	0.05	0.4	0.35	0.30	0.06	0.09	4.6	3.4
49X-5, 103–104	460.23	0.04	0.3						
49X-6, 31–32	461.01	0.04	0.3	0.50	0.46	0.08	0.14	6.1	3.3
50X-1, 91–92	463.61	0.04	0.3						
50X-2, 119–120	465.39	0.80	6.7	0.36	0.00	0.06	0.68		
50X-4, 75–76	467.95	3.18	26.5	3.56	0.38	0.06	0.82	6.4	0.5
50X-CC, 4–5	474.31	8.07	67.2	8.22	0.15	0.04	0.07	3.4	2.2
51X-2, 80–81	474.60	0.05	0.4						
51X-6, 80–81	480.60	0.08	0.7	0.33	0.25	0.07	0.09	3.5	2.9
52X-2, 102–103	484.42	0.08	0.7						
52X-4, 102–103	487.42	0.07	0.6	0.27	0.20	0.07	0.10	3.1	2.1
53X-3, 114–115	495.64	0.07	0.6						
53X-5, 50–51	498.00	0.07	0.6	0.34	0.27	0.06	0.11	4.2	2.4
54X-4, 44–45	506.04	1.38	11.5	1.81	0.43	0.05	0.43	7.9	1.0
54X-6, 68–69	509.28	0.56	4.7						
55X-4, 119–120	516.39	8.74	72.8	8.27	0.00	0.03	1.08		
55X-7, 9–10	519.79	0.08	0.7	0.29	0.21	0.07	0.81	3.2	0.3
56X-2, 46–47	522.36	0.04	0.3						
56X-5, 102–103	527.42	2.51	20.9	2.97	0.46	0.06	0.47	8.1	1.0
57X-2, 80–81	532.30	0.03	0.2	0.41	0.38	0.07	0.10	5.7	4.0
58X-1, 47–48	540.07	0.12	1.0	0.26	0.14	0.06	0.10	2.4	1.4
59X-2, 38–39	551.08	0.04	0.3	0.29	0.25	0.06	0.14	3.9	1.7
61X-2, 114–115	570.44	6.76	56.3	6.49	0.00	0.04	0.12		
61X-3, 108–109	571.76	0.05	0.4	0.28	0.23	0.06	0.06	3.7	3.5
61X-4, 127–128	573.45	5.74	47.8	6.37	0.63	0.07	0.00	9.6	
62X-1, 120–121	579.40	0.05	0.4	0.26	0.21	0.05	0.04	4.0	5.0
Average:		0.63	5.2	1.28	0.35	0.06	0.32	5.7	2.2
Maximum:		8.74	72.8	8.27	2.30	0.15	5.10	15.8	15.2
Minimum:		0.02	0.2	0.22	0.00	0.03	0.00	0.5	0.3

Notes: IC = inorganic carbon, $CaCO_3$ = calcium carbonate, TC = total carbon, TOC = total organic carbon, TN = total nitrogen, TS = total sulfur, C/N = total organic carbon/total nitrogen ratio, and C/S = total organic carbon/total sulfur ratio.

The contact between geotechnical Units G2 and G3 is well defined on most of the physical properties profiles, and represents a change in the downhole trend of water content, porosity, grain density, and natural gamma radiation. The upper part of Subunit G3A is associated with free and/or adsorbed long-chained nonbiogenic hydrocarbons (highest concentrations were found in the upper part of the subunit) and low-salinity pore water (see "Inorganic Geochemistry" and "Organic Geochemistry" sections, this chapter). Although hydrocarbons appeared in small concentrations, they may have affected the pycnometer analyses even after the samples had been dried at 100°C for more than 24 hours.

In summary, the physical properties in the upper 98 mbsf at Site 985 show values associated with the late Cenozoic climatic cooling (69–98 mbsf) and glacial-interglacial variations (seafloor to 69 mbsf). Between 98 and 290 mbsf, the physical properties reflect large-scale changes in accumulation of clastic material (silt) and organic production during the late Miocene to early Pliocene. Below 290 mbsf, an abrupt change in all properties marks the transition into a suite of more homogeneous sediments, and the physical properties show a gradual downhole effect of increased overburden. The physical properties in Hole 985A suggest two periods of reduced sedimentation rate, corresponding with geotechnical Subunit G2C (seismic Reflector R1) and the contact between geotechnical Units G2 and G3 (seismic Reflector R2).

SEISMIC STRATIGRAPHY

The drilling proposal for ICEP-3 (Site 985) was based on two single-channel seismic lines acquired by the University of Bergen, Norway, in 1989. The records from this survey appear noisy and do not show much seismic structure between the seafloor and acoustic basement. As weather conditions were good during the site survey for ICEP-3, the survey was designed to duplicate both the pre-cruise crossing seismic lines, in order to improve the quality of the seismic data over the site. The 80-in.^{3} water gun was used as a source and both the 3.5-kHz and 12-kHz PDR systems were run during the survey (see "Explanatory Notes" chapter, this volume). Total survey length was 17 nmi, consisting of three lines, 985-S1, -S2, and -S3 (Fig. 21). After evaluation of the survey data, Site 985 was drilled within 100 m of the originally proposed site. As the attempt to log Hole 985A failed (see "Operations" section, this chapter), interval velocities used for time-depth conversion are taken from the laboratory measurements (see "Physical Properties" section, this chapter).

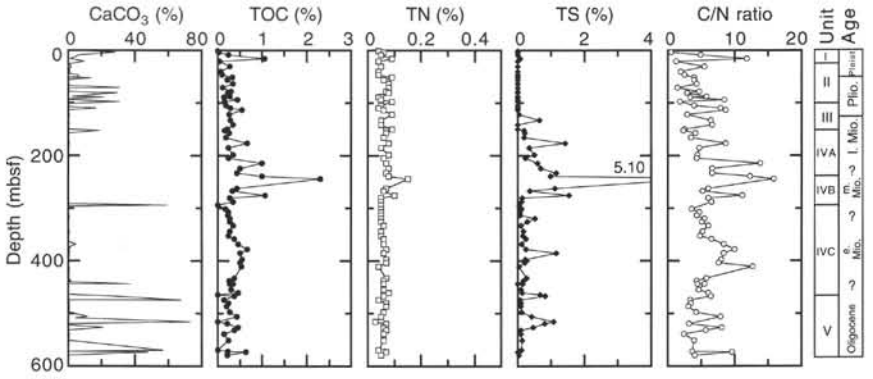

Figure 17. Calcium carbonate ($CaCO_3$), total organic carbon (TOC), total nitrogen (TN), and total sulfur (TS) contents, and TOC/TN (C/N) ratio, lithostratigraphic unit, and age in Hole 985A.

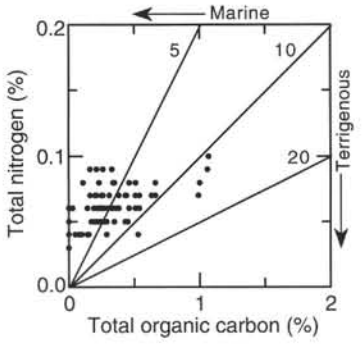

Figure 18. Total organic carbon vs. total nitrogen in Hole 985A. Lines show C/N ratios of 5, 10, and 20.

Based on comparison with velocities measured by the wireline logging at Sites 982 and 984, the laboratory velocities in the APC-cored part of the section (upper 155 mbsf) were corrected by +2% and +4% in the upper 0–100 and 100–155 mbsf, respectively, to compensate for core expansion during recovery.

Description of Seismic Stratigraphic Units

The area adjacent to Site 985 has a sedimentary section of an approximate thickness of 1.0 s two-way traveltime (TWT) above acoustic basement.

The new seismic data at Site 985 partly confirmed the generally featureless seismic character seen in the pre-cruise data, but displayed a somewhat larger variation. Three seismic units, IC-I to IC-III, have been defined, based on changes in seismic character across Reflectors R1 and R2 (Fig. 22).

The interval from the seafloor at 3.87 to 4.15 s TWT is defined as seismic Unit IC-I. Using a *P*-wave velocity of 1.58 km/s, the thickness of this unit is 220 m, and it is characterized by weak, discontinuous acoustic stratification, conformable with the seafloor.

Reflector R1, which displays an undulating character, marks a change to the more disturbed character of seismic Unit IC-II. Near Site 985, this unit is defined from 4.15 to 4.27 s TWT, which corresponds to a thickness of 100 m using an interval velocity of 1.66 km/s. Frequent diffraction hyperbolae are seen within Unit IC-II, which may result from the relief of Reflector R1. The unit appears to thin by approximately 25 m from west to east along survey Line 985-S3 (Fig. 22), but the vague character of Reflector R2 makes this estimate uncertain.

The definition of Reflector R2 is based on discontinuous reflector segments forming a coherent zone that parallels Reflector R1 and forms the base of the disturbed character of Unit IC-II. The lowermost seismic Unit IC-III is acoustically transparent, with the exception of few, low-amplitude, discontinuous reflectors (Fig. 22). The base of this unit is Reflector R3, which is acoustic basement in the area. The bottom of Hole 985A at 588 mbsf corresponds to a two-way traveltime of 4.58 s, using an interval velocity of 1.73 km/s for the drilled part of seismic Unit IC-II. Extrapolation using the velocity gradient seen in the lowermost 50 m of Hole 985A (see "Physical Properties" section, this chapter) gives a basement depth of approximately 900 mbsf. A high-amplitude reflector 0.1 s above basement may, however, be a high-velocity volcanic bed which may increase the basement depth estimate toward 950 mbsf, depending on the thickness of the layer.

Relationship to Core Data

The drilled section at Site 985 has been divided into five lithostratigraphic units and three geotechnical units, respectively, both of which are further divided into subunits (see "Lithostratigraphy" and "Physical Properties" sections, this chapter). The seismic data, on the other hand, show limited response to the relatively frequent downhole changes in lithology and physical properties. The low-amplitude, discontinuous acoustic stratification within seismic Unit IC-I

Table 13. Rock-Eval data for Hole 985A samples.

Core, section, interval (cm)	Depth (mbsf)	TOC (%)	T_{max} (°C)	S_1	S_2	S_3	PI	S_2/S_3	PC	HI	OI
162-985A-											
2H-6, 52–53	15.72	1.06	546	0.08		0.74					69
24X-2, 76–77	214.86	0.99	464	0.16	7.49	0.90	0.02	8.30	0.64	755	91
26X-5, 100–101	238.80	1.00	490	0.04	4.00	0.92	0.01	4.35	0.34	401	92
27X-2, 58–59	243.58	2.30	518	0.06		1.52					66
30X-4, 73–74	275.53	1.07	546			0.73					69
37X-5, 104–105	344.74	0.28	510	0.07	2.36	1.29	0.03	1.84	0.20	853	464
38X-4, 63–64	352.43	0.24	521	0.07		1.06					449

Notes: TOC = total organic carbon obtained by NCHS elemental analysis, T_{max} = temperature (°C) of maximum hydrocarbon generation from kerogen, S_1 (mg HC/g rock) = volatile hydrocarbons, S_2 (mg HC/g rock) = kerogen-derived hydrocarbons, S_3 (mg CO_2/g rock) = organic CO_2 from kerogen, PI ($S_1 + S_2$) = productivity index, S_2/S_3 = kerogen-type index; PC ($0.083 \cdot [S_1 + S_2]$) = petroleum potential, HI ($100 \cdot S_2$/TOC) = hydrogen index, and OI ($100 \cdot S_3$/TOC) = oxygen index.

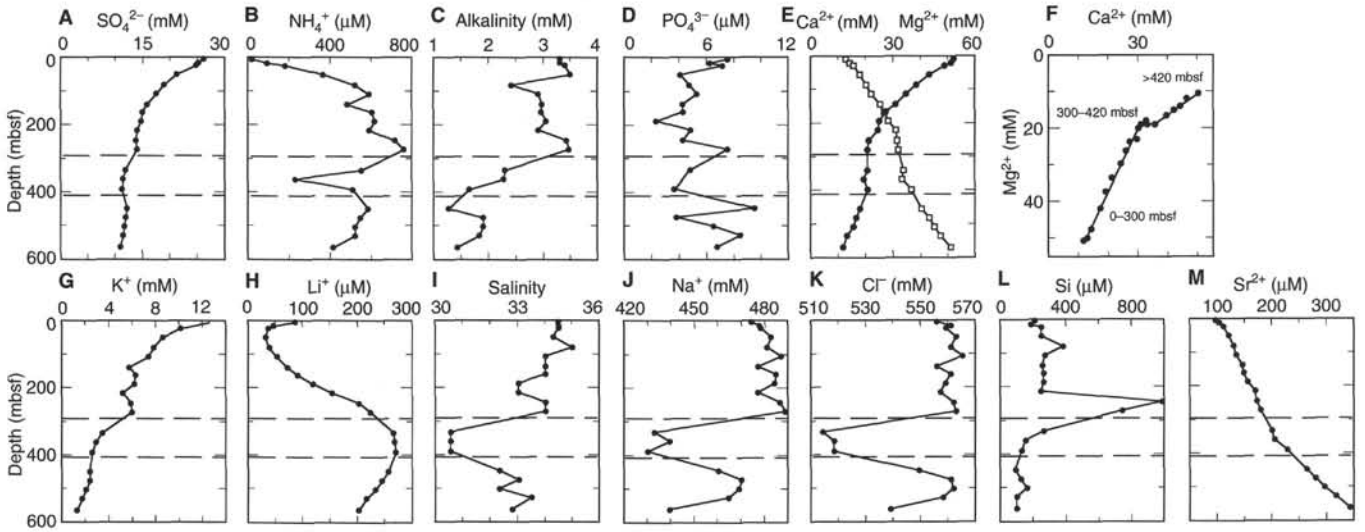

Figure 19. Vertical profiles of sulfate (**A**), ammonium (**B**), alkalinity (**C**), phosphate (**D**), calcium and magnesium (**E**), calcium vs. magnesium (**F**), potassium (**G**), lithium (**H**), salinity (**I**), sodium (**J**), chloride (**K**), silica (**L**), and strontium (**M**) in Hole 985A. Horizontal dashed lines represent depths of high *P*-wave-velocity layers.

Table 14. Composition of interstitial waters in Hole 985A.

Core, section, interval (cm)	Depth (mbsf)	Na (mM)	K (mM)	Li (μM)	Mg (mM)	Ca (mM)	Sr (μM)	Cl (mM)	SO_4 (mM)	NH_4 (μM)	Si (μM)	PO_4 (μM)	pH	Alkalinity (mM)	Salinity
162-985A-															
1H-3, 145–150	4.45	472	12.6	86.0	51.0	11.3	95	556	26.3	10	206	7.6	7.61	3.308	34.5
2H-4, 145–150	13.65	487	11.3	46.0	50.2	12.7	102	561	25.3	88	183	6.2	7.71	3.306	34.5
3H-4, 145–150	23.15	485	10.1	35.0	47.8	13.9	110	559	24.7	175	245	7.1	7.73	3.404	34.5
6H-4, 145–150	51.65	488	8.6	31.0	42.0	16.7	120	563	21.2	365	243	4.1	7.63	3.513	34.3
9H-4, 145–150	80.15	476	7.8	38.0	37.4	18.8	129	561	18.9	520	378	4.7	7.89	2.422	35.0
12H-4, 145–150	108.65	484	7.3	51.0	33.4	20.8	133	565	17.5	591	268	5.3	7.67	2.917	34.0
15H-4, 145–150	137.15	475	5.7	72.0	29.7	23.9	146	556	15.7	487	252	4.2	7.58	2.972	34.0
18X-4, 145–150	161.15	481	6.2	89.0	26.1	25.4	148	561	15.0	607	263	4.2	7.76	2.970	34.0
21X-4, 145–150	189.75	478	6.1	118.0	23.7	26.7	154	559	14.6	614	259	2.2	7.96	3.064	33.0
24X-4, 145–150	215.55	475	5.2	153.0	22.9	29.6	169	557	13.8	590	242	4.8	7.76	2.914	33.0
27X-4, 145–150	247.45	486	5.8	202.0	20.0	30.0	171	562	13.6	717	982	4.2	7.81	3.429	34.0
30X-3, 145–150	274.70	483	5.9	224.0	19.2	30.6	177	563	14.0	761	736	7.6	8.16	3.482	34.0
36X-4, 145–150	334.00	444	3.4	266.0	19.2	32.7	199	514	11.9	553	257	4.8	7.94	2.307	30.5
39X-4, 145–150	362.80	423	2.9	268.0	18.1	32.3	204	518	11.2	228	149		8.04	2.286	30.5
42X-4, 145–150	391.40	433	2.5	271.0	19.2	35.6	227	518	11.1	508	124	3.6	8.08	1.644	30.5
48X-4, 145–150	449.50	456	2.3	257.0	16.6	39.4	264	549	12.1	584	88	9.6	7.80	1.251	32.3
51X-4, 145–150	478.20	471	2.3	245.0	15.3	41.8	280	561	11.8	545	117	3.8	7.80	1.888	33.0
54X-3, 145–150	505.50	471	2.0	234.0	14.0	43.9	296	562	11.6	523	156	6.5	7.80	1.888	32.3
57X-2, 145–150	532.90	463	1.7	217.0	12.0	46.1	318	558	11.4	521	97	8.5	8.23	1.818	33.5
60X-4, 145–150	564.75	441	1.2	203.0	10.6	50.1	344	539	10.8	415	97	6.8	8.31	1.425	32.8

Table 15. Index properties of samples from Hole 985A.

Core, section, interval (cm)	Depth (mbsf)	Water content (wet %)	Water content (dry %)	Wet bulk density Method C (g/cm^3)	Grain density Method C (g/cm^3)	Dry bulk density Method C (g/cm^3)	Porosity Method C (%)	Void ratio Method C
162-985A-								
1H-1, 47–49	0.47	48.0	92.5	1.50	2.63	0.78	70.4	2.38
1H-1, 99–101	0.99	40.8	69.0	1.62	2.72	0.96	64.7	1.83
1H-2, 35–37	1.85	42.9	75.0	1.60	2.75	0.91	66.8	2.02
1H-2, 129–131	2.79	34.0	51.5	1.73	2.70	1.15	57.6	1.36
1H-3, 78–80	3.78	31.1	45.0	1.80	2.73	1.24	54.6	1.20
1H-3, 108–110	4.08	45.5	83.6	1.54	2.64	0.84	68.3	2.15
1H-4, 20–22	4.70	40.2	67.2	1.63	2.71	0.98	64.0	1.78
1H-4, 47–49	4.97	31.1	45.1	1.80	2.73	1.24	54.6	1.20
1H-4, 117–119	5.67	45.4	83.1	1.56	2.79	0.85	69.3	2.26

Only part of this table is reproduced here. The entire table appears on the CD-ROM (back pocket).

Table 16. Compressional-wave velocity measurements from Hole 985A.

Core, section, interval (cm)	Depth (mbsf)	Velocity (m/s)	Temperature (°C)	Direction
162-985A-				
1H-1, 45	0.45	1536	20.9	z
1H-1, 99	0.99	1548	20.7	z
1H-2, 41	1.91	1508	21.0	y
1H-3, 16	3.16	1596	20.9	y
1H-3, 79	3.79	1616	21.1	y
1H-3, 109	4.09	1557	20.8	y
1H-4, 19	4.69	1573	20.8	y
1H-4, 48	4.98	1725	21.5	y
1H-4, 132	5.82	1527	21.2	y

Note: For explanation of measurement directions see "Explanatory Notes" chapter (this volume).

Only part of this table is reproduced here. The entire table appears on the CD-ROM (back pocket).

Table 17. Undrained shear strength measurements from Hole 985A.

Core, section, interval (cm)	Depth (mbsf)	Undrained shear strength (kPa)	Spring no.	Penetrometer (kPa)
162-985A-				
1H-1, 46	0.46	5.4	1	
1H-1, 100	1.00	4.4	1	
1H-2, 34	1.84	3.2	1	
1H-2, 125	2.75	9.8	1	
1H-3, 32	3.32	9.9	1	
1H-3, 78	3.78	14.9	1	
1H-3, 109	4.09	9.5	1	
1H-4, 21	4.71	20.0	1	
1H-5, 130	7.30	8.2	1	

Only part of this table is reproduced here. The entire table appears on the CD-ROM (back pocket).

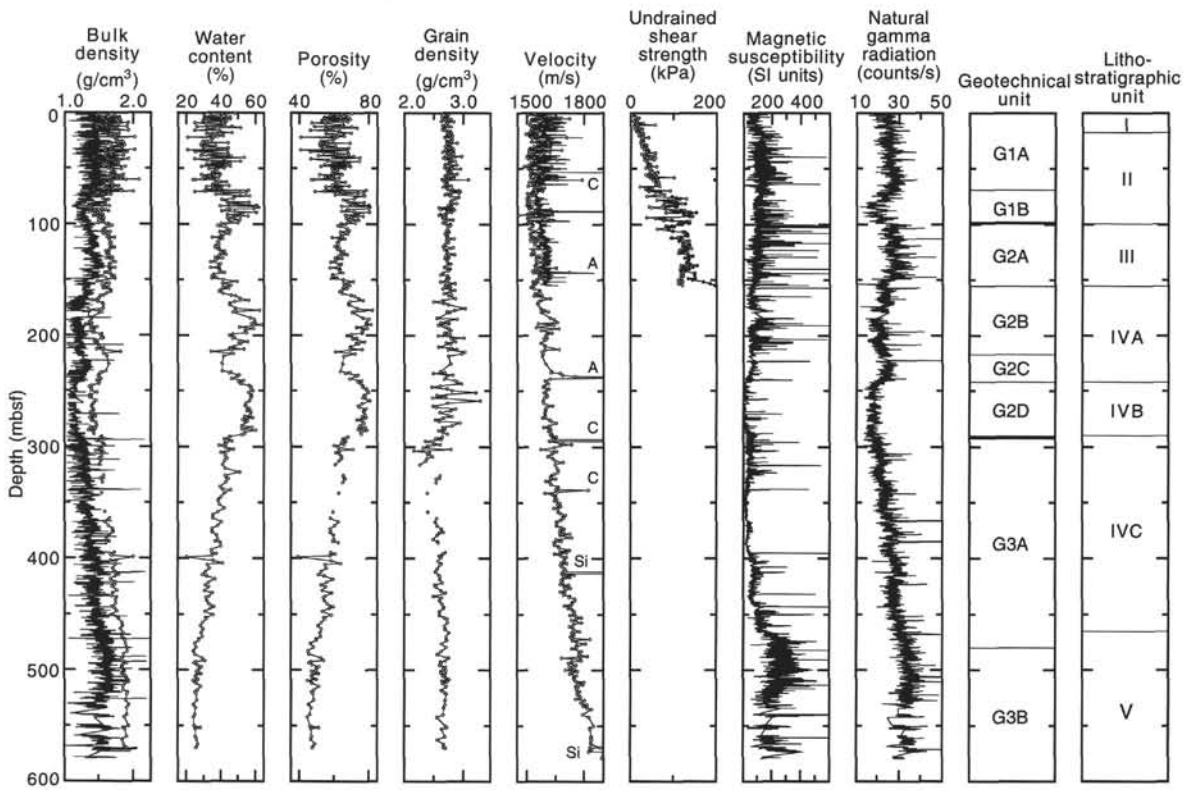

Figure 20. Physical properties data from Hole 985A: bulk density (GRAPE = continuous line; gravimetric = line with open circles), water content, porosity, grain density, compressional wave velocity (PWL = continuous line; split-core measurements = line with open circles; C = carbonate layer; A = ash layer; Si = chert layer), shear strength measured with the vane (open circles) or pocket penetrometer (solid circles), magnetic susceptibility, natural gamma radiation, and geotechnical and lithostratigraphic units.

most likely results from the variations in the relative amounts of the main sediment constituents clay, silt, nannofossils, and ash, which are also reflected in the variable character of the upper four geotechnical units (Fig. 23).

Reflector R1 is the only high-amplitude reflector between basement and the seafloor that can be followed through the length of the seismic survey. The reflector corresponds to a depth within a few meters to the upper boundary of geotechnical Unit G2C (see "Physical Properties" section, this chapter), which is a 23-m-thick unit with lower porosity and higher *P*-wave velocity and bulk density than the sediments above and below. Given the small thickness of geotechnical Subunit G2C, reflections from both its upper and lower boundaries probably interfere to give Reflector R1 its relatively broad character. Given the physical properties of geotechnical Subunit G2C and the character and relief of Reflector R1, possible erosion at this level cannot be excluded.

The disturbed character of seismic Unit IC-II is mainly due to diffractions from Reflector R1, caused by topography and possibly small faults (Fig. 22). Although Reflector R2 is indistinct and difficult to define, seismic Unit IC-II seems to encompass lithostratigraphic Subunit IVB, characterized by an increased content of biosilica, which causes the increased porosity and decreased density and seismic velocity seen in geotechnical Subunit G2D. Although the lower boundary of the biosiliceous unit may add to the character of

Reflector R2, a potentially more important change is found in the upper part of lithostratigraphic Subunit IVC and geotechnical Subunit G3A. A thin (40-cm) high-velocity (3.8 km/s) carbonate layer is observed at 293 mbsf, below which there is a distinct drop in chloride as well as salinity between approximately 300 and 420 mbsf (see "Lithostratigraphy," "Physical Properties," and "Inorganic Geochemistry" sections, this chapter). A peak in the methane content of the sediments was detected at 340 mbsf (see "Organic Geochemistry" section, this chapter). Hence, there is a set of changes in the sediments between 293 and 343 mbsf that may contribute to the character of Reflector R2.

Gas-bearing sediments are a possible cause for the homogeneous and nonreflective character of Unit IC-III, as well as for occasional high-amplitude events such as those seen near a small fault in the eastern part of Line 985-S3 (Fig. 22). However, as no high gas concentrations were noticed below the methane peak at 340 mbsf, the explanation for the character of Unit IC-III lies in the character of the sediments. The lithologic changes, causing relatively distinct changes in, for example, magnetic susceptibility between lithostratigraphic Subunit IVC and Unit V, do not produce responses in the seismic data.

In summary, changes in seismic character at Site 985 are related to variations in porosity and lithology between clay, silt, biogenic components, and ash layers. The most distinct reflector, R1, displays a relief that may indicate erosion at this level.

REFERENCES

Baldauf, J.G., 1984. Cenozoic diatom biostratigraphy and paleoceanography of the Rockfall Plateau region, North Atlantic, Deep Sea Drilling Project Leg 81. *In* Roberts, D.G., Schnitker, D., et al., *Init. Repts. DSDP,* 81: Washington (U.S. Govt. Printing Office), 439–478.

Berggren, W.A., Hilgen, F.J., Langereis, C.G., Kent, D.V., Obradovich, J.D., Raffi, I., Raymo, M.E., and Shackleton, N.J., 1995. Late Neogene chronology: new perspectives in high-resolution stratigraphy. *Geol. Soc. Am. Bull.,* 107:1272–1287.

Cande, S.C., and Kent, D.V., 1992. A new geomagnetic polarity time scale for the Late Cretaceous and Cenozoic. *J. Geophys. Res.,* 97:13917–13951.

————, 1995. Revised calibration of the geomagnetic polarity timescale for the Late Cretaceous and Cenozoic. *J. Geophys. Res.,* 100:6093–6095.

Eide, L., Beyer, I., and Jansen, E., in press. Comparison of Quaternary interglacial periods in the Iceland Sea. *J. Quat. Sci.*

Elderfield, H., 1986. Strontium isotope stratigraphy. *Palaeogeogr., Palaeoclimatol., Palaeoecol.,* 57:71–90.

Eldholm, O., Thiede, J., Taylor, E., et al., 1987. *Proc. ODP, Init. Repts.,* 104: College Station, TX (Ocean Drilling Program).

Eldholm, O., Thiede, J., and Taylor, E., 1989. Evolution of the Vøring volcanic margin. *In* Eldholm, O., Thiede, J., Taylor, E., et al., *Proc. ODP, Sci. Results,* 104: College Station, TX (Ocean Drilling Program), 1033–1065.

Fronval, T., and Jansen, E., in press. Late Neogene paleoclimates and paleoceanography in the Iceland-Norwegian Sea: evidence from the Iceland and Vøring Plateaus, Legs 151 and 104. *In* Thiede, J., Myhre, A.M., Firth, J.V., Johnson, G.L., and Ruddiman, W.F. (Eds.), *Proc. ODP, Sci. Results.,* 151: College Station, TX (Ocean Drilling Program).

Henrich, R., 1989. Diagenetic environments of authigenic carbonates and opal-CT crystallization in lower Miocene to upper Oligocene deposits of the Norwegian Sea (ODP Site 643, Leg 104). *In* Eldholm, O., Thiede, J., Taylor, E., et al., *Proc. ODP, Sci. Results,* 104: College Station, TX (Ocean Drilling Program), 233–247.

Henrich, R., and Baumann, K.H. 1994. Evolution of the Norwegian Current and the Scandinavian Ice Sheets during the past 2.6 m.y.: evidence from ODP Leg 104 biogenic carbonate and terrigenous records. *Palaeogeogr., Palaeoclimatol., Palaeoecol.,* 108:75–94.

Holemann, J.A., and Henrich, R., 1994. Allochthonous versus autochthonous organic matter in Cenozoic sediments of the Norwegian Sea: evidence for the onset of glaciations in the northern hemisphere. *Mar. Geol.,* 121:87–103.

Imbrie, J., Boyle, E.A., Clemens, S.C., Duffy, A., Howard, W.R., Kukla, G., Kutzbach, J., Martinson, D.G., McIntyre, A., Mix, A.C., Molfino, B., Morley, J.J., Peterson, L.C., Pisias, N.G., Prell, W.L., Raymo, M.E., Shackleton, N.J., and Toggweiler, J.R., 1992. On the structure and origin of major glaciation cycles, 1. Linear responses to Milankovitch forcing. *Paleoceanography,* 7:701–738.

————, 1993. On the structure and origin of major glaciation cycles, 2. The 100,000-year cycle. *Paleoceanography,* 8:699–736.

Kaminski, M.A., Gradstein, F.M., Goll, R.M., and Greig, D., 1990. Biostratigraphy and paleoecology of deep-water agglutinated foraminifera at ODP Site 643, Norwegian-Greenland Sea. *In* Hemleben, C., Kaminski, M.A., Kuhnt, W., and Scott, D. (Eds.), *Paleoecology, Biostratigraphy, Paleoceanography and Taxonomy of Agglutinated Foraminifera.* NATO ASI Ser. C, 237:345–386.

Koç, N., and Jansen, E., 1994. Response of high latitude Northern Hemisphere to orbital climate forcing: evidence from the Nordic Seas. *Geology,* 22:523–526.

Locker, S., and Martini, E., 1989. Cenozoic silicoflagellates, ebridians, and actiniscidians from the Vøring Plateau (ODP Leg 104). *In* Eldholm, O., Thiede, J., Taylor, E., et al., *Proc. ODP, Sci. Results,* 104: College Station, TX (Ocean Drilling Program), 543–585.

Myhre, A.M., and Thiede, J., 1995. North Atlantic–Arctic Gateways. *In* Myhre, A.M., Thiede, J., Firth, J.V., et al., *Proc. ODP, Init. Repts.,* 151: College Station, TX (Ocean Drilling Program), 5–26.

Myhre, A.M., Thiede, J., Firth, J.V., et al., 1995. *Proc. ODP, Init. Repts.,* 151: College Station, TX (Ocean Drilling Program).

Okada, H., and Bukry, D., 1980. Supplementary modification and introduction of code numbers to the low-latitude coccolith biostratigraphic zonation (Bukry, 1973; 1975). *Mar. Micropaleontol.,* 5:321–325.

Peters, K.E., 1986. Guidelines for evaluating petroleum source rock using programmed pyrolysis. *AAPG Bull.,* 70:318–329.

Shipboard Scientific Party, 1987. Site 643: Norwegian Sea. *In* Eldholm, O., Thiede, J., Taylor, E., et al., *Proc. ODP, Init. Repts.,* 104: College Station, TX (Ocean Drilling Program), 455–616.

Smalley, P.C., Qvale, G., and Qvale, H., 1989. Some ages from Leg 104 Site 642 obtained by RB-SR glauconite dating and SR isotope stratigraphy. *In* Eldholm, O., Thiede, J., Taylor, E., et al., *Proc. ODP, Sci. Results,* 104: College Station, TX (Ocean Drilling Program), 249–253.

Talwani, M., and Eldholm, O., 1977. Evolution of the Norwegian-Greenland Sea. *Geol. Soc. Am. Bull.,* 88:969–999.

Talwani, M., Udintsev, G., et al., 1976. *Init. Repts. DSDP,* 38: Washington (U.S. Govt. Printing Office).

Weaver, P.P.E., and Clement, B.M., 1986. Synchroneity of Pliocene planktonic foraminiferal datums in the North Atlantic. *Mar. Micropaleontol.,* 10:295–307.

Wolf, T.C.W., and Thiede, J., 1991. History of terrigenous sedimentation during the past 10 m.y. in the North Atlantic (ODP Legs 104 and 105 and DSDP Leg 94). *Mar. Geol.,* 101:83–102.

Wright, J.D., and Miller, K., 1993. Southern Ocean influences on late Eocene to Miocene deepwater circulation. In *The Antarctic Paleoenvironment: A Perspective on Global Change.* Antarct. Res. Ser., 60:1–25.

Ms 162IR-108

Note: For all sites drilled, core description forms ("barrel sheets") and core photographs can be found in Section 3, beginning on page 391. Forms containing smear slide data can be found in Section 4, beginning on page 1147. On the CD-ROM enclosed in the back pocket of this volume are all tables from this chapter (including an extended coring summary table) and shipboard measurements (files containing GRAPE density, *P*-wave velocity, natural gamma radiation, magnetic susceptibility, index properties, and spectral reflectance data).

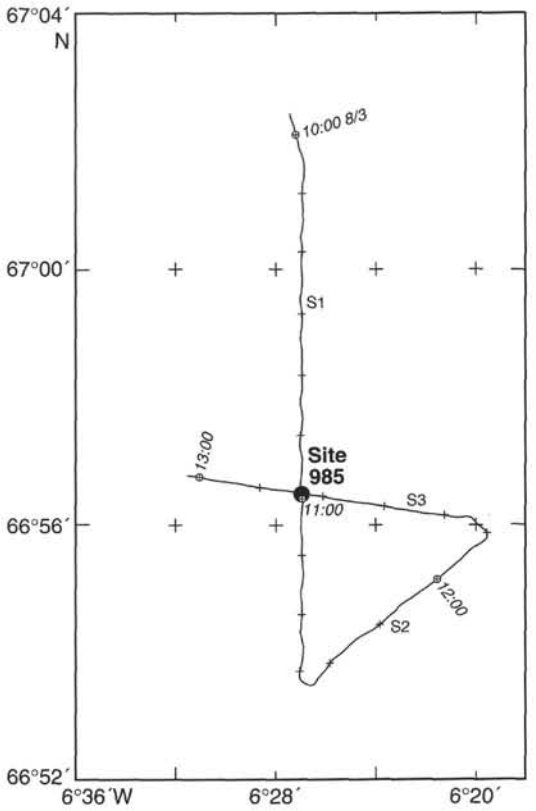

Figure 21. Map showing the site survey track lines near Site 985.

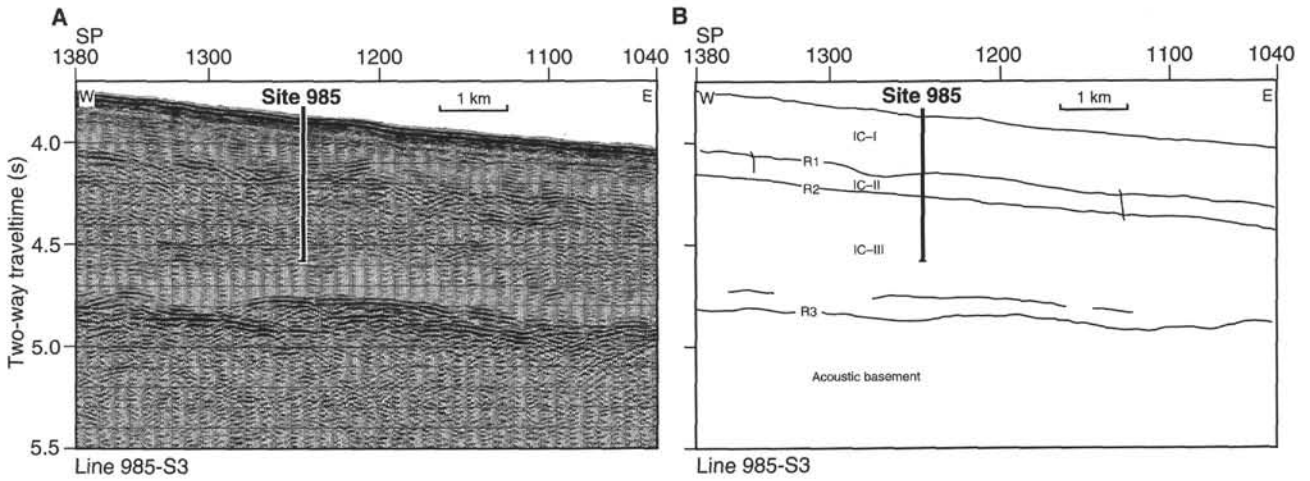

Figure 22. **A.** Seismic Line 985-S3. **B.** Interpretation of Line 985-S3, with seismic units and reflectors shown. Two possible faults are indicated. See Figure 21 for location of the profile. The profile shown is the entire line.

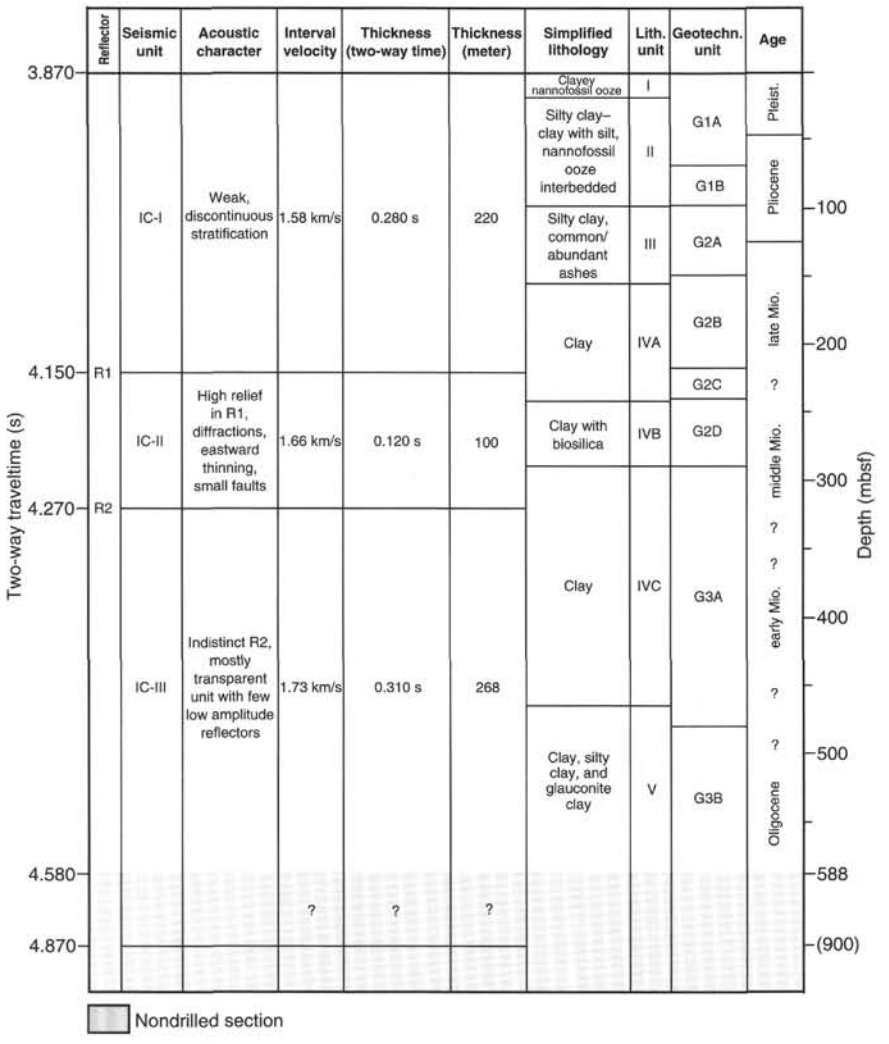

Figure 23. Relationships between seismic stratigraphy, lithostratigraphy, and geotechnical stratigraphy. The depth scale in mbsf is linear within the depths drilled, but note that the figure is not to scale below the drilled depth.